NEW DESIGNS OF MICROWAVE FRACTAL RESONATORS FOR MODERN WIRELESS APPLICATIONS

YAQEEN SABAH MEZAAL DAYYENI

DECEMBER 2014

NEW DESIGNS OF MICROWAVE FRACTAL RESONATORS FOR MODERN WIRELESS APPLICATIONS

A THESIS SUBMITTED TO
THE GRADUATE SCHOOL OF NATURAL AND APPLIED
SCIENCES OF
ÇANKAYA UNIVERSITY

BY
YAQEEN SABAH MEZAAL DAYYENI

IN PARTIAL FULFILLMENT OF THE REQUIREMENTS FOR THE
DEGREE OF
DOCTOR OF PHILOSOPHY
IN
THE DEPARTMENT OF
ELECTRONIC AND COMMUNICATION ENGINEERING

DECEMBER 2014

Title of the Thesis : **New Designs of Microwave Fractal Resonators for Modern Wireless Applications.**

Submitted by **Yaqeen Sabah Mezaal DAYYENI**

Approval of the Graduate School of Natural and Applied Sciences, Çankaya University.

Prof. Dr. Taner ALTUNOK
Director

I certify that this thesis satisfies all the requirements as a thesis for the degree of Doctor of Philosophy.
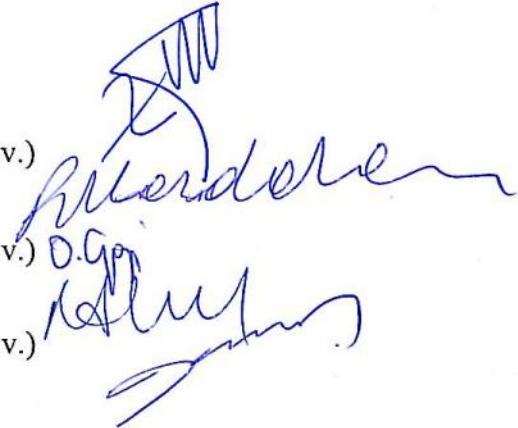
Prof. Dr. Halil Tanyer EYYUBOĞLU
Head of Department

This is to certify that we have read this thesis and that in our opinion it is fully adequate, in scope and quality, as a thesis for the degree of Doctor of Philosophy.

Prof. Dr. Halil Tanyer EYYUBOĞLU
Supervisor

Examination Date: 17.12.2014

Examining Committee Members

Prof. Dr. Halil Tanyer EYYUBOĞLU	(Çankaya Univ.)	
Assoc .Prof. Dr. Fırat HARDALAÇ	(Gazi Univ.)	
Assoc .Prof. Dr. Orhan GAZİ	(Çankaya Univ.)	
Assoc .Prof. Dr. Nursel AKÇAM	(Gazi Univ.)	
Assist. Prof. Dr. Göker ŞENER	(Çankaya Univ.)	

STATEMENT OF NON-PLAGIARISM PAGE

I hereby declare that all information in this document has been obtained and presented in accordance with academic rules and ethical conduct. I also declare that, as required by these rules and conduct, I have fully cited and referenced all material and results that are not original to this work.

Name, Last Name: Yaqeen Sabah Mezzal, DAYYENI

Signature   :

Date   : 17.12.2014

ABSTRACT

**NEW DESIGNS OF MICROWAVE FRACTAL RESONATORS FOR
MODERN WIRELESS APPLICATIONS**

DAYYENI, Yaqeen Sabah Mezaal

Ph.D, Department of Electronic and Communication Engineering

Supervisor: Prof. Dr. Halil T. EYYUBOĞLU

Co-Supervisor: Prof. Jawad K. ALI

December 2014, 132 pages

In this dissertation, new microstrip bandpass and bandstop filters based on fractal resonators have been presented in an attempt to construct filter designs with smaller size for almost modern wireless applications. The proposed bandpass filter structures have been generated based on Moore, Hilbert, Hilbert-zz and Sierpinski fractal geometries while the proposed bandstop filter is based on Hilbert Fractal resonators. The space-filling property and the self-similarity of the configurations related to the consecutive iteration levels of these fractal geometries have been found to create compact filter structures with accepted performance results.

Narrowband compact Moore fractal filters from 2nd and 3rd iteration levels have been designed for 2.4 GHz band application using a relative dielectric constant of 10.8 and dielectric thickness of 1.27 mm with good performance results in their quasi elliptic responses. For 3rd iteration Moore bandpass filter, size reduction percentage

as compared with 2nd iteration one resonating at the same frequency and using the same substrate material for 3rd iteration structure is 43% .The simulated and measured results are well-matched to each other .

Stepped impedance Hilbert microstrip bandpass filters have designed with characteristics of compacted sizes and narrow band responses which are the requisites of recent wireless communication systems. These filters are built from two edge coupled resonators, each resonator has been achieved by applying step impedance resonator generator on 1st and 2nd iterations of Hilbert fractal resonators on each segment for each fractal iteration . They have been proposed for the ISM band applications at center frequency of 2.4 GHz using a substrate with a dielectric coefficient of 9.6 and thickness of 0.508 mm. Results show that these filters own satisfactory output frequency responses. Size reduction percentage as compared with 1st iteration stepped impedance Hilbert bandpass filter operating at similar frequency and using similar substrate material for 2nd iteration structure is 63.34% .

New fractal design scheme based on Hilbert-zz curve has been used to produce compact microstrip bandpass filter .This fractal filter has been realized using two coupled resonators using additional coupling stubs .The material substrate has relative dielectric constant of 9 and thickness of 1.27 mm. Simulation graphs demonstrate that these filters possess good transmission and return loss features for the resultant frequency responses.

It should be mentioned that Moore, stepped impedance Hilbert resonator and Hilbert-zz bandpass filters exhibit higher harmonics eliminations in out of passband regions of their frequency responses which are much desired properties in modern wireless communications.

Miniaturized microstrip bandpass filters have been designed using Sierpinski fractal curves from 0th to 3rd iteration levels. The intended filter designs have been performed using dual-mode square slotted microstrip resonator in accordance with adopted fractal iterations. These microstrip bandpass filters have less bandwidth and sharper transmission responses than those of the single mode resonator and traditional square patch filter. Filter structures generating from the successive

iterations of the applied fractal geometries exhibit a noticeably low insertion loss, and sharper response of about 1% fractional bandwidth as compared with the conventional microstrip square patch filter of 3% fractional bandwidth constructed at the same resonant frequency of 5.33 GHz and using substrate material of dielectric coefficient of 10.8 and thickness of 1.27 mm.

A new dual-band microstrip bandpass filter has been designed using Peano fractal geometry at resonant frequencies of 2.25 GHz and 4.825 GHz using a substrate of a relative dielectric constant of 10.8 and thickness of 1.27 mm. The topology of this filter consists of dual edge coupled resonators constructed from 1st iteration of Peano fractal geometry. Simulated responses show that this filter has well frequency responses as well as dual bands gained which are highly requested in current communication systems.

On the other hand, new designs of Wide Bandpass Filter (WBPF) and Narrow Bandstop Filter (NBSF) based on Hilbert fractal resonators have been investigated using Sonnet simulator. The frequency responses properties of the proposed filters have been studied to observe the corresponding broad bandpass and narrow bandstop behaviours at the frequency around 2GHz.Moreover, the phase dispersion and surface current density details about proposed filters have been presented and analyzed. The proposed fractal filters have been found to possess compact sizes with flexible designs in addition to good frequency responses.

The modeling, simulation and performance evaluation have been performed using the method of moment (MoM) package Microwave Office 2009 from Advanced Wave Research (AWR) and a full-wave based electromagnetic simulator Sonnet software package which are very commonly used in electronics industry and research institutions.

Keywords: Microstrip Fractal Resonators, Compact Bandpass and Bandstop Filters, Narrow Bandpass Filters, Wide Bandpass Filter, Narrow Bandstop Filter, Frequency Harmonic Suppressions.

ÖZ

MODERN KABLOSUZ UYGULAMALAR İÇİN MİKRODALGA FRAKTAL REZONATÖRLERİNİN YENİ TASARIMILARI

DAYYENI, Yaqeen Sabah Mezaal

Doktora, Elektronik ve Haberleşme Mühendisliği Anabilim Dalı

Tez Yöneticisi: Prof. Dr. Halil T. EYYUBOĞLU

Eş Tez Yôneticisi: Jawad K. ALI

Aralık 2014, 132 sayfa

Bu tezde, yeni fraktal mikroşerit bant geçiren ve bant durduran filtre tasarımları modern kablosuz uygulamalar için daha küçük boyutu ile filtre tasarımlar üretmek amacıyla geliştirmiştir.

Önerilen Bant-geçiren filtre yapıları Moore, Hilbert, Hilbert-zz ve Sierpinski fraktal geometrilerine dayanarak oluşturulurken. Önerilen bant durduran filtresi Hilbert Fraktal rezonatörlere dayanmaktadır.

Bu dallanmış geometrilerin ardışık yineleme seviyelerine karşılık gelen yapıların boşluk doldurucu özelliği ve kendi kendine benzerliği kabul edimiş performanslı indirgenmiş boyutlu filtre yapılarnın üretilmesi için tespit bulunmuştur.

İkinciden Üçüncü yinelemeye dar bant kompakt Moore fraktal filtreleri, nispi dielektrik sabiti 10.8 ve dielektrik kalınliği 1.27 mm olan ve yarı eliptik sonuç

performansları iyi olan durumları kullanılarak 2.4 GHz bant uygulaması için tasarlanmıştır. Üçüncü yinelemeli Moore bant-geçiren filtre için, ikinci yinelemeye göre aynı frekansta boyut küçültme yüzdesi için % 43 tur , üçüncü yineleme için aynı substrate materyalini kullanarak. Simülasyon ve ölçülen sonuçlar birbirine uyumludur.

Kademeli empedans Hilbert mikroşerit bant-geçişli filtreler Modern telsiz iletişim devrelerinin gereksinimleri kompakt büyüklükte ve dar bantlı tepkilerinin özellikleri ile tasarladık.Bu filtreler çift kenar kuplajlı rezonatörden inşa edilmiştir, her rezonatör her fraktal yineleme için her segmentinde Hilbert fraktal rezonatörlerin birinci ve ikinci yineleme adım empedans rezonatör jeneratör uygulanmasına dayanmaktadır.Bu filtreler 9.6 nispi dielektrik sabiti ve 0.508 mm kalınlık ile 2.4 GHz merkez frekansında ISM bant uygulamaları için tasarlanmıştır.Sonuçlar bu filtrelerin iyi iletime sahip ve geri dönüş kaybı özellikleri olduğunu göstermektedir. İkinci yinelemeli Kademeli empedans Hilbert mikro bant-geçişli filtre için,ilk yinelemeye göre aynı frekansta boyut küçültme yüzdesi için % 63,34 'tür, İkinci yineleme filtere için aynı substrate materyalini kullanarak.

Hilbert-zz eğrisine dayalı yeni fraktal tasarım 9 nispi dielektrik sabiti ve 1.27 mm kalınlığında bir substrat kullanılarak ek bağlantı taslakları ile iki kutup kapasitif birleştiğinde mikro bant-geçiren filtre kompakt oluşturmak için getirilmiştir. Sonuçlar bu filtrelerin iyi iletime ve çıkış frekans tepkisinin ve geri dönüş kaybı özellikleri sahip olduğunu göstermektedir.

Moore , kademeli empedans Hilbert rezonatör ve Hilbert-zz bant geçiren filtreleri kendi freakrans tepkilerinin bant geçiren bölgelerin dışında yüksek harmonik bastırma özelliği sergiler , ki bunlar modern telsiz iletişimi için çok istenen ve şaşırtıcı özellikerdir.

Minyatür mikroşerit bant geçiren filtreler, üçüncü yineleme seviyelere sıfırıncı gelen Sierpinski fraktal eğrileri kullanılarak dizayn edilmiştir.Önerilen filtre tasarımı,

terçih edilen fraktal yinelemeye göre çift modlu, kare oluklu mikroşerit rezonatörün kullanımına dayanmaktadır .Bu mikro bant geçiren filtreler tek modlu rezonatör ve geleneksel kare yama filtre daha dar ve keskin % 1 fraksiyonel bant genişliği tepkisi göstermektedir. Geleneksel mikroşerit yama kare filtresi ise aynı frekansta , dielektrik sabiti 10.8 ve kalınlığı 1.27 mm olan substrat malzeme kullanılarak % 3 tür fraksiyonel bant genişliği tepkisi vermektedir.

Yeni çift bantlı mikroşerit bant geçiren filtre Peano fraktal geometrisi kullanılarak dizayn edilmiştir.Bu filtre, dielektrik sabiti 10.8 ve kalınlığı 1.27 mm olan yüzey malzeme kullanılarak 2.25 GHz ve 4.825 GHz rezanatörler frekansları tasarlanmıştır. Bu filtre Peano fraktal geometri ilk yineleme inşa çift kenar birleştiğinde rezonatörlerin oluşur.Simüle tepkiler bu filtrede frekans tepkilerini yanı sıra son derece güncel haberleşme sistemlerinde istenen kazanılan çift bant olduğunu göstermektedir.

Öte yandan, Hilbert fraktal rezenatörlerde dayalı geniş bant geçiş filtresi ve dar bant durduran filtre yeni tasarımlar Sonnet simülatörü kullanılarak incelenmiştir. Önerilen filtrelerin frekans yanıtları özellikleri 2 GHz civarında frekansta gelen geniş bant geçiren ve dar bant durduran davranışlarını gözlemlemek için çalışılmıştır. Ayrıca, önerilen filtreleri hakkında faz dağılımı ve yüzey akım yoğunluğu ayrıntıları sunulmuş ve analiz edilmiştir.Önerilen fraktal filtreler, iyi bir frekans yanıtları vardır, ek olarak, esnek tasarımları ile kompakt boyutlarda sahip oldukları bulunmuştur.

Modelleme, simülasyon ve performans değerlendirme çok yaygın elektronik sanayi ve araştırma kurumlarında kullanılan AWR2009 ve Sonnet simülatörleri kullanarak yapılmıştır .

Anahtar Kelimeler: Mikroşerit Fraktal Rezonatörler, Kompakt Bant Geçiren ve Bant Durduran Filtreler, Dar Bant Filtreler, Geniş Bant Geçiren Filtre, Dar Bant Durduran Filtre, Frekans Harmonik Bastırma.

ACKNOWLEDGEMENTS

TABLE OF CONTENTS

LIST OF FIGURES

FIGURES

FIGURES

FIGURES

FIGURES

FIGURES

FIGURES

LIST OF TABLES

TABLES

LIST OF ABBREVIATIONS

2D	Two Dimensional
3D	Three Dimensional
AWR	Advanced Wave Research
BW	Bandwidth
BPF	Bandpass Filter
CPW	Coplanar Waveguide
DF	Dielectric Filter
DGS	Defected Ground Structure
EM	Electromagnetic
EMI	Electromagnetic Interference
FD	Fractal Dimension
FBW	Fractional Bandwidth
GPS	Global Position System
GSM	Global System for Mobile
HTS	High Temperature Superconductivity
ISM	Industrial Scientific Medical
IL	Insertion Loss
L_R	Return Loss
LTCC	Low Temperature Cofired Ceramic
MIC	Microwave Integrated Circuit
MoM	Method of Moment
PCB	Printed Circuit Board
RF	Radio Frequency
SIR	Step Impedance Resonator
SiP	System in Package
TEM	Transversal Electromagnetic Wave

ABBREVIATIONS

WBPF	Wide Bandpass Filter
NBSF	Narrow Bandstop Filter

LIST OF SYMBOLS

SYMBOLS

C	Speed of Light
d	Coupling Gap, Stub Length , Pertubation Side Length
D	Capacitive Gap
E	Electric Field Intensity
F_N	Polynomial Function
g	Spacing Between Strips
H	Magnetic Field Intensity
ε_r	Relative Dielectric Constant
ε_{eff}	Effective Dielectric Constant
λ_0	Corresponding Wavelength at Resonant Frequency
λ_g	Guided Wavelength
J_s	Current Density
$k_{i,j}, K_{i,j}$	Coupling Factor
ι_c	Geometric Conductor Parameter
N	Filter Order
n,k	Fractal Iteration Order
n ,m	Mode Numbers
β	Phase Constant
ω	Angular Resonant Frequency
Q	Quality Factor
Q_c	Conductor Losses Quality Factor
Q_d	Dielectric Losses Quality Factor
Q_{ext}	External Quality Factor
Q_r	Radiation Losses Quality Factor
Q_u	Unloaded Quality Factor

SYMBOLS

$\emptyset_{21}$	Phase Shift Constant of S_{21} Coefficient
S, L	Microstrip Side Length
$S_n, L(k)$	Iterative Overall Fractal Perimeter
R	Connecting Segment Length
Sc	Conductor Surface
S_{21}	Transmission Coefficient
S_{11}	Reflection Coefficient
α	Attenuation Constant
γ	Propagation Constant
P	Normalized Frequency
P_{diss}	Dissipated Power
P_{EST}	Flowing Power via Specified Port
P_{inc}	Incident Power in Two Port Network
P_{tran}	Transmitted Power in Two Port Network
Ω	Normalized Angular Frequency
$g_o, g_1, \dots, g_i$	Chebychev Reactance Elements
ϵ	Ripple Constant
ε_0	Absolute Dielectric Constant
ε_{eff}	Effective Permittivity
ε_r	Relative Dielectric Constant
f_o, f_0	Resonant Frequency
f_1, f_{c1}	Lower Frequency
f_2, f_{c2}	Upper Frequency
α_c	Conductor Attenuation Constant
σ	Conductivity
δf	Transition Region

SYMBOLS

μ	Permeability
R_S	Surface Resistance
V	Resonator Volume
$\mathrm{v_T}$	Wave Velocity
Γ	Effective Resonator Volume to Conducting parts Surface Ratio
W	Stored Electromagnetic Energy
W	Microstrip Width
T	Microstrip Thickness
H	Substrate Thickness
$\tan \delta$	Tangent Loss
α_d	Dielectric Loss
Z_0	Characteristics Impedance

CHAPTER 1

INTRODUCTION

1.1 Background

Microwave bandpass and bandstop filters are available in all satellite, radar, and wireless communication systems, and are used to pass certain range of frequencies from a spectrum of frequencies and reject another according to the requirements of these systems. They are generally realized using one or more resonators, coupled to each other. In fact, a resonator is any physical component that stores both magnetic and electric energy in a frequency-dependent way. At the resonance frequency, the electric and magnetic current distributions in the resonator are equally stored. An ideal resonator can be designed simply by a capacitor/inductor system, where at resonance the magnetic and electric energy is exchanged to each other between inductor and capacitor [1,2].

Passive filter types can be classified according to physical structures as follows :

1.At Lower Frequencies

- **Lumped Element Filters**

Lumped elements have been used in microwave circuits for more than 30 years. The basic theory of filters [1,3-11] is corresponding to connected lumped inductors and capacitors as illustrated in **Figure 1**. This graph represents a lowpass filter, and we can construct a prototype design with 1 Ω input–output impedance and a 1-rad cutoff frequency. From here, it is basically a matter of scaling the g values for different elements to get the preferred frequency response and insertion loss. Moreover, other classes of filter such as highpass, bandpass, and band-stop simply involve a transformation in addition to the scaling to achieve the most wanted characteristics. For radio wave frequencies or the least

limit of the microwave frequency bands, passive filters can be realized by using coil inductors and parallel plate chip capacitors to build printed circuit board (PCB) connections. Several hybrid microwave integrated circuit (MIC) technologies such as thin film, thick film, and cofired ceramic are being adopted to build up such circuits. Lumped-element filters can be employed simply .By using presently obtainable surface-mounted components ,these filters can meet size and cost targets in high-volume production as in Ceramic Lumped-Element Filters and Superconducting Lumped-Element Filters .
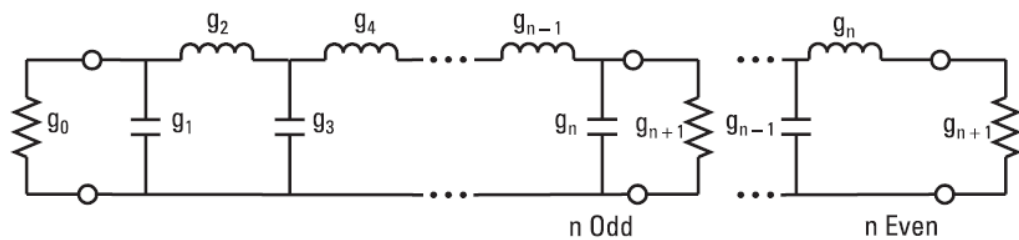
Figure 1 Lowpass filter prototype

2. At Higher Frequencies

- **Dielectric Filters**

Dieletric filters (DFs) are suitable for bandpass filtering. Against the two-dimensional plane (2D), three dimensional (3D) of the device is also classified as a DR filter. In the category of 3D devices, designers selected firstly metallic empty cavities or waveguides to meet their requirements for very narrow bandwidth filtering. But after 1980s, the high dielectric constant material with low loss and good thermal stability, have become available. DF solution has been adopted for many applications, especially the spatial uses. This technique permits us to eliminate the size of the cavity and waveguide devices and increase their performances. In the cases of DF as compared to cavity, some values of average ratios can be given for dual-mode resonators :

1 : 4 in volume

1 : 2 in mass

Furthermore, DF structure with excited mode can be selected to provide a specific response required. DFs are typically used on the number of devices, especially in the microwave filters using various topologies according to their functions. The main

functions can be done by treating extremely narrow bandwidth filtering and power signals [12-14].

- **Microstrip Line Filters**

Figure 2 shows the cross section of strip transmission line and microstrip on printed PCB. For stripline the mode of propagation is essentially TEM because of the conducting plate is bounded by the same dielectric material. Namely that $\varepsilon_e = \varepsilon_r$, the dielectric constant of the medium. For microstrip line, the propagation mode consists of TE and TM modes since the upper dielectric of a micostrip line is usually air while the bottom dielectric is PCB dielectric. For TEM mode, the electromagnetic phase velocities in air and the PCB are different, due to non-matching at the air-dielectric boundary. However quasi-TEM may be applied at frequency of 6GHz or lower where the axial H and E fields are small enough . For microstrip line the effective dielectric constant ε_e limits between unity and ε_r. In situations of low frequencies , the electromagnetic field is mostly distributed in the air, while at larger frequencies, the electromagnetic field concentrates on PCB dielectric. So, the microstrip line is dispersive [1,6,8]. **Figure 3** shows the effective regions of dielectric constant of microstrip and strip line.
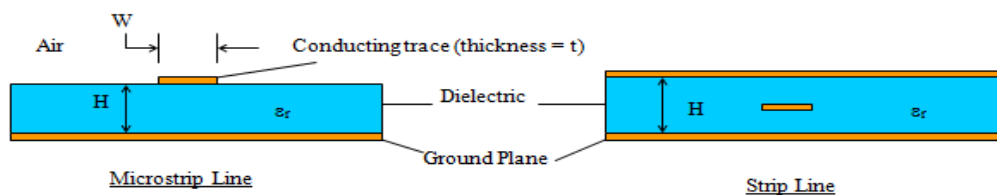
Figure 2 Cross section view of microstrip and strip transmission line as implemented on a printed circuit board
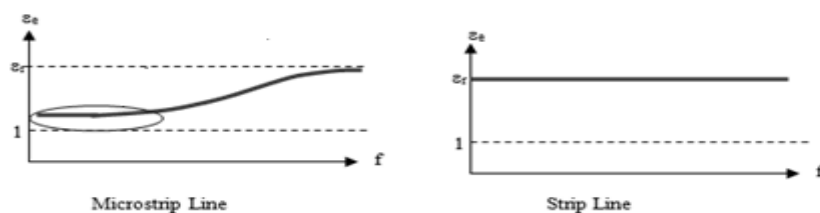
Figure 3 Effective dielectric constant of microstrip and stripline

- **Coplanar Waveguide (CPW) Filters**

Coplanar waveguide is a kind of electrical transmission line which can be produced using printed circuit board technique, and is used to transmit microwave-frequency signals. On a smaller scale, coplanar waveguide transmission lines are also constructed into monolithic microwave integrated circuits. Conventional coplanar waveguide as depicted in **Figure 4** has one conducting track printed onto a dielectric substrate, together with dual return conductors, one to either side of the track. All previous conductors are on the same side of the substrate, and hence are coplanar. The return conductors are separated from the middle track by a small gap, which has an unvarying width along the length of the line. Away from the cental conductor, the return conductors typically enlarge to an indefinite but large distance, so that each is notionally a semi-infinite plane.
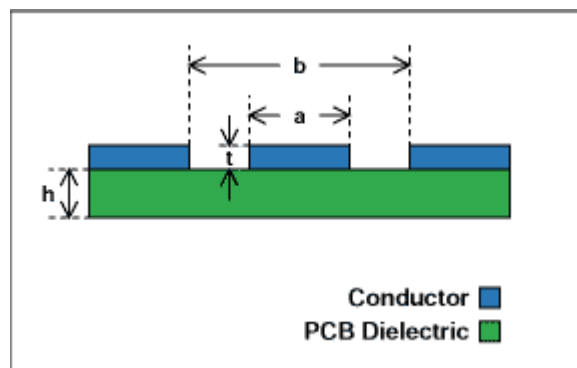
Figure 4 Conventional coplanar waveguide (CPW)

CPW structure is very useful to alter the microstrip planar filter designs because of its independency to the thickness of substrate. Different contributions on parallel-coupled CPW bandpass filters (BPFs) are reported as in [15-17]. The filters with excellent selectivity and high performance interference rejection levels are still desired in modern communication applications. Relatively, the four-pole filter with dual transmission zeros was indicated in [18]. In [19], the quasi-elliptic CPW BPFs based on capacitive cross-coupling effect and stepped-impedance resonators (SIR) were suggested to implement compact size and satisfactory selectivity. As well as transmission zeros, an enhancement of the stopband rejection is also necessary. Until now, the achieved CPW BPFs to exclude the spurious responses are still limited [20-

21]. A specific pattern of double-surface CPW filter using via holes was used to reduce the spurious responses.

Another four-pole BPF was presented in [21] using dual asymmetric parallel-coupled CPW stages at the input/output terminal to produce two transmission zeros for excluding the harmonic passband around triple of the center frequency (3 f_0). However, at the same time, the CPW structures with miniaturized size, good selectivity, and good stopband rejection are difficult to be realized.

- **Waveguide Filter**

A waveguide filter is an electronic device in which its internal metal tubes are with hollow so that an electromagnetic wave may be sent. Waveguide filters are essential elements in communication and electronic engineering designs and have diverse applications. These include limitation of noise and selection of signals. Waveguide filters are often applied in the microwave frequencies band when they have adequate size and low loss. Microwave filters are used widely in broadcasting, satellite communications, and telephone networks. There are many types of waveguide filter. The most widespread consists of several coupled resonant cavities. However within this class of waveguide filter, there are huge number of subtypes, primarily differentiated by coupling means. These coupling types include irises, posts and apertures. Other types of waveguide filters classified to stub filters, dielectric resonator filters, insert filters, and corrugated-waveguide filters. Several waveguide designs have applied filter basics but their application is something other than to filter signals. For examples, directional couplers, diplexers and impedance matching components. These designs frequently may take on the form of a filter, or at least in part.

The common manufacturing principle of substandard waveguide in mostly used simple term is the hollow metal type as shown **Figure 5**, but other waveguide technologies are possible [22]. The wave is mostly embraced by conducting material. There is possibility to build waveguides out of dielectric rods ,[23] the most well known sample being optical fibres.

High performance narrow-band microwave waveguide bandpass filters are largely favourite for the next generation of modern wireless communication systems. To satisfy this purpose, there is big interest in the compact microstrip filters because of their ease of fabrication, low loss, miniaturized size and low weight [22,23].
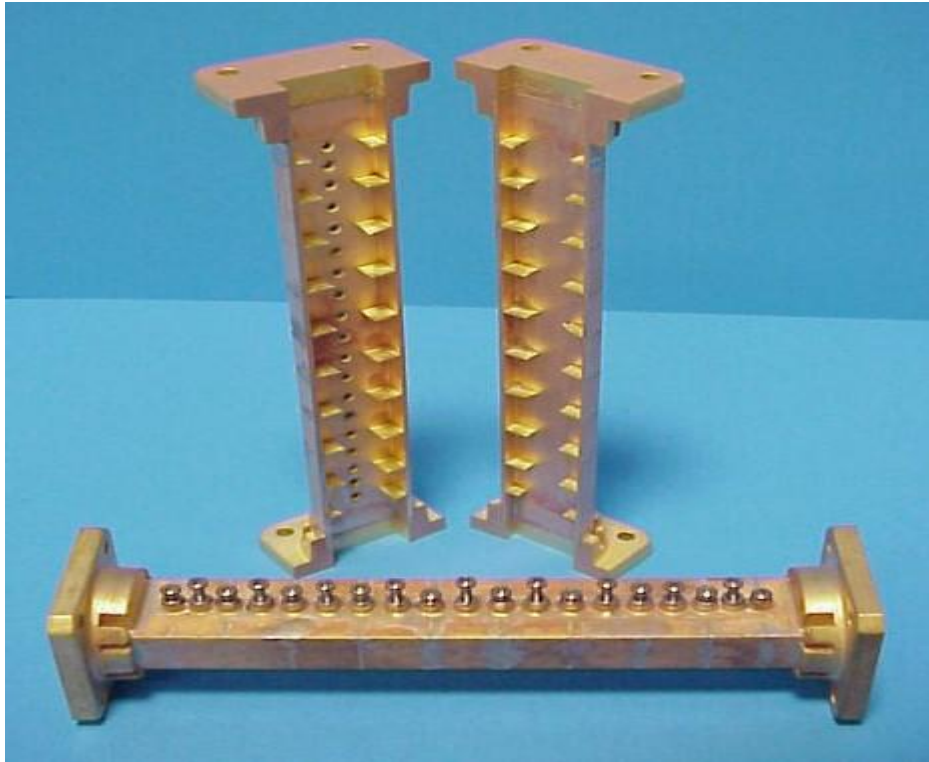
Figure 5 Waveguide filters

1.2 Some Miniaturization Techniques of Microstrip BPF and BSF

1.2.1 Using high dielectric constant substrate

It is most intuitive miniaturization method related to the choice of dielectric substrates with high ε_r. Indeed, this produces a reduction of the wave propagation velocity on the transmission line and the consequent reduction of the wavelength for a given frequency. However, in order to be used as substrate for thin films, a dielectric material has to satisfy very stringent requirements, such that, presently, only $LaAlO_3$ and MgO are really used in the filter design. It is clear that $LaAlO_3$ offers the best miniaturization perspectives but, in many practical applications, its low ε_r uniformity makes more reliable the use of MgO [24].

1.2.2 Use of slow wave transmission line

Slow wave resonators are generally realized by loading basic transmission lines by a large number of planar inductances and/or capacitances, with very small dimensions. In this way, periodic structures are obtained, where the wave propagation constant is strictly dependent on the frequency (high dispersion). Usually, they present also an increasing spacing between harmonics with an improved out-of-band rejection for the filter response. A typical slow wave resonator is reported in **Figure 6**. In this case, the inner region of a basic $\lambda_g/2$ resonator is removed and loaded by a series of capacitive fingers, which increase the equivalent capacitance C. The consequent reduction of the wave velocity (v_T) is strictly dependent on the number and dimensions of the fingers. By this technique, a resonant frequency reduction between 20-30% can be obtained, even if the smaller dimensions of the loading elements (in some cases around few tens of microns) can make the design particularly sensitive to the photolithography process quality [24].
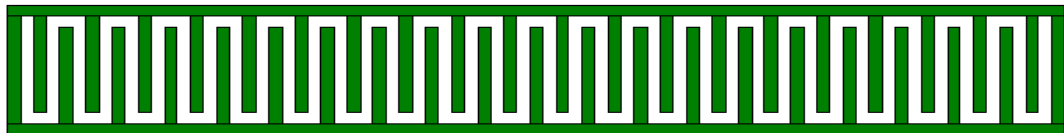
Figure 6 Slow wave resonator loaded by capacitive fingers

1.2.3 Use of microstrip lumped element circuit

As far as the microstrip lumped elements are concerned, they can be considered as the result of an extreme application of the meandering technique. In these structures, similarly to what happens in a LC couple, the resonator parts, where the magnetic field is stored, are separated from the parts where the electric field is stored. A typical example, where the inductive and the capacitive regions are evidenced, is shown in **Figure 7**.

The use of quasi lumped elements leads to a significant size reduction of a filter and is very interesting above all for applications in UHF range (lower than 1GHz). However, due to the presence of extremely miniaturized sections, the reduction of

the quality factor can be significant, with values in some cases lower than 10^4 [25-29].
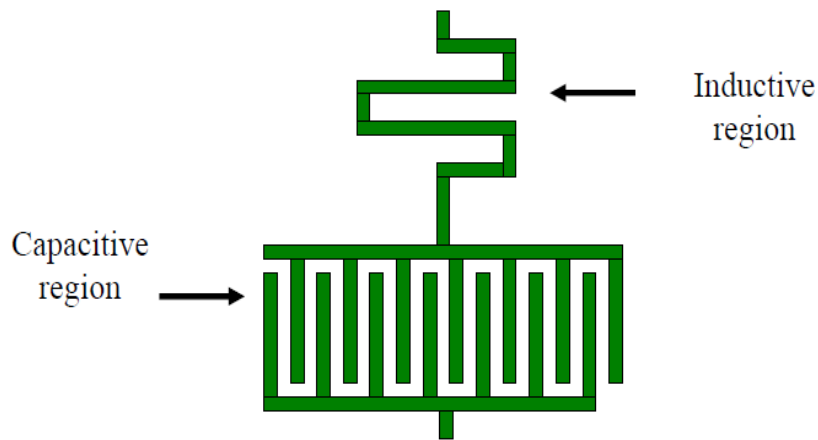
Figure 7 A microstrip lumped element

1.2.4 High temperature superconductivity (HTS) microstrip filter technique

High-Temperature Superconductivity (HTS) thin films possesses very lower surface resistance (Rs) as compared with normal metals. HTS is most modern filter technology that affects continuously on the design of electronic systems ,communication systems, medical instrumentation, and military microwave systems. Because HTS uses thin film, it is the best solution for compact HTS filter devices. Consequently, by HTS Filters, narrow band responses in the available RF frequency spectra and compact devices using different transmission-line structures have been adopted and characterized. Because of high power dissipation of these types of filter, an efficient cooling is needed. Thin film technology was available mainly due to the advancement in semiconductor industry especially in the fields of wireless communication [1, 30-32].

1.2.5 Low temperature cofired ceramic (LTCC) filters technique

Low temperature cofired ceramic LTCC is one of the most sufficient ways for miniaturizing and packaging technologies, as LTCC can bundle both passive and active components into a single module to meet the system-in-a-package (SiP)

requirement. These circuits may become wire bonded to ceramic-based hybrids. This technology can reduce discontinuities and air gaps present in conventional stripline assemblies, which will improve the output responses of these circuits. All of these advantages can effectively reduce the cost, size, mechanical complexity and weight for stripline devices [1, 33].

1.2.6 Dual and multi mode filters technique:

Up to date, dual-mode microstrip filters have remarkable properties, because of their high selectivity characteristics. They can be used as a double tuned circuit, therefore, a desired n order is equivalent to its half order of minaturized filter. Namely, each element is two pole filter in single structure. Dual mode microstrip filters can consist of one or more dual mode microstrip line resonator in form of square patch, triangle, ring, disk or whatever [1,24,34].

However, triple mode filter is more miniaturized than dual mode filter, because each resonator represents three poles in single structure as compared with dual mode structure[24,35]. Different orders of multimode resonator filters represent the number of poles for these components which can be accomplished by applying the SIR elements in circuit configuration [36-39].

Another way to reduce dual-mode resonators is to use (cross slotted patch), miniaturized by the application of surface cuts which, increase the current path length, produce a decrease in the resonance frequency without changing the external dimensions [36].

1.2.7 Fractal microstrip filters

Mandelbrot defined Fractals as in [40] as method of classifying structures whose dimensions were not integers. These curves have been adopted previously to specify unique natural phenomena that where difficult to define with Euclidean geometries, as in the density of clouds, length of coastline and branched trees. The term fractal is basically taken from the Latin word fractus, which indicates irregular or broken fragments. Therefore, there is need for a geometry that handles these complex shapes

better than Euclidean geometry, where the Euclidean geometry have a whole number of dimensions as in a one dimensional line and two dimensional planes [40].

In antennas, filters and other microwave circuit designs, the use of fractal shapes makes the operational frequency of component which depends on the ratio of the electromagnetic signal's wavelength to the physical size of the component independent of its scale. This means that a fractal device structure can be constructed in small sizes, yet possessing a broad frequency range. The reasons for using fractal antennas and filters appears are firstly because of self-similarity especially for antennas (which means number of copies of itself can be appeared at several scales) to operate in same way at several wavelengths. Secondly, because by using space-filling properties of some fractal shapes, many microwave and RF microstrip devices can be folded and packaged in smallest areas [40].

Research results explained that, because of increase of the total length of microstrip line on a given substrate, using fractal curves may decrease resonant frequency of microstrip resonators, and gives narrow band responses[41-42].

1.3 Thesis Objectives

The aim of this thesis is to present compact microstrip bandpass filter designs based on Sierpinski, Moore, Hilbert and Hilbert-zz fractal geometries as well as microstrip narrow bandstop filter using Hilbert fractal resonators suitable for use in various wireless mobile applications. The proposed filter designs have been modeled, simulated and evaluated using reliable AWR2009 and Sonnet EM software packages.

1.4 Thesis Outline

This Ph.D dissertation is arranged as follows:
- Chapter two includes the fundamental principles of fractal geometry and applications.
- Chapter three provides basics and parameters of the bandpass and bandstop filters.

- Chapter four shows the design and simulated results of proposed fractal bandpass filters.

- Chapter five presents the design and the simulation results of proposed wide bandpass filter and narrow bandstop filter based on Hilbert fractal geometry.

- Chapter six includes the conclusions and suggestions for future work.

CHAPTER 2

FRACTAL GEOMETRY CONCEPTS AND APPLICATIONS

2.1 Introduction

The mathematician scientist, Benoit Mandelbrot defined and expanded Fractals as in [40] as method of assorting structures whose dimensions were not complete number. These curves have been harnessed previously to clarify some natural phenomena that are hardly defined with Euclidean geometries, as in the density of clouds, blood vessels, and branched trees .The term fractal is basically quoted from the Latin word fractus, which means broken parts or fragments. Therefore, there is serious reqiurement for a geometry that handles these complex shapes better than Euclidean geometry, where the Euclidean geometry have one dimensional line, or two dimensional planes...etc as in dots, squares and cubes [40].

2.2 Types of Fractals

Generally, fractals can be divided into two types, natural (random) and mathematical (deterministic). Natural fractals are all those that are available in nature - clouds, mountains, trees, leaves, valleys, the human respiratory system. Mathematical fractals are fractals developed using mathematical formulas and the concepts of iteration, recursion etc. Widely known mathematical fractals are Mandelbrot set, Julia set, Van Koch curve, Sierpinski triangle etc [40, 43]. **Figures 8-15** show some examples of fractals that they can seen from nature or from Mandelbrot set.

Figure 8 Oak Tree – a natural fractal object
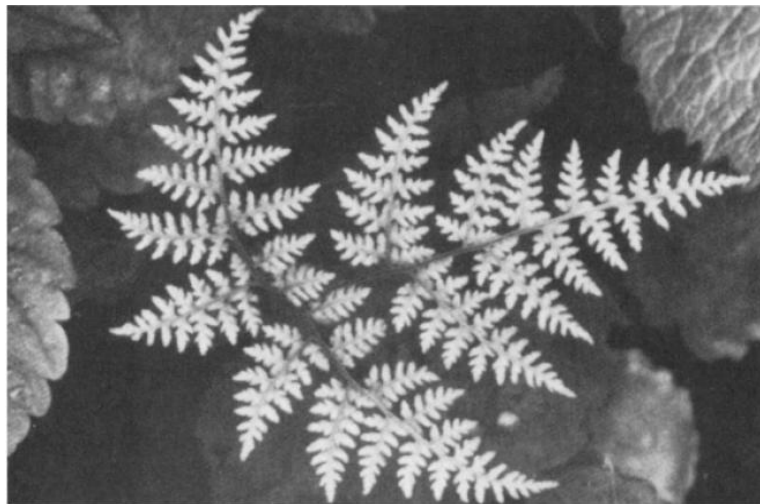
Figure 9 Fern leaf- a natural fractal object
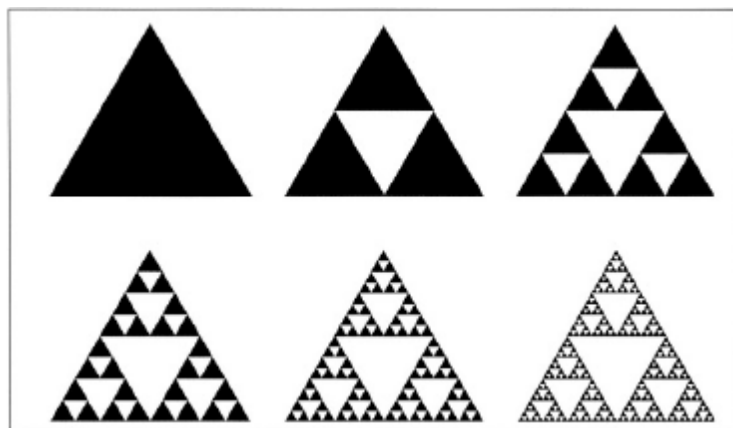
Figure 10 Sierpinski Triange - a mathematical fractal object
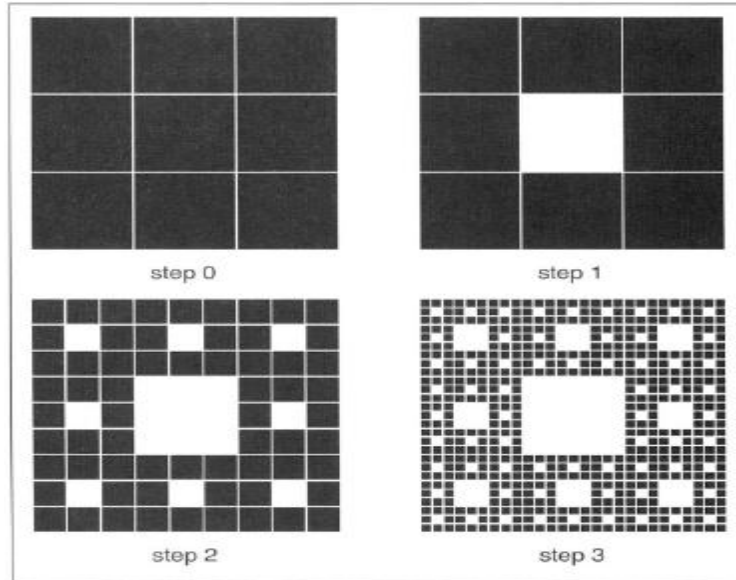
Figure 11 Sierpinski Carpet- a mathematical fractal object
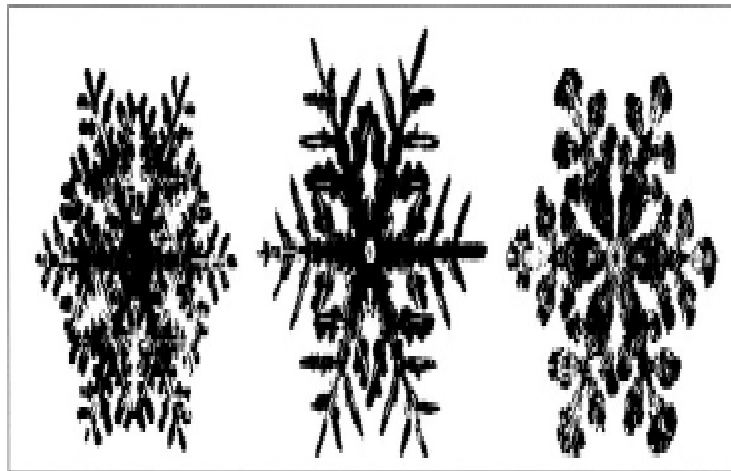
Figure 12 Natural flakes
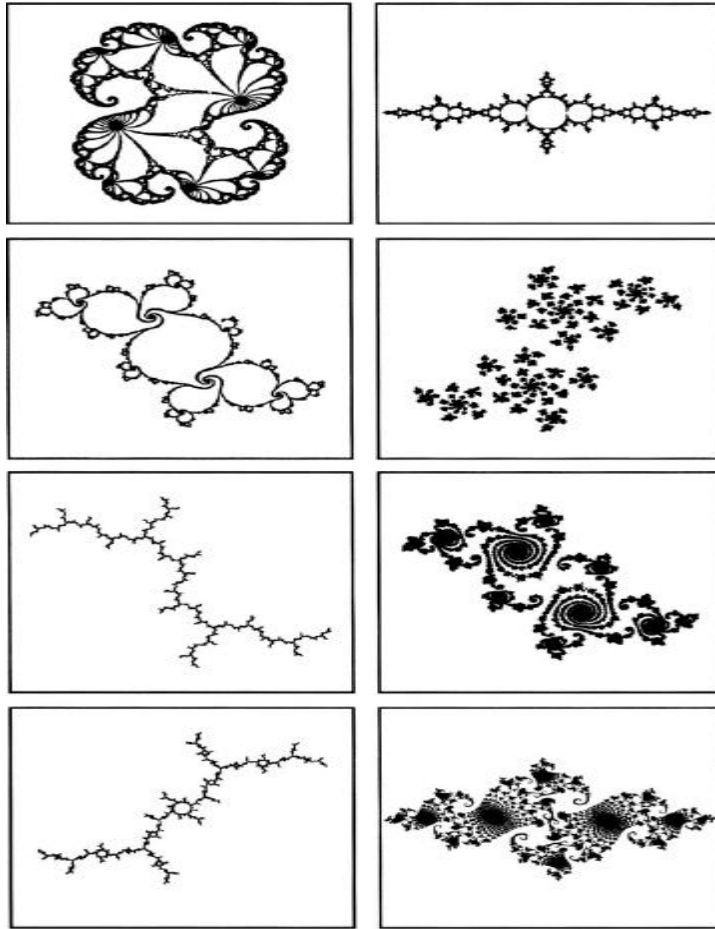
Figure 13 Julia set
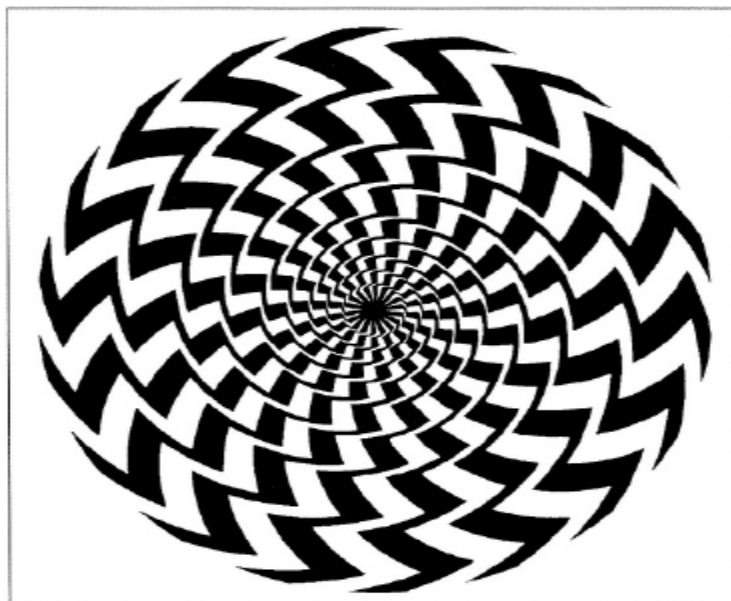
Figure 14 Spiral or not, visual illusion

Figure 15 Fractal forgery

2.3 Fractal Concepts and Euclidian geometry

Firstly, fractals are a decidedly modern invention. Although possessed of turn- of-the- century ancestors, they have been well-known as main contributed scientists only over the last ten years. Fractal shapes are called to be self-similar and independent of scale or scaling. Secondly, Euclidean geometry supplies concise exact definitions of man-made objects but is inappropriate for natural shapes. It yields cumbersome and inaccurate descriptions. Machine shops are essentially Euclidean factories: objects easily described are easily built. Fractals, on the other hand, submit a superior characterization of many natural structures and have already given computer imagery a natural flavor. Euclidean shapes are typically explained by a simple algebraic formula, fractals are generally the results of recursive algorithms which can be made by computer programs [40, 43, 44].

Euclidian	Fractal Geometry
(1) Traditional (>2000 years)	(1) Modern
(2) Based on characteristic size or scale	(2) No specific size or scaling
(3) Suits human made objects.	(3) Appropriate for natural shapes
(4) Described by formula.	(4) Recursive algorithm

Table 1 Comparasion Between Euclidian and Fractal Geometry

2.4 Properties of Fractal

Fractals are a modern group of geometrical objects that have three main properties: self similarity, space filling and fractal dimensions.

The first property is the self-similarity property. A self similar object is one which can be split into any number of similar parts. An essential characteristic of fractals that differentiates them from the more Euclidean shapes is the characteristic that magnified subsets look like the whole and to each other. [40]. The second property is the space filling property; the possibility of these fractal curves to pack longer geometries in to smallest areas. This property is considered as best candidate instead of the Euclidean geometries to design a very small size filter compared with the design wavelength. The last property is the fractal dimensions; this requirement recognizes fractals from the Euclidean geometries, which own integer dimensions. The basic idea of dimension is represented as topological dimension. A point, a line

segment, a square and a cube, as shown in **Figure 16** have integer dimensions zero, one, two and three, respectively.
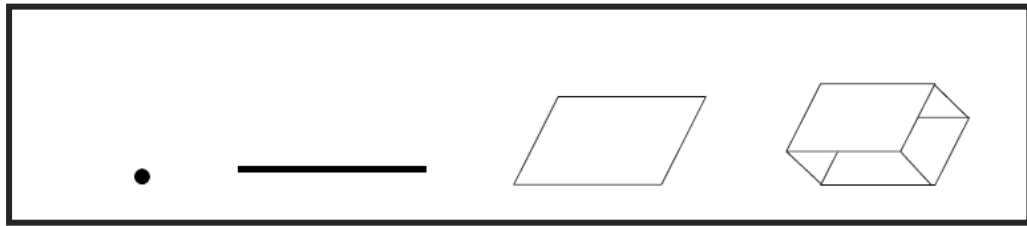
Figure 16 Euclidean geometries

The concept of self similarity is closely associated dimension concept.

$$D = \log N / \log (1/r) \tag{2.1}$$

where N is the total number of distinct copies, and $(1/r)$ is the reduction factor value which means how will the length be of the new side with respect to the original side length.

An object usually described as one-dimensional, for example, a line segment, also possesses same scaling property. It can be split into N similar portions each of which is scaled down by the ratio r=1/N of the whole. Similarly a two-dimension object such as a square area in the plane, can be split into N self-similar parts each of which is constricted by a ratio $r = 1/N^{1/2}$.

A three-dimensional object as in a solid cube may be divided into N small cubes each of which is scaled down by a ratio $r = 1/ N^{1/3}$. A D-dimensional self-similar object can be divided into N smaller replcas of itself each of which is dimensionally reduced by a factor r where $r = 1/N^{1/D}$ or $N=1/r^{D}$.

The fractal dimension as compared with Euclidean dimension does not need to be an integer. Clouds have a fractional dimension of approximately 3.3 as shown in **Figure 17** . Van Koch curve, a mathematical fractal, has a dimension of 1.26 as shown in **Figure 18** [40,43].

Figure 17 Fractal cloud
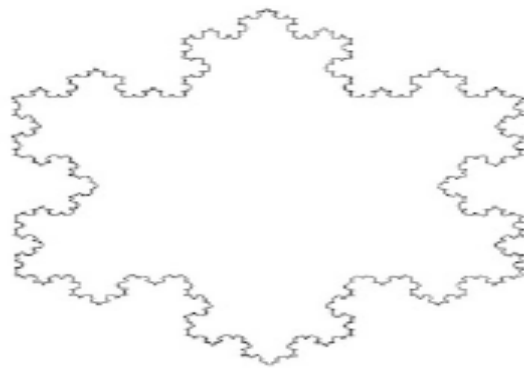
Figure 18 Van Koch snowflake

2.5 Some Types of Deterministic Fractal Geometry

2.5.1 Cantor set

Cantor fractal, or cantor set, shown in **Figure 19** is a simple example of a fractal geometry. A common construction is the middle third Cantor set generated by iterative process. This can be said the most simple fractals and a good place to discuss the nature of fractal geometries. The Cantor set has unlimited set of hidden line segments in the unit interval. The best method to understand the generation process of Cantor set fractal is its construction illustration. This is given in **Figure 19** for the simplest form of Cantor set, namely the triadic Cantor set. The set is constructed by process of middle third removal of the unit line segment as in stage 1 in the figure. From the dual remaining line segments, each one third in length, the

middle thirds are again deleted as in stage 2 in the figure and so on. This fractal also called as a Cantor discontinuum or Cantor dust [40, 43].

Stage 0 (*n*=0)

Stage 1 (*n*=1)

Stage 2 (*n*=2)

Stage 3 (*n*=3)
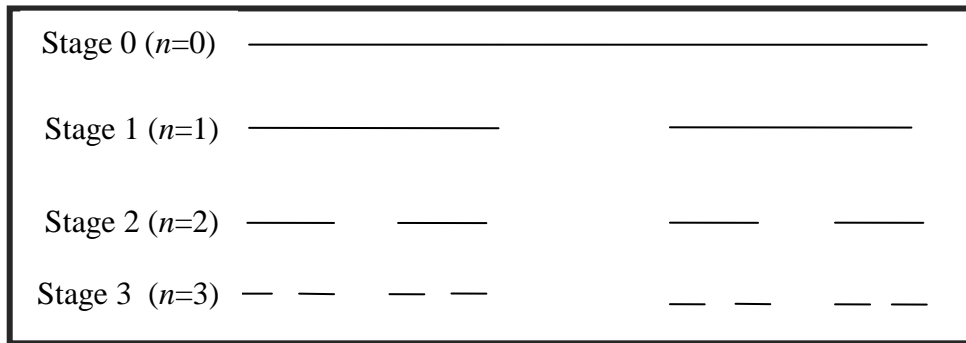
Figure 19 The first four stages in the construction of the Cantor set

2.5.2 Koch curve

The construction method of the Koch curve is shown in **Figure 20**. As same as Cantor set, the Koch curve is easily built using an iterative algorithm started with line segment initiator as in *n* = 0 in the figure . The initiator is divided into thirds, and the middle third deleted. Then, the middle third is replaced with dual identical segments, both one-third in length, which produce an equilateral triangle as in *n*= 1; this step represents Koch curve generator. Similarly, the middle third is deleted from each of the four segments as in *n*= 2 and each is replaced with dual similar segments as before and so on for *n*= 3 and 4 .An obvious property of the Koch curve is it is like infinite in length. This can be distinguished from the generation process. At each generation step *n*, the length of the fractal curve raised as $L_{n-1}^{\frac{4}{3}}$, where L_{n-1} is the previous step length of the curve in. As generations step increases, the length of the curve also increases [44].

2.5.3 Sierpinski gasket

The generation procedure of the Sierpinski gasket is shown in **Figure 21**. The initiator here is a solid triangle in this figure. The middle triangular portion is cut from triangle initiator. By the same way, the middle triangular portions are deleted from the remaining triangular elements as in *n* = 2 and so on for *n* = 3,4 and 5 . Each

fractal iteration in this generation consists of three smaller copies of the previous stage, each copy dimensionalized by scaling factor of one half [40, 44-45].

2.5.4 Sierpinski carpet

The Sierpinski carpet, **Figure 22**, is a mathematical fractal which can be considered as two dimensional geometry [44,46]. The Sierpinski carpet is constructed analogously to the Sierpinski gasket, but it use squares instead of triangular. To generate this fractal curve, it must start with a filled square in the plane, and then divided it into nine smaller identical squares where the central square is removed. The remaining squares are split into nine smaller similar squares which each central are removed [44]. This process can be continued to infinite.
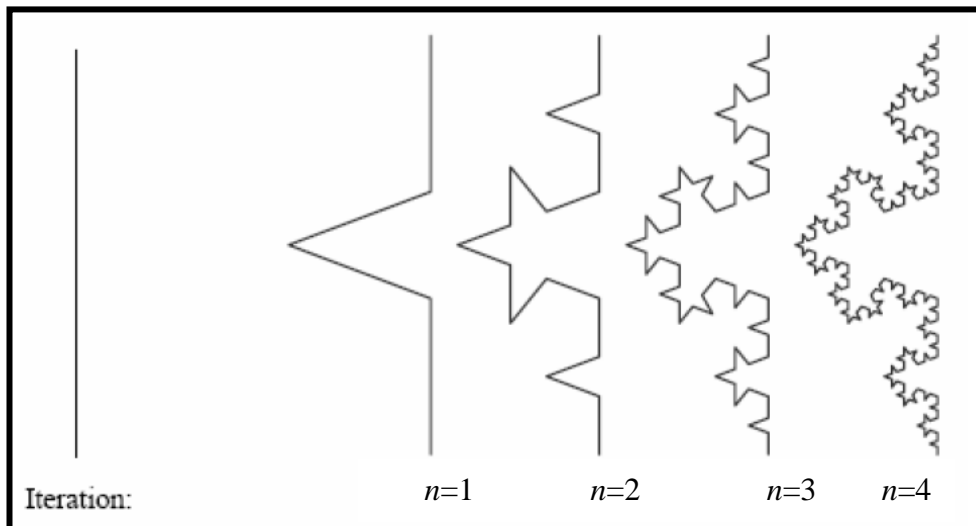
Figure 20 The first four stages in the construction of the Koch curve
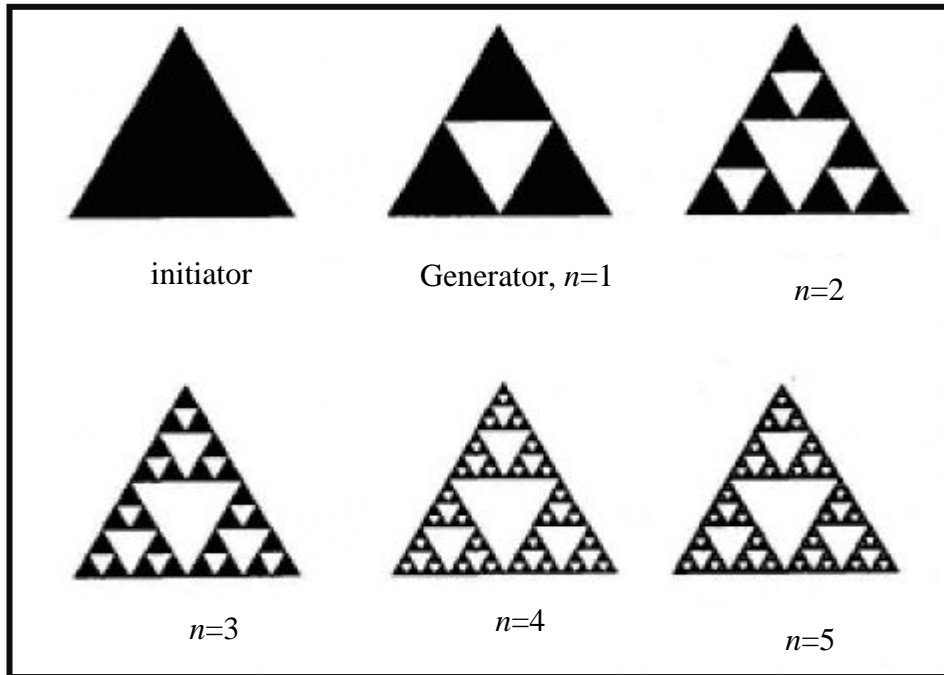
Figure 21 The first five stages in the construction of the Sierpinski gasket
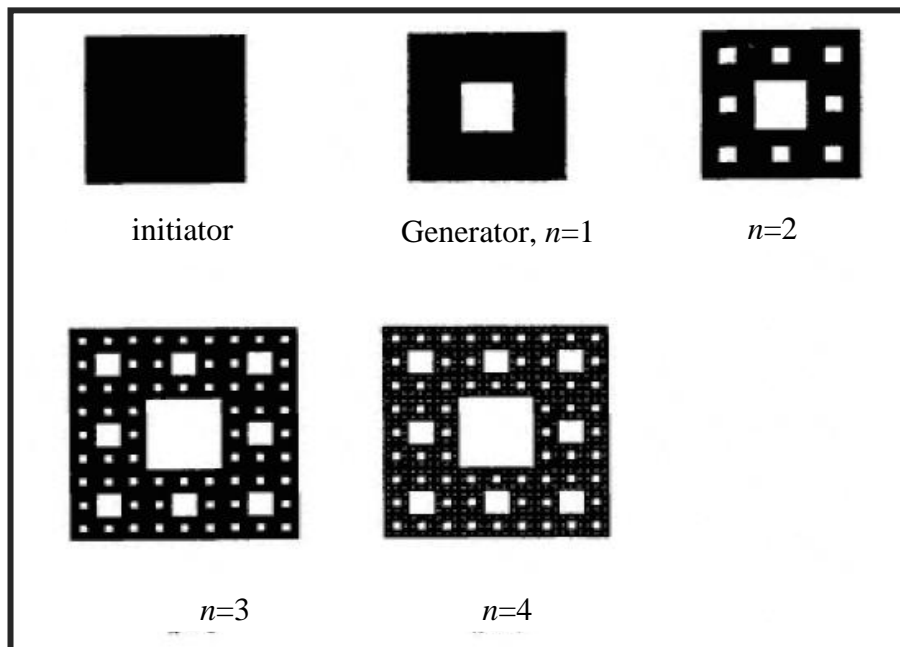
Figure 22 The first four stages in the construction of the Sierpinski carpet

2.5.5   T- Fractal geometry

It is also called Koch Minkowiski; the initiator of this fractal geometry is a Euclidean square as in **Figure 23**. Each of the four straight line segments of the starting shape is replaced with the generator, as shown in **Figure 23** below. The generating steps can be continued to infinite number of iterations. The final fractal structure is a geometry with unlimited complex underlying structure which cannot be differentiable at any point [24,47].
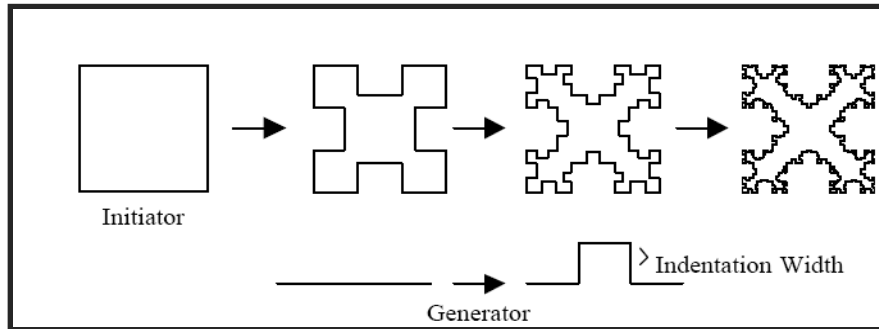
Figure 23 The iterative generation procedure of a T- fractal geometry

2.5.6   Hilbert fractal geometry

Hilbert fractal geometry is well-known as the space-filling curves (SFCs). The geometry of this fractal can be constructed from a long metallic strip compacted within a microstrip patch as in **Figure 24**. As the fractal iteration increases, this geometry can space-fill the patch. Hilbert fractal geometries have been used in wide variety of miniaturized antenna designs as compared to filter designs[24,41,48].
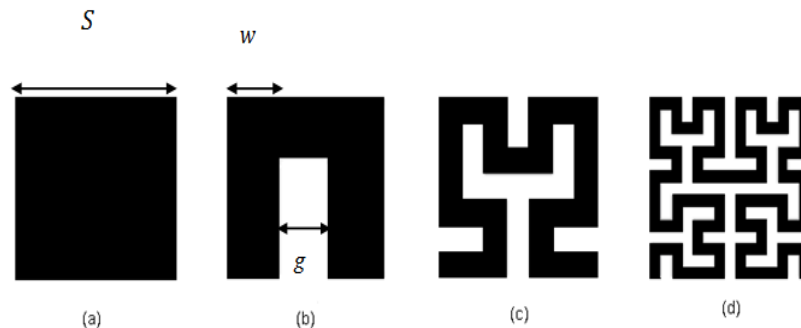
Figure 24 Hilbert fractal iterations (a)Original ,0th iteration (b) 1st iteration(c) 2nd iteration (d) 3rd iteration

The fractal curve can be suitable in a square section of S as external side. In accordance with Hilbert fractal resonators with side length S and iteration k, the total sum of conducting line segments $L(k)$ can be calculated by [24]:

$$L(k) = (2^k + 1)S \qquad (2.2)$$

The general aim in designing antennas and filters by using Hilbert fractal geometry is to increase SFC fractal iteration as far as possible so as to match the resonator in more miniaturized area. However, it has been concluded that, there is an obvious inversely proportional relationship for this type of SFCs between compactness level and quality factor of the resonator. The strip width w and the gap between the strips g are important factors which relatively define this relation [24]. The external side S are connected with w, g and iteration level k ($k \geq 2$) by:

$$S = 2^k(w + g) - g \qquad (2.3)$$

2.5.7 Peano fractal geometry

Peano fractal geometry was proposed by Peano in 1890 as space-filling curve [49]. The most amazing property of the Peano-curve algorithm is its larger packaging or folding rate than the Hilbert fractal generation procedure in filling a 2-D region, which expects that the Peano resonator may have lower resonant frequency as compared with Hilbert resonator of the same iteration order k. The Peano fractal curve, as in **Figure 25**, fits in a square section of S as external side. The total strip length $L(k)$ of Peano fractal geometry can be calculated by [50,51]:

$$L(k) = (3^k + 1)S \qquad (2.4)$$

On the other hand, the side length S of Peano microstrip resonator can be determined from the values of strip width w and gap between the strips g within iteration level k ($k \geq 2$) by [50,51]:

$$S = 3^k(w + g) - g \qquad (2.5)$$

The fractal dimension gives details about space filling processing and a prominent irregularities measure when viewed at very small scales. A dimension contains

much   information about the geometrical properties of a fractal like self similarity and compression levels [24,50,51].
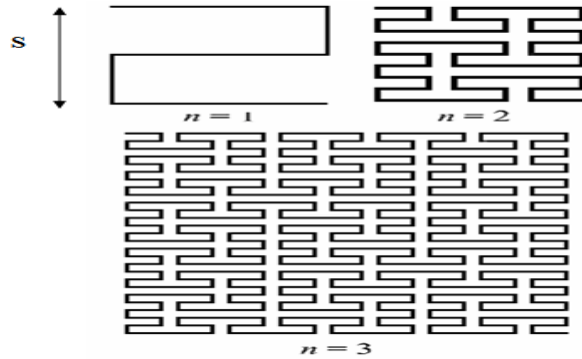
Figure 25 The first three iteration levels of Peano fractal curve generation process

2.8.5 Moore fractal geometry

First of all, the Moore fractal geometry is a closed curve as compared to   Hilbert fractal geometry as stated in **Figure 26**. It can be drawn by connecting some copies of the Hilbert curves placed end to end by using suitable orientations [52]. The 2nd ,3rd , and 4th iterations of Moore space-filling curves have been shown in **Figure 26** (b) .
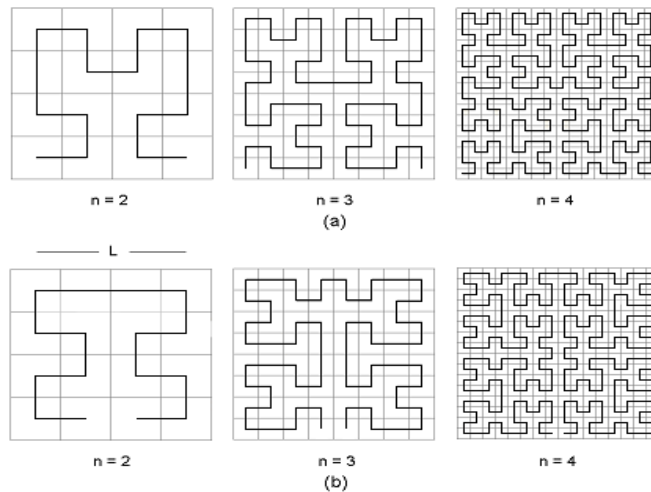
Figure 26 The 2nd iteration, $n = 2$, the 3rd iteration, $n = 3$, and the 4th iteration, $n = 4$, for (a). Hilbert and (b). Moore fractal curves [52]

For a Moore fractal resonators constructed from conducting trace with a side length L and iteration n, the length of each line segment d_n is given by:

$$d_n = \frac{L}{2^n - 1} \qquad (2.6)$$

Because of Moore geometry is a closed as compared to Hilbert geometry of the same iteration, the all line segments forming the perimeter of Moore fractal geometry equals to that of Hilbert plus one, where the all line segments for the Hilbert space filling curve can be evaluated by [24]:

$$S_n = (2^n + 1)L \qquad (2.7)$$

So, the corresponding perimeter of Moore fractal curve of the same iteration level, n, order will be [8]:

$$S_n = ((2^n + 1) + \frac{1}{2^n - 1})L \qquad (2.8)$$

By strip width w, and the spacing between strips g, the side length of Moore resonator can be given as [24,52] :

$$L_n = 2^n(w + g) - g \qquad (2.9)$$

2.6 Applications of Fractal Geometries in Science and Engineering

2.6.1 1/f Noise and fractals in DNA base sequence

Standard special density measurement techniques are applied in a new manner to single base positions in DNA sequences. Measurements verified the ubiquitous low-frequency noise and long 1/fb fractal association in addition to outstanding short-range periodicity. The classification of data bank on behalf of large banks (primates, invertebrates, plants, etc.) display system average spectral index changes and evolution categories [53,54].

2.6.2 Fractal geometry of music

A parallelism of the fractal geometry of natural landscape and that of music suggests that music can be investigated through a visual representation of acoustic signals. The parallelism inspires us to make musical abstracts by scaling the original down to half, quarter or eight of its original length. An algorithm for this has been devised. The self-similarity of Bach's music has been demonstrated by this analysis. Bird songs, nursery rhymes and classical music are distinguished by their diatomic scale. Bird songs and nursery rhymes are not well structured successions of tones, dominated by unison or seconds (i = 0,1,2….). A proper combination of selected songs can however, include enough variety to achieve fractal geometry. The progress to baroque and classical composers is manifested by the approximation to fractal geometry in Bach's and Mozart's music, simulating the harmony of nature. This is absent in modern music [55, 56].

2.6.3 On the synthesis and processing of images and fractal signals

Some techniques are available for generating random images and fractal signals. The methods are basically obtained from a Fourier based description of a random scaling fractal and are therefore able to utilize a Fast Fourier Transform. This provides the potential for constructing a real time facility by implementing the available DSP hardware, the principle intention for developing the techniques [44].

2.6.4 Positive wavelet representation of fractal signals and images

With appropriate choice of an analyzing positive pulse wavelet, information concerning the structure of a signal is concentrated economically in the local maxima and minima of the function of two variables, position and scale given by the wavelet transformation. This information is extracted by process of co-relation detection, in which the analyzing wavelet is regarded as a multiple-scale matched filter. Identification of local extrema corresponds to the detection of signal wavelets [44].

2.6.5   Application in geological site characterization

Fractal geometry can be applied to a problem of practical significance in geo-sciences that of generating a rock transmissivity field with realistic detail over a range of length scales from a relatively small number of measured values [57].

2.6.6   Image compression

Fractal techniques (Affine transformation and the concept of attractors) can be employed to achieve phenomenal compression of images of natural scenery [44].

2.6.7 Microwave circuit applications

Recent developments in wireless communication systems have introduced new challenges to design and produce very good compact components. These challenges encourge microwave circuit designers and filter designers to find key solutions by adopting different types of fractal geometries [24, 41-42, 58].

By self-similarity property of fractal structures , multi-band fractal antennas, such as Sierpinski carpet and Sierpinski gasket antennas have been successfully applied, while the space-filling charcterisics can be used to minimize antenna and filter size. Fractal geometries have unique space-filling properties. Research results explained that, because of increase of total length of the microstrip line fractal resonators, the use of fractal curves can decrease resonant frequency and offers narrow resonant peaks [42,58].

Fractals are going toward a new generation of compact RF and microwave passive networks for wireless devices. Any wireless system depends on an RF front-end which includes antennas, filters and diplexers, along with other passive elements such as capacitors, inductors and resistors. There is no problem whether the system is as influential as a cellular base-station, as sensitive as a super conducting satellite receiver or as small as a system-on-chip wireless device, the compactness and integration of such a front-end becomes always a key issue in terms of performance, robustness, packaging and cost.Fractal technology has been already applied in the miniaturization of another essential part of the wireless front-end. Compact fractal

antennas for handsets, PDAs, cellular base-stations and high-speed data applications have been used in every small corner of the wireless world. The size compression and multiband qualifications of fractals allow well-organized, broadband and multipurpose devices to be packed in places that were at length unreachable due to size, weight, or appearance constraints. Based on an analogous principle to filter and antenna miniaturization capabilities, fractal technology has been recently proven to become the most efficient way in packaging RF and microwave networks as well [59,60].

2.7 Literature Survey of Fractal Microwave Filters

Among the earliest use of fractals in the design and manufacturing filters is Yordanov *et. al*, [61].

In 1999, Yordanov, *et. al* , [61] had designed and prospected Cantor fractal filter as shown in **Figure 27** below. The transmission and reflection properties had been studied from multilayered slab made from two kinds of dielectrics. The relative permittivity between them is assumed to be a complex number. The pattern of the slab follows the Nth of the Cantor fractal set construction. In order to consider easy for fabrication slabs, the values of N are restricted to 3,4 or, maximum, 5.
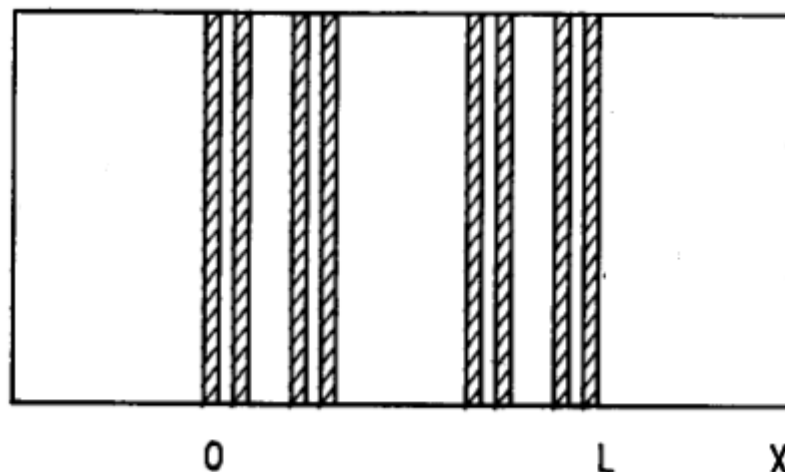
Figure 27 Example of Cantor fractal media

In 2004, Barra, [24] had designed and fabricated highly miniaturized superconducting filters, using resonators based on fractal layouts. His attention has been focused on Hilbert and Koch-Minkowiski space filling curves as shown in

Figure 28. He explored the miniaturization levels achievable by these resonators, emphasizing the parameters which allow obtaining a good trade-off between compact size and losses. Several prototype four pole filters, with Chebychev and quasi elliptic responses, have been designed and fabricated. The main experimental measurements are reported as well.
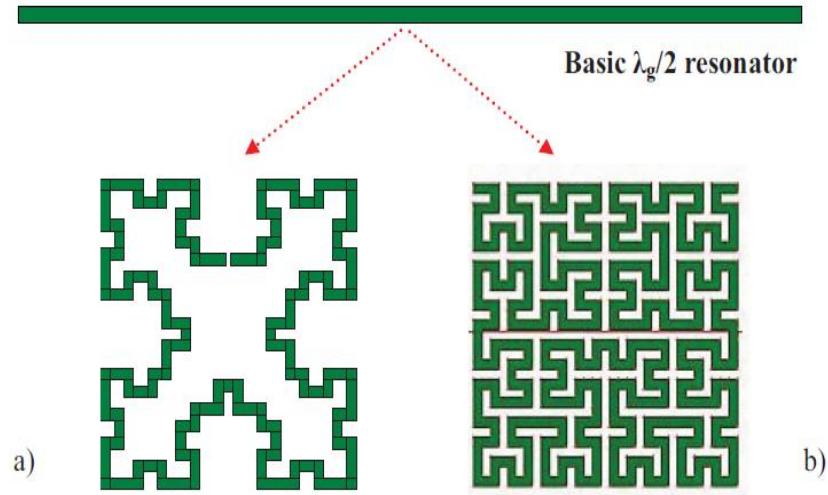
Figure 28 a) Koch-Minkowski and b) Hilbert resonator examples

Typical and simplified cross-coupled spiral resonators with Hilbert configuration (CCSR-H) based on 3rd and 4th fractal iterations have been introduced in [62] for a large coupling coefficient with comparison between each other. All introduced designs in [62] have low insertion loss, high out-of-band rejection level and wider band frequency responses. Moreover, surface current distributions simulated by IE3D software package have been used to analyze the coupling regions in spiral and Hilbert configurations. These configurations are shown in **Figures 29-30** respectively.
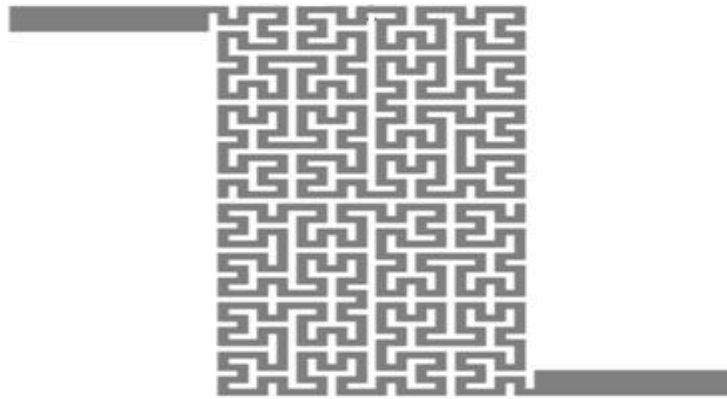
Figure 29 Typical CCSR-H based on 4th Hilbert fractal iteration

Figure 30 Typical CCSR-H based on 3rd Hilbert fractal iteration

Narrow band dual loosely coupled resonators microstrip bandpass filters based on Hilbert fractal geometry with coupling stubs have been proposed for wireless application as in [41] within ISM band at fundamental frequency of 2.4 GHz. The proposed filter design topology is based on a single-mode microstrip resonators constructed from 2nd and 3rd iteration levels of Hilbert fractal geometry. The performance of each propsed filter has been analyzed using a method of moments (MoM) based software package, Microwave Office 2007, from Advanced Wave Research Inc. The new filters have small sizes and low insertion loss as well as high performances, which are very essential features in microstrip filter design theory.These filter structures are shown in **Figures 31-32** .
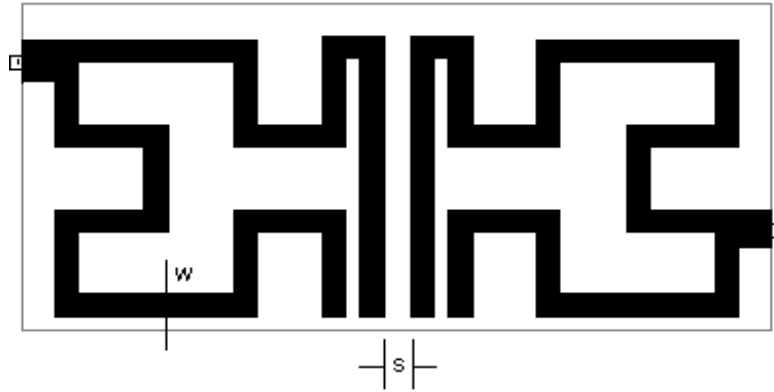
Figure 31 The modeled microstrip bandpass filter with two resonators based on 2nd iteration Hilbert curve geometry
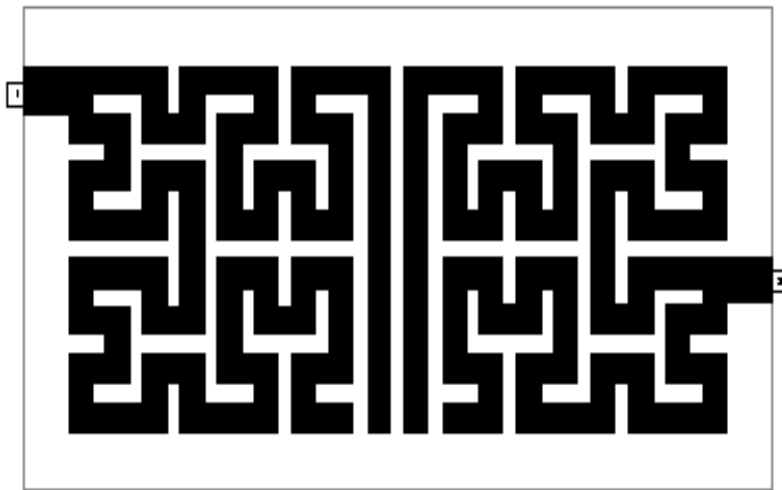
Figure 32 The modeled microstrip bandpass filter with two resonators based on 3rd iteration Hilbert curve geometry

In 2006, Bengin, *et. al,* [63] had investigated the use of Sierpinski fractal geometry in the fabrication of a complementary split ring resonator bandpass filter as stated in **Figure 33**. This filter using square Sierpinski fractal curves has been implemented to lessen resonant frequency of the structure and obtain more enhanced frequency responses.
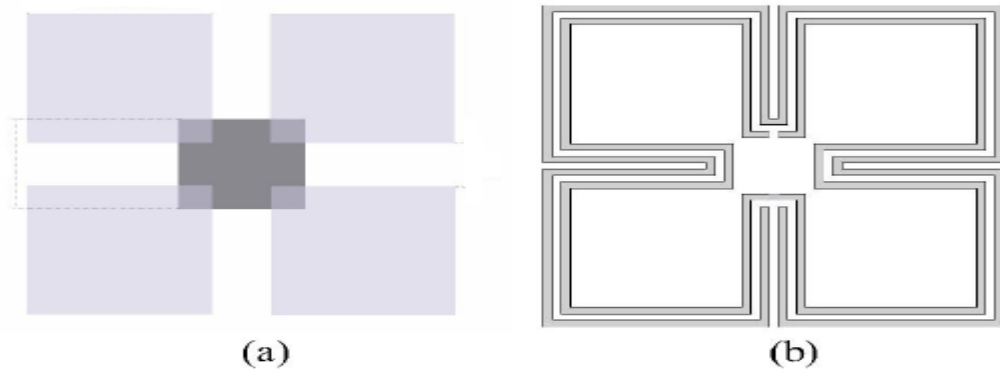
Figure 33 (a) Sierpinski fractal curve of the second order, (b) Sierpinski double split ring configuration

In 2006, Kim ,*et.al,* [64] have been used Koch fractal geometry to design parallel coupled BPF geometry with blocked hramonics.This type of fractal named after the mathematician Helge von Koch, is excellent choice which has been applied to minimize different conventional filters. This has two basic properties: the iteration factor and the iteration order. The iteration factor means the procedure of the fractal geometry generation, while iteration order represents the current achieved iteration for fractal structure. **Figure 34** shows Koch shape bandpass filters. Koch − Minkowski curve have been applied on the edges of the filter coupled sections. According to the generator in **Figure 34**, the iteration factor is ¼ and the orders are zero, 1st and 2nd iterations parallel coupled BPF as shown in **Figure.2.27**.
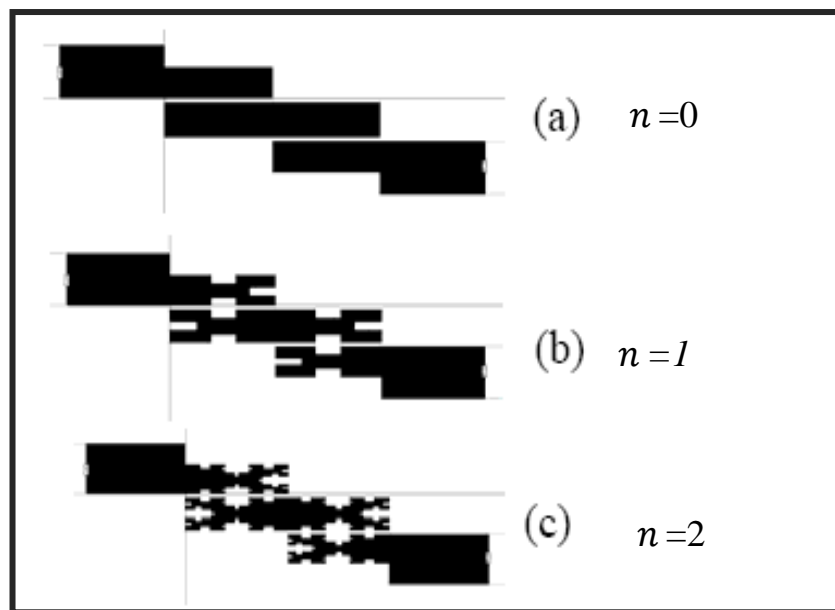
Figure 34 The fractal layout of parallel coupled BPF geometry: a- Zero iteration, b-The first iteration, c- The second iteration

In 2007, Xiao, *et.al,* [65] had introduced new properties of microstrip equilateral triangular patch resonator with fractal defection as explained in **Figure 35** .This fractal filter has been introduced to achieve high quality output response filters with multiple transmission zeros, low insertion loss and wide passband and stopband, in addition to compact sizes.
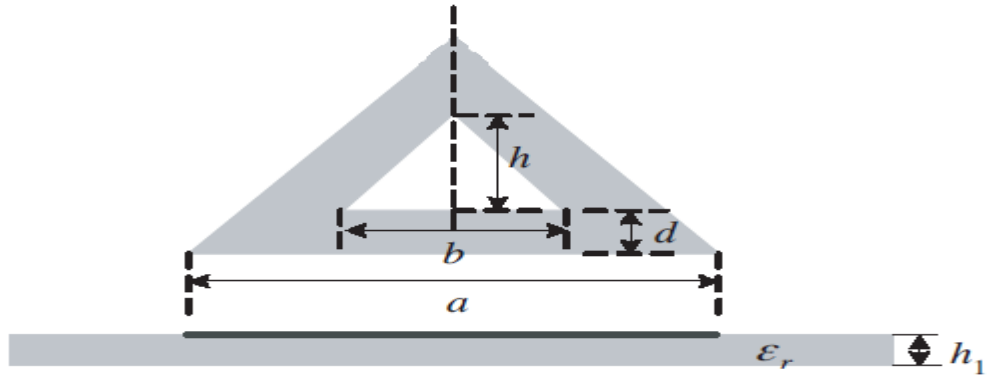
Figure 35 Microstrip equilateral triangular resonator with fractal shaped defection

Chen, *et. al,* [66] had proposed in 2007, Hilbert fractal curve ring with defected ground structure (DGS) to design a lowpass filter as in **Figure 36**. The DGS structure has a flat lowpass characteristic and a sharp band-gap property compared with the conventional dumbbell DGS. To improve the out-band suppression, an improved Hilbert fractal curve ring DGS cell model loaded with open-stubs was proposed. Based on the improved model, a compact L-band microstrip low-pass filter with periodic Hilbert curve ring DGS was designed and fabricated.
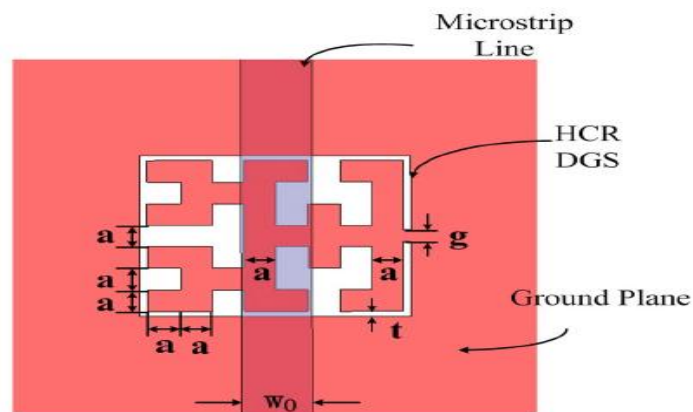
Figure 36 HCR DGS cell model

Ali[42] presented in 2008 new filter topologies based on Minkowski-like pre-fractal curve .He proposed capacitively coupled dual mode microstrip bandpass filters to obtain more selectivity in the resulting filter performance as compared with using a single mode resonator. Minkowski-like pre-fractal curve iterations and generation method can been recognized in **Figure 37**.
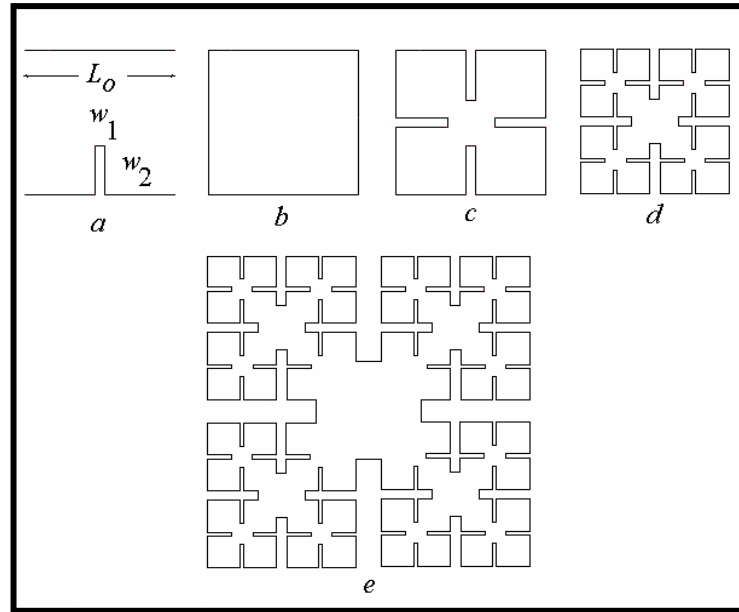
Figure 37 The iterations of the Minkowski-like pre-fractal structure; (*a*) the generator, (*b*) the square ring resonator, (*c*) the 1st iteration, (*d*) the 2nd iteration, and (*e*) modified and enlarged copy of the 3rd iteration

In 2009 [58], Ali and Hussain introduced a dual mode ring resonator with Koch fractal shape to obtain miniaturized microstrip bandpass filter with accepted performance.The proposed filters have narrow bandwidths which are very useful to enhance immunity of wireless systems against frequency interferences. The generation iterations of the proposed fractal microstrip patch filters based on fractal Koch curve are shown in **Figure 38**.
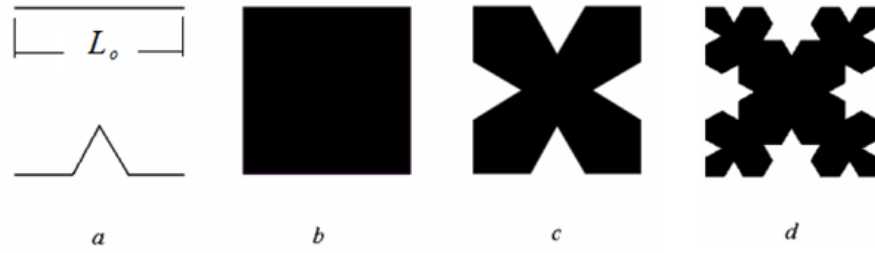
Figure 38 The generation process of the proposed fractal microstrip patch structures based on fractal Koch curve. (a) the generator. (b) the square patch initiator, (c) the 1st iteration, and (d) the 2nd iteration.

In 2010 , the design of bandstop filter based on Hilbert fractal defected ground structure (HDGS), has been developed and optimized using fuzzy genetic algorithm as stated in [67]. This filter has been designed at 2.4 GHz center frequency with flat pass-band characteristics .The simulation results showed that this method has faster convergence rate than the traditional genetic algorithm.The structure of this bandstop filter is shown in **Figure 39**.
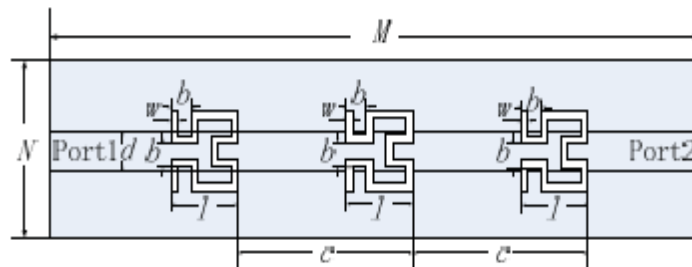
Figure 39 HDGS filter [67]

More recently, a Peano fractal shaped open stub has been used to eliminate the second harmonic of the compact dual-mode ring based microstrip bandpass filters as explained in **Figure 40**. Modeling and performance evaluation of the presented filters have been performed using a full-wave electromagnetic EM simulator, from Sonnet Software Inc. Simulation results show that the introduction of the proposed stub almost maintains the physical size of the filters under test and improves the filter performance by reducing the harmonics to adequate levels. This method can be used in the miniaturized UWB antenna design as a simple means to create the required notch in the antenna response [68].
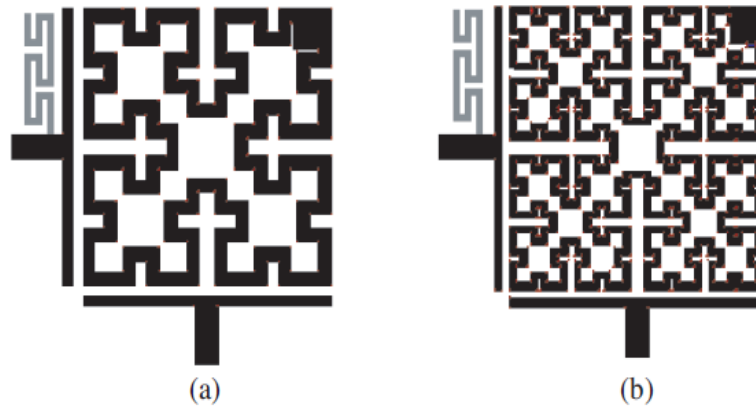
Figure 40 The modeled dual-mode microstrip bandpass filter structures with the Peano shaped open stubs connected at their inputs [68]

A minaiturized dual-mode dual-band microstrip BPF, with its ground plane being defected using fractal based CSRR, is presented in [69]. The internal ring of the conventional square CSRR has been adapted by applying Minkowski like pre-fractal curve to its sides. This produces more compact microstrip BPF with two passbands. The upper band is a result of the dual-mode ring structure while the lower band is attributed to embedded CSRR structure in the filter ground plane. The configuration of the proposed filter has two parts as illustrated in **Figure 41**. The first one is the conventional microstrip dual-mode BPF configuration which comprises the upper side of the whole structure. The second part stands for the proposed CSRR as a DGS in the ground plane.
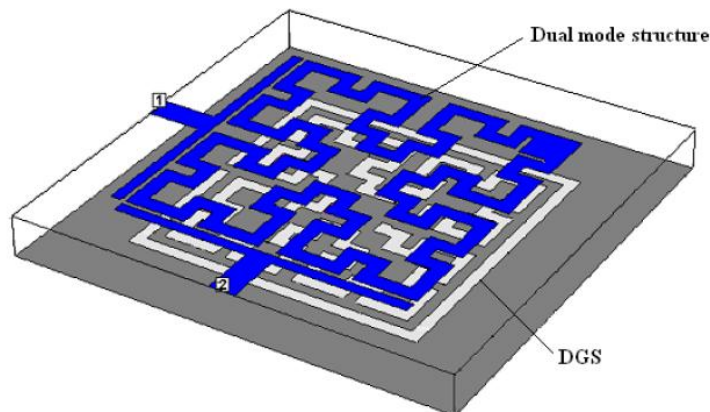
Figure 41 The layout of dual-mode dual-band BPF showing the top dual-mode structure and the bottom CSRR DGS in the ground plane [69]

A miniaturized dual-mode dual-band microstrip BPFs using the same design method reported in [69] but with different fractal iterations for inner ring have presented in [70]. The Application of different iteration levels to the inner ring results in filter responses with different resonant frequency ratios. Experimental results have been achieved on produced filter prototypes, with respect to different iteration levels, are in high conformity with those theoretically obtained. The top view of this structure, **Figure 42**(a), stands for dual-mode BPF with the combined input/output ports. The ring resonator of this filter has the structure related to the 2nd iteration Minkowski pre-fractal geometry. The bottom views, **Figure 42** (b) and (c), show the fractal based CSRR structures related to the 1st and 2nd iterations Minkowski pre-fractal geometry that should be embedded in the implemented filter ground plane.

(a) (b) (c)
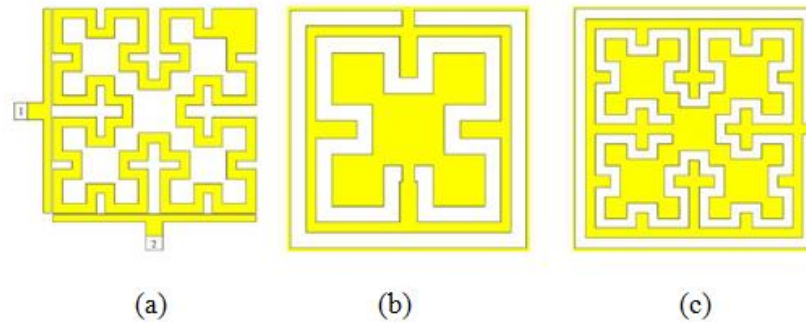
Figure 42 The implemented microstrip dual-band dual-mode BPF structure: (a) the dual-mode fractal based ring structure (top view), (b) and (c) CSRRs with Minkowski fractal shaped inner ring of the 1st and 2nd iterations respectively (bottom views) [70]

CHAPTER 3

BANDPASS AND BANDSTOP MICROSTRIP FILTER BASICS AND PARAMETERS

3.1 Introduction

Microstrip bandpaass and bandstop filters play very considerable roles in many RF and microwave system applications. Excellent performance, more compact size, lighter weight, and cheaper filters have been increasingly adopted in various microwave circuits and systems, because they are essential with rapid development of wireless communication systems [1,24,41,42] .

This chapter presents the features of bandpass and bandstop filters. Main attention has been dedicated to introduce the concepts of coupling, external quality factor for the microstrip resonators , main review about losses of microwave filters, dual mode filters and fundamentals of bandstop (notch) filters .

3.2 Bandpass Filter Basics

An analog bandpass filter is a two port network, as in **Figure 43**, which works by allowing signals in a specific band of frequencies to pass, while signals at all other frequencies are stopped. Basically, a filter is realized by a set of resonators electromagnetically coupled each other and coupled to an external feed circuit. The number and the type of the couplings between the resonators determine the overall performances of the device [1, 25].
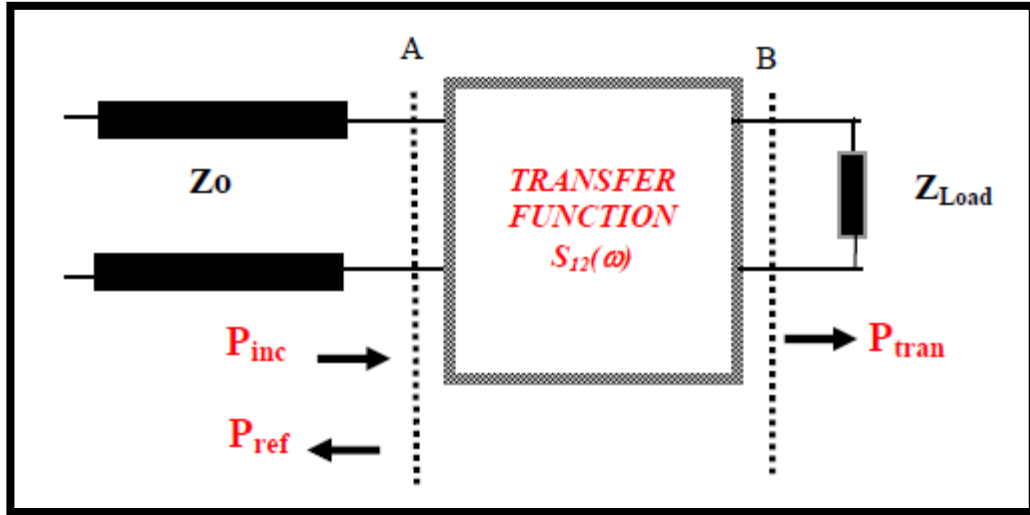
Figure 43 Filter as a two port network

The filter response is defined by its transfer function which, in the microwave range, is used to provide a desired expression to the transmission coefficient $S_{21}=|S_{21}|e^{-i\,\emptyset_{21}}$. An important parameter describing the filter characteristics is the group delay (τ_D) which represents the overall delay of a signal due to filtering, expressed as:

$$\tau_D = \frac{d\emptyset_{21}}{d\omega} \tag{3.1}$$

where $\emptyset_{21}$ is in radians and ω is in radians per second. However, in many practical applications, the filter specifications are mainly referred to the amplitude function $|S_{21}|$ (or $|S_{12}|$ for a reciprocal network[1]) which describes how the magnitude of the response varies with frequency. This is also done by the so called insertion loss (*IL*) response, defined as [1, 3]:

$$IL|_{dB} = 10log\left(\frac{P_{inc}}{P_{tran}}\right) = 10log\left(\frac{1}{|S_{21}|}\right) = -|S_{21}|_{dB} \tag{3.2}$$

where P_{inc} and P_{tran} are incident and transmitted power respectively in the two port network. In the ideal case as shown in **Figure 44** (a), a filter presents a perfectly rectangular amplitude response, where $|S_{21}|_{dB}$ is zero within the pass-band and $-\infty$ elsewhere. Moreover, the phase response would be linear as a function of the frequency, implying a constant group delay. Provided these conditions, the input spectral components, contained in the pass-band, would be perfectly replicated in the output signal, while the spectral content outside the pass-band would be completely

reflected. Since such an ideal filter cannot be realized, in real cases a small but finite pass-band insertion loss IL_{BW} is always found as in **Figure 44** (b) .
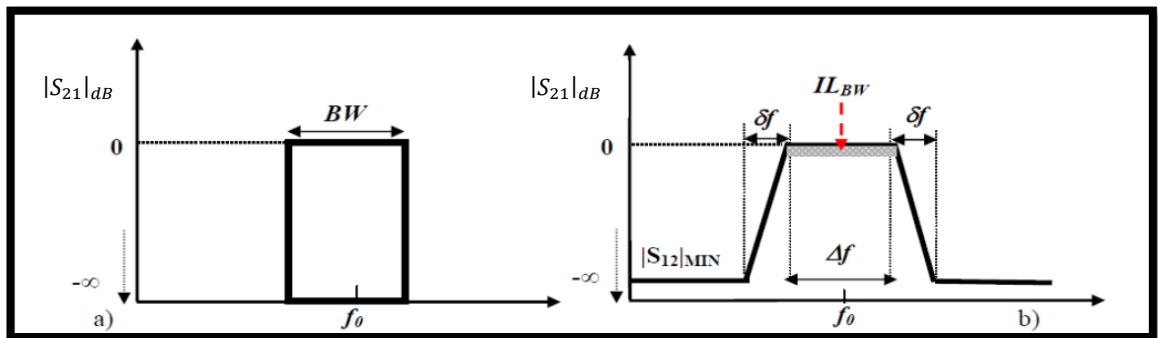
Figure 44 (a) Ideal filter amplitude response (b) Real filter amplitude response

Furthermore, there is transition region δf, between the pass-band and the stop-band ($|S_{21}|_{dB} = |S_{21}|_{min}$), which determines the so called filter selectivity. A key objective in telecommunication systems is usually to keep δf as small as possible, to make the filter able to reject the interference of strong signals operating in the adjacent bands.

3.3 Microstrip Technology

The microstrip resonators are composed by two conducting planes separated by a dielectric layer with a permittivity ε_r and a thickness h as in **Figure 45** while *w* and *t* represent the width and thickness of upper conductor plane on dielectric substrate [1].
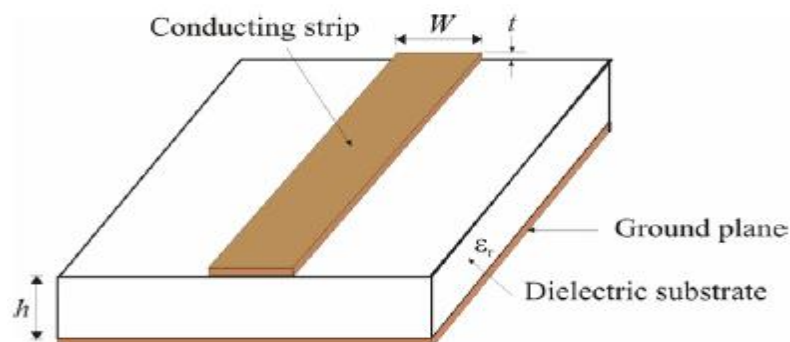
Figure 45 Microstrip transmission line

While one of the two conducting planes is used as ground plane, the other one can be patterned by photolithographic processes, giving rise to different resonator types. The microstrip technology is very interesting since it offers a very easy way to fabricate frequency selective devices which, owing to their low size and weight, can be largely integrated with other devices and systems. The fields in the microstrip distribute within dual air medias, in the upper and lower dielectric section, therefore the structure is not homogeneous. Because of this inhomogeneous section, the microstrip does not back up a pure TEM wave. This is because a pure TEM wave has just transverse components, and its propagation velocity relies only on the material specifications such as the permeability and permittivity. However, with existing the dielectric substrate and the air which they act as guided-wave medias, the waves in a microstrip line will not have hidden longitudinal components of electric and magnetic fields, and their propagation velocities will depend on the physical dimensions of the microstrip as well as material properties [1].

The simplest way to realize a microstrip resonator is to consider a straight line with open-circuit ends as in **Figure 46** (a). According to the elementary transmission line model, if the microstrip line has length L, the modes resonate at the frequencies at which:

$$L = \frac{n\lambda_g}{2} = \frac{n}{2f_o\sqrt{\varepsilon_0\mu_0\varepsilon_{eff}}} \tag{3.3}$$

where λ_g is the wavelength in the considered dielectric substrate (basic $\lambda_g/2$ resonator), n is mode number, and ε_{eff} is the effective permittivity, which takes into account the fringing fields and depends on ε_r, h and also on the microstrip width w [1,71].
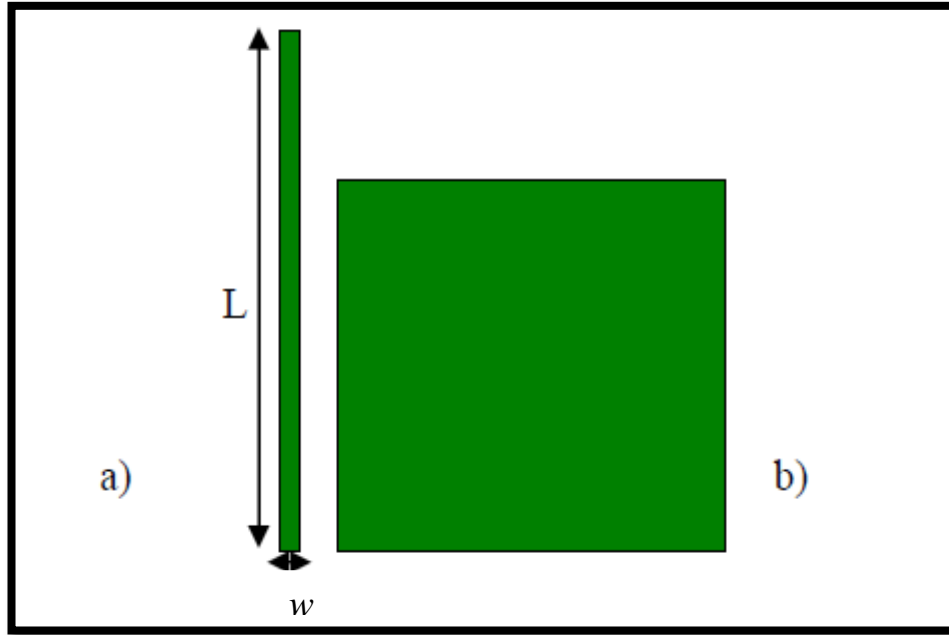
Figure 46 Basic planar resonators

Another type of basic planar resonator can be realized by enlarging the transverse dimension *w*, in order to obtain structures, also called patch resonators, which possess a two dimensional set of modes with two mode numbers (n,m). A typical example is a square resonator as in **Figure 46** (b). In this case, the symmetrical geometry provides also the possibility to generate two modes at the same frequency, thus having a two pole filter with only one patch (dual mode resonator). In the realization of a microstrip filter, the resonators are placed next to each other in specified distances d and are coupled simply by the fringing fields. Currently, patch resonators are widely used in planar filters application, for they have more small sizes, ease of fabrication, less loss and higher power handling capabilities, compared with the line-based resonator filters [72].

Considering the basic $\lambda_g/2$ resonator, **Figure 47** shows some typical Chebychev configurations, where the resonators have been coupled magnetically, putting close their long sides in the backward and forward configurations as in **Figure 47** (a) and **Figure 47** (b) respectively or electrically through the edge-coupled configuration as shown in **Figure 47** (c) [24,71].

Figure 47 Basic microstrip filter layouts: a) Backward coupling, b) Forward coupling and c) Edge coupling

Similarly, different approaches can be followed for the feed line configuration. Usually, the 50Ohm microstrip feed lines are coupled to the external resonators by a capacitive gap d as in **Figure 48** (a) or by a direct connection (tapped line configuration as in **Figure 48** (b) .
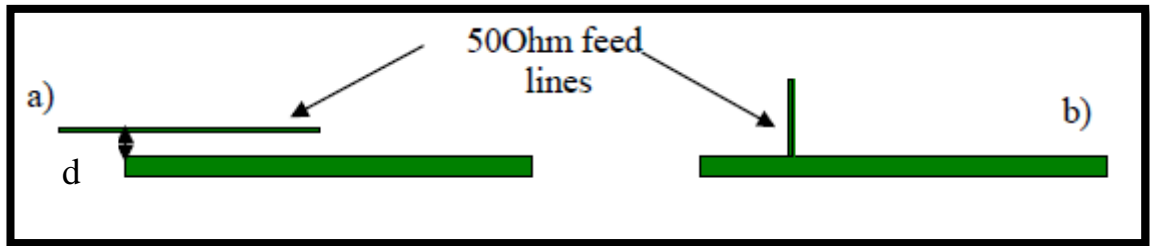
Figure 48 a) Feed line configurations: a) capacitive gap and b) direct connection

3.3.1 Source of Losses in Microstrip Filters

In most conventional microstrip line filter, there are three different losses, which are conductors or ohmic loss, dielectric loss, and radiation loss. These losses may damage or affect the entire components of the electromagnetic (EM) wave propagation.The wave propagation constant in integrated microstrip filters is given by $\gamma = \alpha + j\beta$, where $\alpha = \alpha_c + \alpha_d + \alpha_r$ stands for overall attenuation constant orginating from the conductor losses, dielectric losses and radiation losses while β is phase constant. The unloaded quality factor of a resonator in accordance with single loss contribution is given by [32,73]:

$$Q_i = \frac{\omega_0 W}{P_{diss,i}} \qquad (3.4)$$

where W is the overall stored electromagnetic energy and P_{diss} is average dissipated power over time. When various losses are considered, total dissipative loss can be added approximately ,independent from each other[5,31]:

$$P_{diss} = \sum_i P_{diss,i} = \sum_i \frac{\omega_0 W}{Q_i} = \omega_0 W \sum_i \frac{1}{Q_i} \tag{3.5}$$

From this, the total unloaded quality factor Q_0 can be calculated as:

$$\frac{1}{Q_0} = \sum_i \frac{1}{Q_i} \tag{3.6}$$

or, it can be linearly expressed by [1,31]:

$$\frac{1}{Q_0} = \frac{1}{Q_c} + \frac{1}{Q_d} + \frac{1}{Q_r} \tag{3.7}$$

where $Q_c, Q_{d,}$ and Q_r are the quality factors related to conductor losses, dielectric losses and radiation losses, respectively. For better filter performance, it is very necessary to eliminate or reduce these losses as far as possible; namely, the quality factor must be increased.

3.3.1.1 Conductor Losses

The conductor losses arise from many factors corresponding to the metal material forming the strip, the walls and ground plane. The sources of these losses are skin effects, conductivity and surface roughness [1,74]. At microwave frequencies, the conducting losses in a given material can be approximately described by the surface resistance Rs, defined as the real part of the surface impedance Zs, while X_s is the surface reactance, defined as imaginary part of the surface impedance Zs . In turn, Zs is defined as the intrinsic impedance encountered by a plane wave which, coming from the free space, is perpendicularly incident on an infinite half plane of the considered material. Z_s is related to the material conductivity σ by the expression[1,32]:

$$Z_s = R_s + jX_s = \sqrt{\frac{j\omega\mu}{\sigma}} \tag{3.8}$$

Once R_s is defined, the dissipative power in the conducting parts of a resonator is given by:

$$P_{diss,c} = \frac{1}{2} R_s \int_{Sc} |H|^2 \, ds \tag{3.9}$$

where *Sc* is the overall conductor surface ,and *H* is the related tangential component of the magnetic field. Similarly, the stored electromagnetic energy can be written by:

$$W = \frac{1}{2} \mu \int_v |H|^2 \, dv \tag{3.10}$$

where *v* represents the overall resonator volume. In this way, the quality factor Q_c will be:

$$Q_c = \frac{\omega \mu}{R_s} \frac{\int_v |H|^2 \, dv}{\int_{Sc} |H|^2 \, ds} = \frac{\Gamma}{R_s} \tag{3.11}$$

where Γ is a parameter, with dimensions of a resistance, representing the ratio between an effective volume of the resonator (a volume weighted with the field) and the corresponding effective surface of the conducting parts. In many cases, this expression is differently rearranged by the introduction of length and equation(3.11) becomes:

$$Q_c = \frac{\Pi Z_0}{\lambda_0 R_s} \frac{2 \int_v |H|^2 \, dv}{\int_{Sc} |H|^2 \, ds} = \frac{\Pi Z_0}{\lambda_0 R_s} \iota_c \tag{3.12}$$

where $Z_0 = \sqrt{\frac{\mu_0}{\varepsilon_0}} = 377$ ohm ,λ_0 and ι_c are respectively intrinsic impedance in free space, the wavelength at resonant frequency and geometric conductor parameter. It is easy to show that both ι_c and Γ increase when resonators with higher ratios between *v* and *Sc* are considered.

Generally, conductor losses are corresponding to various geometry and material parameters. On the one hand, narrowing the strip reduces the total dimensions and weakens simultaneously the higher-order modes. However, narrow strip causes higher conductor losses. Moreover, narrowing the strip while maintaining the characteristic impedance (Z_o) constant must lead to decrease in the substrate thickness (*h*), which may cause hard fabrication tolerances. On the other hand, widening the strip reduces the conductor losses, but increases the radiation losses, as well as larger component size. Thus, there is a conflict issue between the need to have compact structures (with higher losses) and higher structures size (with less losses)[1].

3.3.1.2 Dielectric Losses

The dielectric losses can be written in quality factor Q_d terms given in (3.13), where $tan\delta$ is the dissipation factor [1,73,75]:

$$Q_d = \frac{1}{tan\ \delta} \tag{3.13}$$

$$Q_d = \frac{\pi}{\alpha_d \lambda_g} \tag{3.14}$$

In addition, Q_d can also be written by (3.14) where, α_d and λ_g are the dielectric attenuation constant, guided wavelength of the strip line transmission medium at interested frequency, respectively. In general, using low-loss dielectric substrates helps to reduce the dielectric losses.

3.3.1.3 Radiation Losses

When filter structures are open to air, they will radiate energy. By the way, the radiation losses can be reduced by fully coating and embedding the entire structures within the integration medium. Filters manufactured in such configuration are not only protected from the environment, but also from the electromagnetic interference (EMI). Vice versa for the extremely covered structures [1].

3.4 The Transfer Function of Analog Filter

In the design of practical filters, the ideal rectangular amplitude response is approximated by using some specific polynomials, presenting different features concerning the steepness of the filter skirts and also implying different internal structures.Usually,$|S_{21}|^2$expressed as[1,24] :

$$|S_{21}(\Omega)|^2 = \frac{1}{1+\epsilon^2 F_N^2(\Omega)} \tag{3.15}$$

where

$$\epsilon = \frac{1}{\sqrt{10^{\frac{-L_R}{10}} - 1}} \tag{3.16}$$

and

$$\Omega = \frac{1}{FBW}\left(\frac{\omega}{\omega_o} - \frac{\omega_o}{\omega}\right) \tag{3.17}$$

where Ω represents variable frequency which is normalized to the passband cut-off frequency of the lowpass prototype filter, ω is variable angular frequency of bandpass filter, ω_o is the mid band frequency and FBW is the fractional bandwidth. ϵ is a ripple constant related to a given return loss $L_R = 20\, log\, |S_{11}|$ in dB. The degree N of the polynomial (F_N) represents the number of the resonators and the roots of $[1 + \epsilon^2 F_N{}^2(\Omega)]$ are also called "poles" of the filter. In modern applications, three types of polynomials are really considered: Chebychev, Cauer (elliptic) and quasi elliptic. **Table 2** summarizes the expressions of these three cases and **Figure 49** reports their typical exemplary responses.

Response type	$F_N(\Omega)$
Chebychev	$cos\|N\,cos^{-1}(\Omega)\| \qquad \|\Omega\|\leq1$ $cos\|N\,cosh^{-1}(\Omega)\| \qquad \|\Omega\|\geq1$ where Ω is normalized angular frequency
Quasi elliptic	$cosh\left\|(N-2)\,cosh^{-1}(\Omega) + cosh(\frac{\Omega_a\Omega - 1}{\Omega_a - \Omega}) + cosh^{-1}(\frac{\Omega_a\Omega + 1}{\Omega_a + \Omega})\right\|$ Where $\Omega = \pm\Omega_a$ $(\Omega_a > 1)$ are the frequency locations of a pair of transmission zeros
Cauer elliptic	$M\, \dfrac{\prod_{i=1}^{n/2} (\Omega_i{}^2 - \Omega^2)}{\prod_{i=1}^{n/2}(\frac{\Omega_s{}^2}{\Omega_i{}^2} - \Omega^2)}$ for N even $N\, \dfrac{\Omega\,\prod_{i=1}^{(n-1)/2} (\Omega_i{}^2 - \Omega^2)}{\prod_{i=1}^{(n-1)/2} (\frac{\Omega_s{}^2}{\Omega_i{}^2} - \Omega^2)}$ for N odd and ≥3 where $0 < \Omega_i < 1$ and $\Omega_s > 1$ represent some critical frequencies

Table 2 Polynomials for Filter Response [1,24]
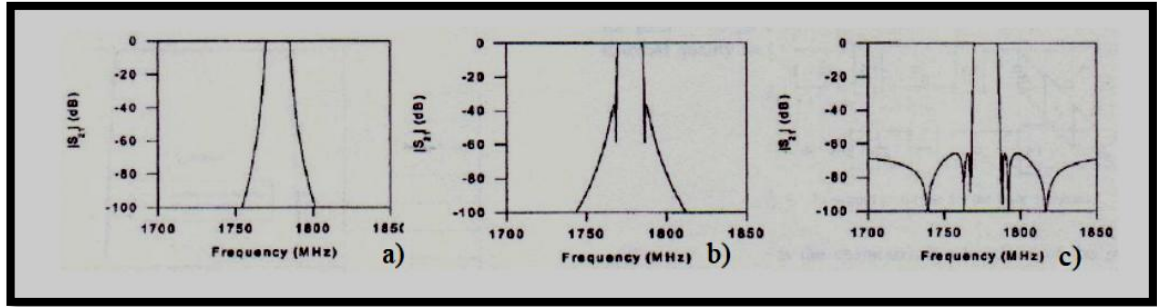
Figure 49 a) Chebychev, b) quasi elliptic and c) elliptic responses

In the quasi elliptic and elliptic cases, S_{21} is characterized by the presence of transmission zeroes (respectively 2 and *N-1*), which can be opportunely positioned very close to the band edges, improving the selectivity performances in comparison with Chebychev filter with same *N*.Indeed, it is easy to show that for every type of response, the degree *N* of the polynomials affects directly the desired selectivity δf, as shown in **Figure 50** for a Chebychev filter.
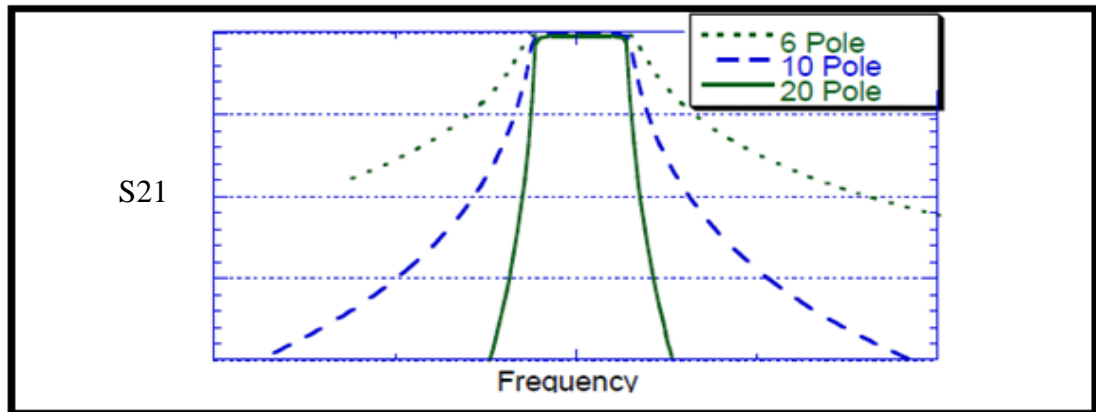
Figure 50 Chebychev filter response as function of the number of poles

3.5 The Coupling Concept

A general expression for the coupling coefficient k_{ij} of two coupled microwave resonators can be given considering the ratio between the coupled energy and the stored energy as in **Figure 51** [1]:

$$k_{ij} = \frac{\iiint \varepsilon\, E_1 . E_2\ dv}{\sqrt{\iiint \varepsilon\, |E_1|^2\, dv}\ *\ \sqrt{\iiint \varepsilon\, E_2{}^2\, dv}} + \frac{\iiint \mu\, H_1 . H_2\, dv}{\sqrt{\iiint \mu\, |H_1|^2\, dv}\ *\ \sqrt{\iiint \mu\, |H_2|^2\, dv}} \qquad (3.18)$$

49
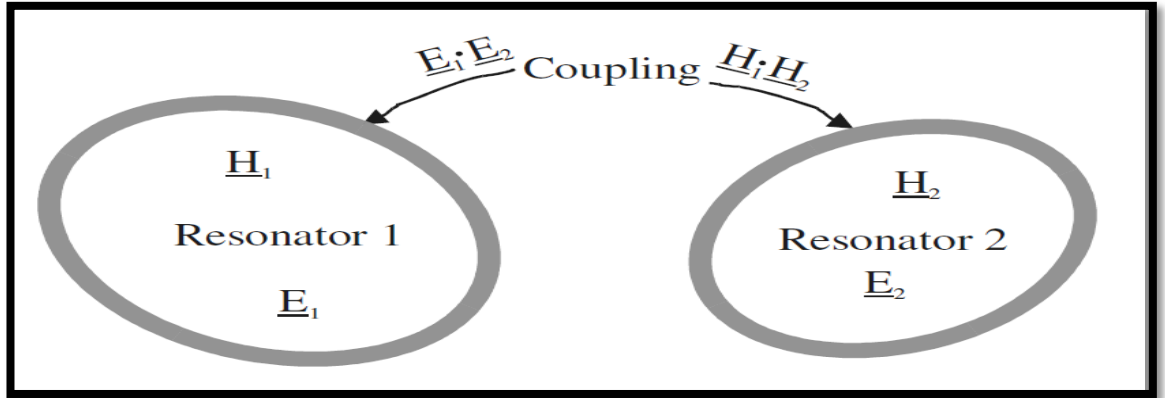
Figure 51 General coupled RF/microwave resonators [1]

where the generic $k_{i,j}$ (coupling coefficient) represents the coupling between the ith and j^{th} resonators, while E and H are the electric and magnetic fields, respectively, evaluated at the resonance frequency. As shown, the overall coupling is composed of two terms, representing separately the electric and the magnetic couplings. It is to be noted that the coupling may have positive or negative sign. In particular, a positive sign indicates that the coupling improves the stored energy of uncoupled resonators, while a negative sign means the inversed effect. Consequently, the electric and magnetic couplings could have similar effect, if they have the same sign, or have the opposite effect, if their signs are different. Beyond the couplings between the resonators, it is also necessary to define the coupling strength of the input and output resonators with the feed circuit. To this end, for these resonators, one can introduce the external quality factor (Q_{ext}) [24,71]:

$$Q_{ext} = \frac{\omega_0 W}{P_{EST}} \tag{3.19}$$

where W is the overall stored electromagnetic energy and P_{EST} is the power flowing out of the corresponding port. Usually, in all practical cases, the desired responses require the same value of P_{EST} for every port. In the following sections, we will shortly introduce the filter design procedure, describing how to get the coupling $k_{i,j}$ and Q_{ext} from the desired $|S_{21}|$ expression. Here, it is worth to remember that in the Chebychev case, considering all resonators having same resonant frequencies

(synchronously tuned), only the ($k_{j,j+1}=k_{j+1,j}$) elements of the coupling matrix [k] have non zero values. This means that a Chebychev response can be obtained by a simple ladder network with only sequential couplings, as shown in **Figure 52** for a four pole filter.
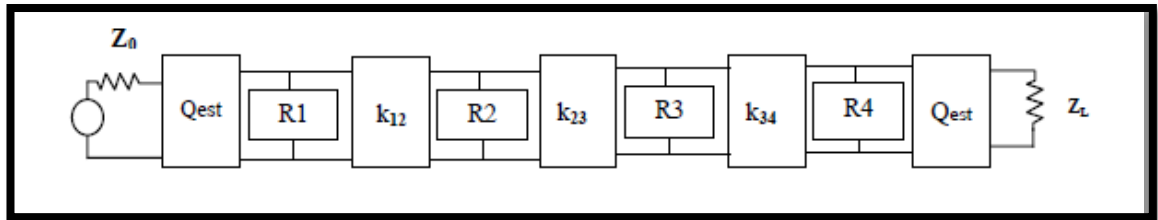
Figure 52 Four pole Chebychev network

On the contrary, the elliptic filters, which offer the best performances in terms of selectivity, require also a very high number of couplings and result practically unrealizable in many cases. To this regard, a very good trade-off is provided by the quasi elliptic model. Indeed, this can be realized starting from the Chebychev model, by adding only one cross coupling as in **Figure 53** [1].
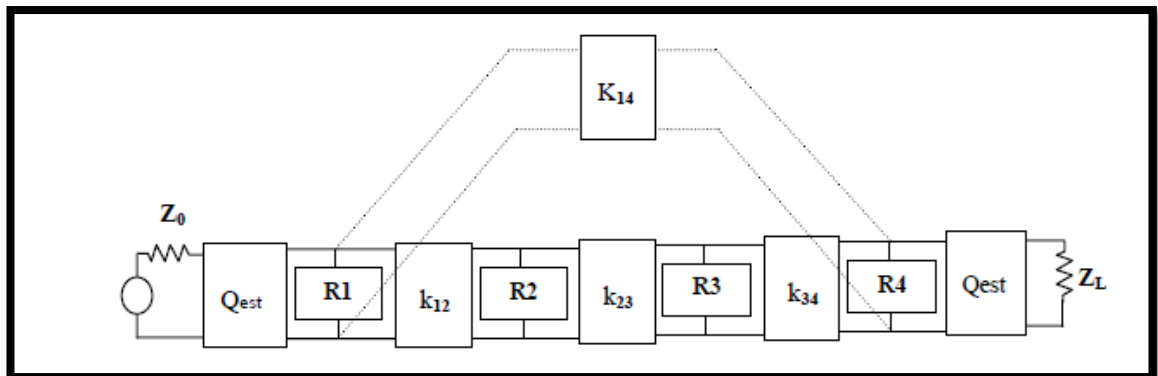
Figure 53 Four pole quasi elliptic network

3.5.1 Coupling Matrix and External Quality Factor

The coupling matrix representation is very quite significant for many coupled-resonator filter topologies [1]. Although coupled-resonator filters with bridge couplings were published widely beginning as early as 1957, those that had the most important microwave filter art were by Atia and Williams in 1972 [76]. The filter synthesis art then rapidly developed, with the result that narrow bandpass filters can be designed for any response such as linear-phase responses, elliptic-function

51

responses and responses that are not symmetric around center frequency. From a normalized coupled-resonator low-pass prototype network, these filters can be designed that is completely characterized by its coupling matrix [77]. This makes a very advantageous formula in terms of coupling coefficients and external quality factors for analysis and synthesis of coupled-resonator filter circuits as shown below [1]:

$$S_{21} = 2 \frac{1}{\sqrt{q_{e1}q_{en}}} [A_{n1}]^{-1} \quad \text{and} \quad S_{11} = \pm(1 - \frac{2}{q_{e1}} [A]_{11}^{-1}) \tag{3.20}$$

$$[A] = [q] + P[U] - j[k]$$

where P is $P = \frac{f_o}{BW}\left(\frac{f}{f_o} - \frac{f_o}{f}\right)$, $[U]$ is the $N \times N$ identity matrix, $[k]$ is the so-called general coupling matrix, which is an $n \times n$ reciprocal matrix (i.e., $k_{ij} = k_{ji}$). Finally, $[q]$ is a NxN matrix with all entries zero except for $q_{11} = \frac{1}{q_{e1}}$ and $q_{nn} = \frac{1}{q_{e2}}$ where q_{e1} and q_{e2} are the scaled external factors given by $q_{ei} = \frac{BW}{f_o} Q_{ext,i}$, for i = 1,2 .

For Chebychev and quasi elliptic responses, this general approach has been widely developed and their synthesis is possible by analytical or numerical formulas. In particular, the specifications of a Chebychev filter are given by: the number of poles N, the centre frequency f_o, the in-band ripple ϵ ,and the equi-ripple bandwidth BW. With these values provided, the coupling coefficients between resonators and Q_{ext} can be evaluated by [1,78]:

$$k_{i,i+1} = \frac{BW}{\sqrt{g_i \cdot g_{i+1}}} \quad \text{for } i = 1 \text{ to } (N-1) \tag{3.21}$$

$$Q_{ex1} = \frac{g_0 \cdot g_1}{BW} \tag{3.22}$$

$$Q_{exN} = \frac{g_N \cdot g_{N+1}}{BW} \tag{3.23}$$

where g_i is the generic parameter of the low-pass prototype filter. The g_i parameters depend only on N and ϵ and can be evaluated by analytical formulas [1, 79]. Some parameters for fixed ϵ values are shown in **Table 3**. The approach to quasi elliptic responses, where the zeroes position with respect to the band edges have also to be

indicated in the specifications, is theoretically more complex, since an exact analytical formulation does not exist.

However, even in this case, tables and approximated expressions are present in literature for the low-pass parameters of some basic quasi elliptic filter configurations with 4, 6 and 8 poles. Once known, $k_{i,j}$ and Q_{ext} for a desired response, the design of a microstrip filter can be realized by the use of electromagnetic simulators which, given the substrate characteristics, allow fixing all the geometric parameters concerning the resonator dimensions, the distances between them and the considered feed line configurations.

Value of n	g_1	g_2	g_3	g_4	g_5	g_6	g_7	g_8	g_9	g_{10}	g_{11}
					0.01-dB Ripple						
1	0.0960	1.0000									
2	0.4488	0.4077	1.1007								
3	0.6291	0.9702	0.6291	1.0000							
4	0.7128	1.2003	1.3212	0.5476	1.1007						
5	0.7563	1.3049	1.5773	1.3049	0.7563	1.0000					
6	0.7813	1.3600	1.6896	1.5350	1.4970	0.7098	1.1007				
7	0.7969	1.3924	1.7481	1.6331	1.7481	1.3924	0.7969	1.0000			
8	0.8072	1.4130	1.7824	1.6833	1.8529	1.6193	1.5554	0.7333	1.1007		
9	0.8144	1.4270	1.8043	1.7125	1.9057	1.7125	1.8043	1.4270	0.8144	1.0000	
10	0.8196	1.4369	1.8192	1.7311	1.9362	1.7590	1.9055	1.6527	1.5817	0.7446	1.1007
					0.1-dB Ripple						
1	0.3052	1.0000									
2	0.8430	0.6220	1.3554								
3	1.0315	1.1474	1.0315	1.0000							
4	1.1088	1.3061	1.7703	0.8180	1.3554						
5	1.1468	1.3712	1.9750	1.3712	1.1468	1.0000					
6	1.1681	1.4039	2.0562	1.5170	1.9029	0.8618	1.3554				
7	1.1811	1.4228	2.0966	1.5733	2.0966	1.4228	1.1811	1.0000			
8	1.1897	1.4346	2.1199	1.6010	2.1699	1.5640	1.9444	0.8778	1.3554		
9	1.1956	1.4425	2.1345	1.6167	2.2053	1.6167	2.1345	1.4425	1.1956	1.0000	
10	1.1999	1.4481	2.1444	1.6265	2.2253	1.6418	2.2046	1.5821	1.9628	0.8853	1.3554

Table 3 Exemplary Parameters of Chebychev Low Pass Prototype Filters

Most of the EM simulators are based on the method of moment, such that they evaluate the filter response by dividing first the resonators in small regions (mesh), less or more fitted according to the desired accuracy, and then solving a set of linear equations derived from an integral equation, whose unknown is the surface current density J_s. Once defined, the shape and the dimensions of the resonators, for a given coupling configuration, the coefficient $k_{i,j}$ as a function of the spacing d can be determined by analyzing the transmission response of two resonators, when they are insufficiently and weakly coupled to the external feed lines. Indeed, provided this

fundamental condition, it is easy to show that the corresponding $|S_{21}|$ presents two characteristic peaks at frequency f_1 and f_2 as in **Figure 54**, symmetrically centered on f_0. The coupling coefficient is given by[1, 80]:

$$K_{12} = \frac{2(f_2 - f_1)}{(f_2 + f_1)} \qquad (3.24)$$
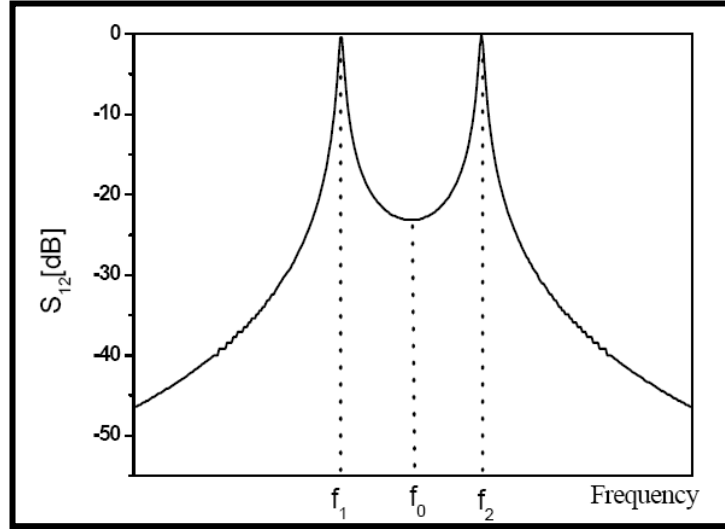
Figure 54 Typical transmission response of two coupled resonators

A similar procedure can be followed for Q_{ext}. The resonator can be coupled only to an input port (singly loaded resonator) or to both input/output ports (doubly loaded resonator) as shown in **Figure 55** [1]. In the former case, Q_{ext} can be extracted from the phase response S_{11} by using the relation:

$$Q_{ext} = \frac{f_{(0^o)}}{f_{(-90^o)} - f_{(+90^o)}} \qquad (3.25)$$

In the latter case, the resonator is used as one pole filter and Q_{ext} can be derived from -3dB bandwidth transmission peak:

$$Q_{ext} = \frac{2f_0}{BW_{3dB}} \qquad (3.26)$$
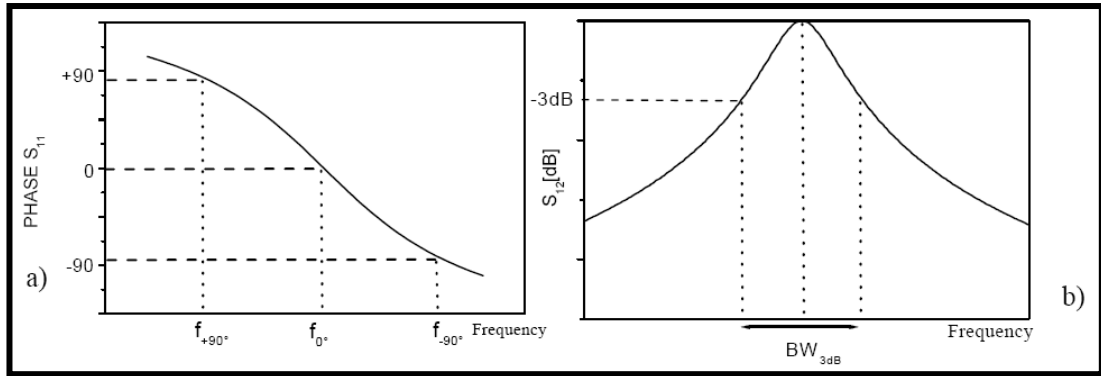
Figure 55 Q_{ext} calculation for (a) Singly and (b) Doubly loaded resonator

3.6 Dual Mode Filters

This section has introduced the basic principles of a dual-mode resonators, also some of theoretical calculations related with dual-mode resonators are presented.

3.6.1 Dual-Mode Square Ring Resonator

Classical microstrip bandpass filters are mostly designed using single-mode resonators. Recently, dual-mode resonators have been widely adopted in microwave and RF wireless communication applications for their high performance and low loss properties. Since they have double resonant nature, a dual-mode bandpass filter of some order requires half as multiple resonators as compared with classical topology [81]. Dual-mode principle for 2D and 3D resonators is well known and has been the subject of extensive studies since the early 70s [82]. This principle is typical of all the resonators provided of geometrical symmetry that, for this reason, are able to give rise to degenerate modes with the same resonant frequency. When the symmetry is kept intact, the two modes are orthogonal and they cannot exchange microwave power. On the contrary, when the geometrical symmetry is opportunely broken, the resonator boundary conditions change allowing the coupling between the modes. Consequently, two modes can be contemporarily present at slightly split frequencies. A main advantage of this type of resonator lies in the property that each of dual-mode resonators can used as dual tuned resonant circuit, and hence the required

number of resonators for a n-order filter is decreased by half, in form of a compact filter configuration [1, 83-85].

3.6.2 Microstrip Dual-Mode Resonators

To discuss this issue, let us start with a microstrip rectangular patch resonator top view in **Figure 56**, represented by a Wheeler's cavity model [86], that in this case the modes are transverse magnetic *TM*, with the magnetic field orthogonal to z-axis. Where the electric walls are found perfectly in the upper and lower side of the cavity while the remaining sides are the perfect magnetic walls.
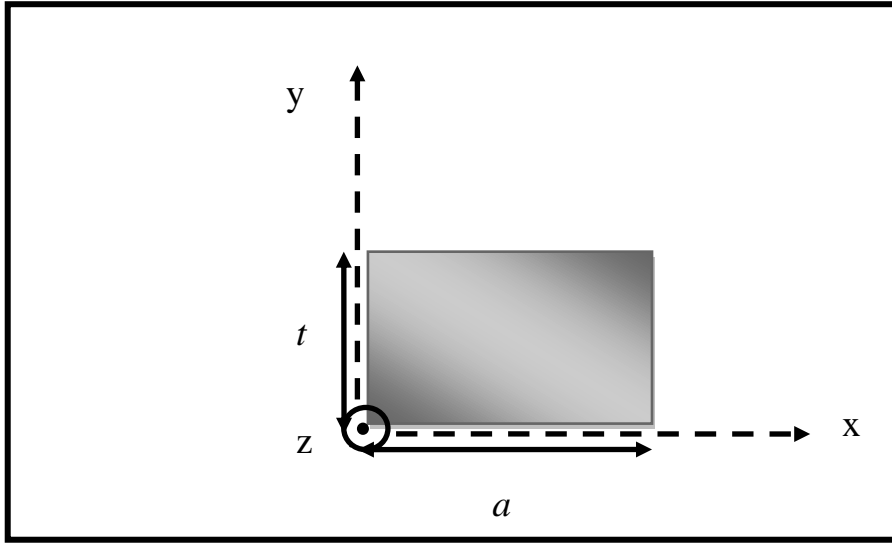
Figure 56 Top view of a generic rectangular patch

The EM fields inside the cavity can be defined in terms of TM_{mn0}^z modes:

$$E_z = A_{mn} \sum_{m=0}^{\infty} \cos\frac{m\pi}{a} x \sum_{n=0}^{\infty} \cos\frac{n\pi}{t} y$$

$$H_x = \left(\frac{j\omega\varepsilon_{eff}}{K_c^2}\right)\left(\frac{\partial E_Z}{\partial y}\right)$$

$$H_y = -\left(\frac{j\omega\varepsilon_{eff}}{K_c^2}\right)\left(\frac{\partial E_Z}{\partial x}\right)$$

$$K_c^2 = \left(\frac{m\pi}{a}\right)^2 + \left(\frac{n\pi}{t}\right)^2 \tag{3.27}$$

where A_{mn} represents the amplitude of mode, ω is the radian frequency, and a and ε_{eff} are the effective width and permittivity .The resonant frequency of the cavity can be determined by:

$$f_{mn0} = \frac{c}{2\pi\sqrt{\varepsilon_r}}\sqrt{\left(\frac{m\pi}{a}\right)^2 + \left(\frac{n\pi}{t}\right)^2}$$

or

$$f_{mn0} = \frac{1}{2\pi\sqrt{\mu\varepsilon_{eff}}}\sqrt{\left(\frac{m\pi}{a}\right)^2 + \left(\frac{n\pi}{t}\right)^2} \qquad (3.28)$$

Actually, there are an infinite number of resonant frequencies related to various field modes or distributions. By analyzing the modes TM_{100} and TM_{010}, it is immediate to prove that in the former of the magnetic field is directed only along the y axis, while in the latter it is directed along the x axis. Consequently, the surface current $J_s = i_z \times H_t$ is oriented only along x in TM_{100}, while it is oriented along y in TM_{010}.

$$f_{100} = \frac{c}{\sqrt{\varepsilon_r}}\frac{1}{2a}$$

and

$$f_{010} = \frac{c}{\sqrt{\varepsilon_r}}\frac{1}{2t} \qquad (3.29)$$

Then, it is evident that for a square patch (a=t), TM_{100} and TM_{010} are degenerate modes, since they have the same resonant frequency and can separately and orthogonally (without power exchange) excited, as shown in **Figure 57**. However, as stated above, the modes can be coupled by introducing an adequate geometry distortion, such that the changed boundary conditions can be satisfied by the contemporary presence of the two modes. The final surface current distribution is then a superimposition of the original orthogonal currents and this justifies, also intuitively, the classical placement at right angle of the feed lines [1].

 A microstrip dual-mode resonator is not restricted with square shape, but typically has two-dimensional (2-D) symmetry. **Figure 58** explains some classical microstrip dual-mode resonators, where D in each resonator refers to its symmetrical dimension, and λ_{go} is the guided-wavelength at its resonant frequency in the associated resonator. It is necessary to indicate a small perturbation has been applied to each dual-mode resonator at offset location that is assumed at a 45° from its two

orthogonal modes. For example, a small cut can be used to disturb the square patch and disk resonators, while a small patch can be inserted to the ring, square loop, and meander loop resonators, respectively. Note that for coupling of the orthogonal modes, the perturbations may also take other forms that are different than those indicated in **Figure 58**. For example, a small elliptical deformation of a circular disk or patch can be used for coupling the two degenerate modes and, by the same way, a square patch can be little bit twisted into a rectangular shape for the coupling. The perturbation dimensions of each filter should be tuned for desired filter responses [1, 84-85], because of behavior and the intensity of the coupling between dual degenerate modes of the dual-mode resonator are essentially depended by the perturbation's size and shape. However, more details about this issue can be found in [87,88].
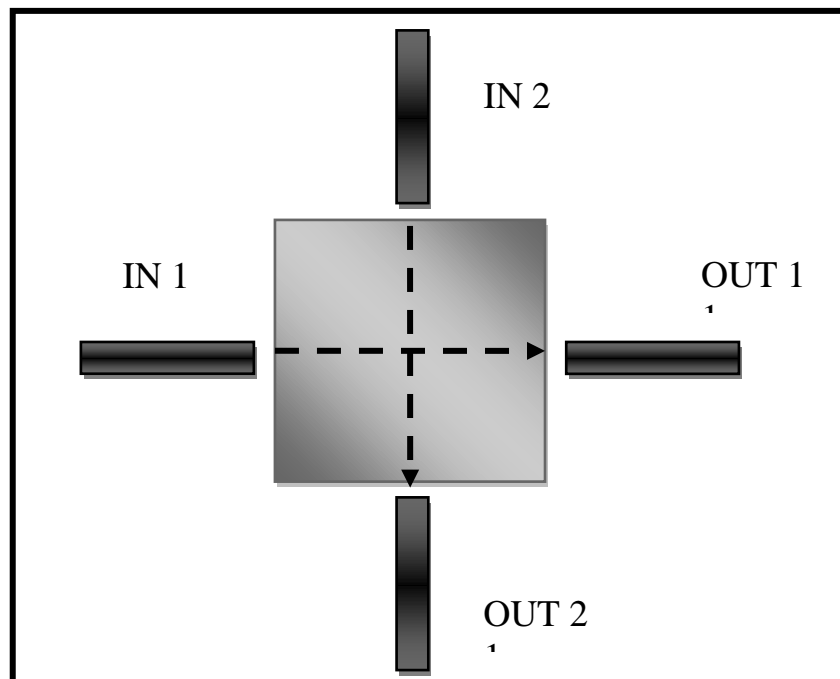
Figure 57 Current distributions of the orthogonal modes in the basic square patch
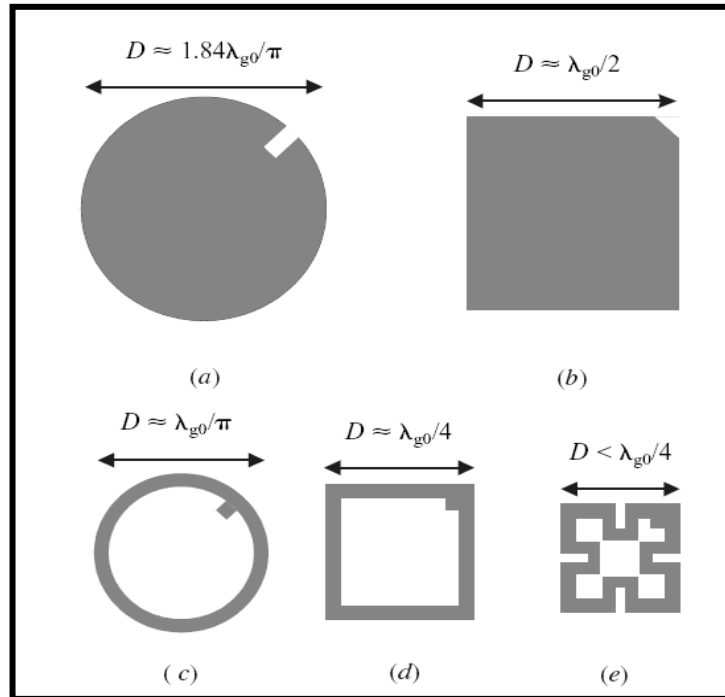
Figure 58 Some microstrip dual-mode resonators (a) Circular disk (b) Square patch (c) Circular ring (d) Square loop (e) Meander loop

3.6.3 Simple Model of Square Ring Resonator

The microstrip ring resonator is a easy fabricated circuit and has been increasingly utilized to calculate dispersion, effective dielectric constant and discontinuity parameters and to measure optimal substrate thickness. Moreover, they are typically used in the circuit design and measurements, as in filters [89], oscillator [90], antennas, and so forth [91]. Also, many complicated circuits can be manufactured by adding a notch, cutting a slit, cascading dual or multiple rings, performing some solid-state devices, and so on.

The square ring resonator is just a transmission line constructed in closed loop. **Figure 59** shows the conventional closed loop microstrip square ring resonator with dual coupling spacings. Power is coupled inside and outside the resonator via coupling gaps and feed lines. It has a big value of insertion loss because of small coupling regions. In the case of large distance between resonator and the feed, the coupling gaps will not have effect on the resonant frequencies of the ring. This type of coupling is called "loose coupling." Loose coupling represents negligible small capacitance of the coupling gap. If the feed lines are positioned closer to the

59

resonator, the coupling becomes stronger and the gap capacitances become more considered. This makes the resonant frequencies of the circuit away from pure resonant frequencies of the ring. So, the capacitances of the coupling gaps for ring resonator design will be more appreciable [89].

The design of ring resonator requires guided wavelength (λ_g) determination for used transmission line. The ring resonates at the frequencies when its average perimeter is a multiple of the guided wavelength and results in, [Appendix A]
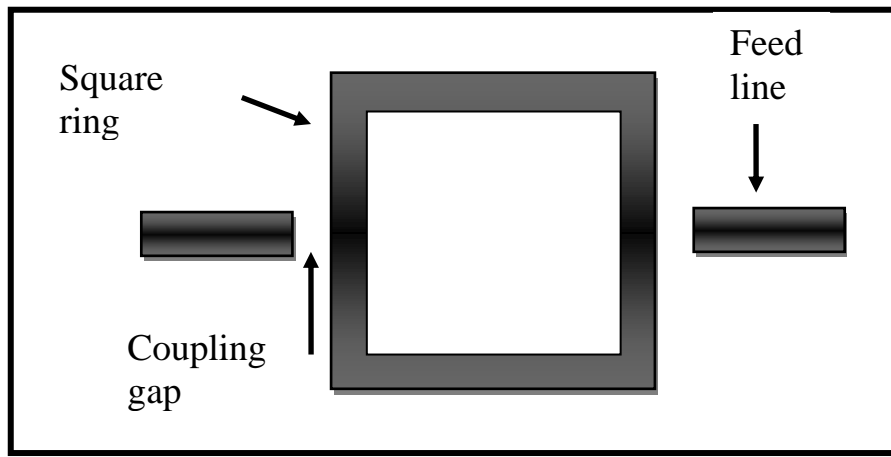
Figure 59 The microstrip square ring resonator

total length $= n\lambda_g$ for square, ring, and meander loop.

$2\pi r = n\lambda_g$, for n = 1, 2, 3, . . .   ring resonator   (3.30)

where *r* is the mean radius of the ring that equals the average of inner and outer radiuses, λ_g is the guided wavelength, and n is the mode number. This relation is valid for the loose coupling condition with no considered coupling gap effects . From this equation, the resonant frequencies for different modes can be determined since λ_g is frequency dependent. For the first mode, the maximum field happens at the coupling gap locations, and nulls take place normally from the coupling gap positions.

3.6.4 Even -Odd -Modes

The two orthogonal modes existing within a ring resonator are used as coupled modes instead of independent, thus, the most typical application of two port devices

are BPF. **Figure 60** illustrates the basic structure of a dual-mode filter using one-wavelength ring resonators that proved in appendix A for any shape (square, ring, and meander) using transmission line theorem. Input and output ports are spatially separated at 90° intervals, and an adequate perturbation or discontinuity is positioned at an equal distance from the input and output (point C or D in the **Figure 60**). The behavior of the combination of two orthogonal resonance modes can qualitatively be explained by applying the travelling wave theory to this figure. For simplicity, it has been assumed that a structure where the resonator is excited by electric coupling, and the input/output ports are capacitive coupled as shown in that figure. First, consider a case eliminating the perturbation or discontinuity within the resonator. The incident wave excited at the input port generates a strong electric field at point A due to electric coupling. The electromagnetic waves due to this electric field propagate clockwise and counterclockwise reaching point B at a reverse phase where the phase of the clock wise wave is 270° while the counterclockwise wave is 90°. The electric field amplitude at point B due to these waves becomes zero, and no response is generated at the output port. In next case, a discontinuity such as stub or notch at point C, as with the previous case, a strong electric field is generated at point A by exciting the input port, and thus two travelling waves are excited. The counterclockwise wave reaches point B at a 90° phase shift. Further propagating to point C at 135° phase shift, a portion of this wave reflected at in-phase or reverse phase due to this discontinuity in the transmission line of the resonator. Considering the reflected wave as in-phase, this wave propagates to point B while encountering a further phase shift of 135°. The total phase shift from point A becomes 360°, and thus the electric field magnitude of this reflected attains its maximum value at this point. This allows the wave to propagate through the output port by electric coupling. Similarly, the reflected wave of the clockwise travelling wave due to the discontinuity can also propagate through the output port [92, 93].
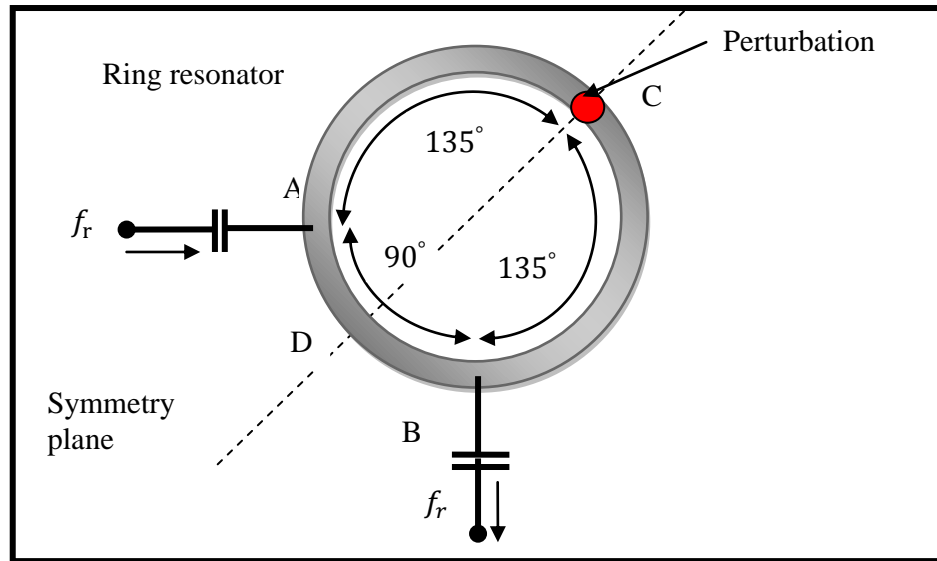
Figure 60 Structure of dual-mode resonator based on a one-wavelength ring resonator [29]

3.6.4.1 Even-Mode

The even-mode equivalent circuit of the ring resonator is shown in **Figure 61** (b). This analysis valid for any shape such as ring, square, and meander, where a magnetic wall is applied along the (Symmetry S–plane), which is an open circuit, and divides the capacitance into one-half. Even-mode excitation, where two in-phase signals of equal amplitude are simultaneously applied to the input and output ports, satisfies open circuited conditions at the symmetrical plane of the circuit. Thus the circuit can be divided into two identical sub-circuits at the symmetrical plane, and analysis is based on either sub-circuit by applying an open-circuited condition to the divided plane [92].

3.6.4.2 Odd-Mode

Similarly for odd-mode excitation, where signals of reverse phase are applied to the input and output ports, an identical circuit satisfying short-circuited condition at the divided plane is considered. As shown in **Figure 61** (c) [92, 94].
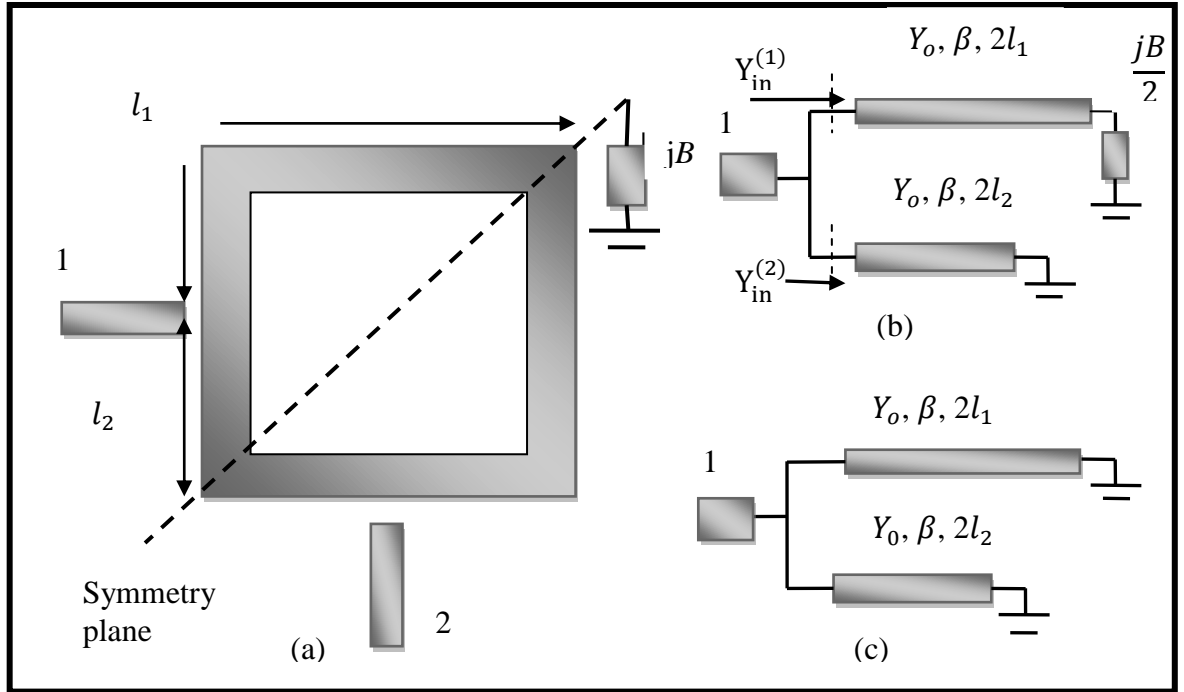
Figure 61 a- Dual-mode resonator b- Even-mode equivalent circuit c- Odd-mode equivalent circuit

3.6.5 Calculation of the Central Frequency and the Coupling Coefficient

The resonance conditions for each mode are analyzed from **Figure 61**, and the derived resonance frequencies are used to obtain the coupling between the two orthogonal resonance modes. The coupling coefficient K between the orthogonal resonance modes can be expressed in the following form using the even- and odd-mode resonance frequencies, respectively expressed as f^e and f^o [92, 95-96].

$$K = \frac{2|f^e - f^o|}{f^e + f^o} \tag{3.31}$$

The resonance condition $Y_{in}^1 + Y_{in}^2 = 0$

Y_{in}^1 represents index 1 refers to length l_1, while Y_{in}^2 represents index 2 refers to length l_2. Since the resonance condition is given by $2(l_1 + l_2)\beta_o = 2\pi$

$$\beta_o = \frac{\omega_o}{\upsilon} = \frac{\pi}{l_1 + l_2} \tag{3.32}$$

where υ is the wave propagation speed along the transmission line, β and ω are the off-resonance, propagation constant and angular frequency:

$$\beta = \frac{\omega}{\upsilon} = \frac{\pi}{l_1 + l_2}\frac{\omega}{\omega_o} \tag{3.33}$$

63

If perturbation B on symmetry axis, $B > 0$ represents capacitor or $B < 0$ represents inductor. Let us consider transmission line section of characteristic admittance Y_o, propagation constant β and the length l connected to a load with the admittance load Y_L. The input admittance is given by the relation:

$$Y_{in} = Y_o \frac{Y_L + jY_o \tan \beta l}{Y_o + jY_L \tan \beta l} \tag{3.34}$$

For the branch l_1 in **Figure 61** the load has admittance:

$$Y_L = \frac{jB}{2} \tag{3.35}$$

Therefore

$$Y_{in}^{(1)} = Y_o \frac{j\frac{B}{2} + jY_o \tan \beta l_1}{Y_o - \frac{B}{2} \tan \beta l_1} \tag{3.36}$$

If we define the normalized susceptance as:

$$b = \frac{B}{Y_o}$$

Then:

$$Y_{in}^{(1)} = Y_o \frac{j\frac{b}{2} + j \tan \beta l_1}{1 - \frac{b}{2} \tan \beta l_1} \tag{3.37}$$

Furthermore; if we define the angle $\emptyset$ such that:

$$\tan \emptyset = \frac{b}{2}$$

Then: $Y_{in}^{(1)} = jY_o \tan(\beta l_1 + \emptyset)$ \hfill (3.38)

Applying the final equation to index 2, then:

$$Y_{in}^{(2)} = jY_o \tan(\beta l_2) \tag{3.39}$$

At resonance $\qquad Y_{in}^{(1)} + Y_{in}^{(2)} = 0 \quad$ then:

$$\beta(l_1 + l_2) = \pi - \emptyset = \pi - \tan^{-1}\frac{b}{2} \qquad \text{for even-mode}$$

$$\beta^e = \frac{2\pi f^e}{v} = \frac{\pi - \tan^{-1}(\frac{b}{2})}{l_1 + l_2} \tag{3.40}$$

When the resonator is unperturbed mode then:

$$\tan^{-1}\frac{b}{2} = 0,$$

and:

$$\beta_o = \frac{2\pi f_o}{v} = \frac{\pi}{l_1 + l_2}$$

(3.41)

Therefore

$$\beta^e = \beta_o(1 - \frac{1}{\pi}\tan^{-1}(\frac{b}{2}))$$

(3.42)

and the resonant frequency for the even-mode is:

$$f^e = f_o(1 - \frac{1}{\pi}\tan^{-1}(\frac{b}{2}))$$

(3.43)

The perturbation does not affect the odd-mode therefore the odd-mode resonant frequency f^o remains the same as in the unperturbed case.

$$f^o = f_o$$

(3.44)

The central resonant frequency is:

$$f_c = \frac{f^e + f^o}{2} = f_o(1 - \frac{1}{2\pi}\tan^{-1}(\frac{b}{2}))$$

(3.45)

The coupling coefficient of the two modes, define as the absolute value of the frequency shift between both even and odd-modes over the central frequency becomes:

$$K = \frac{|f^e - f^o|}{f_c} = \frac{\frac{1}{\pi}\left|\tan^{-1}(\frac{b}{2})\right|}{1 - \frac{1}{2\pi}\tan^{-1}(\frac{b}{2})}$$

(3.46)

note here $b = \frac{B}{Y_o} = \frac{Y_b}{Y_o}tan(\beta_o d)$, where d represents the side length of perturbation, Y_b=characteristic admittance of the perturbation stub as shown in **Figure 62**. Therefore as the length of perturbation increases, this leads to increase of even resonant frequency(f^e), so affecting the resonant frequency(f_c) and coupling coefficient (K). The in-band insertion loss increases, since the even resonant mode increases, while the odd resonant mode remains constant. The configuration with only one perturbation in the symmetry plane as shown in **Figure 62** is a very common case in literature [97] and two perturbations techniques can also be used [98- 102].
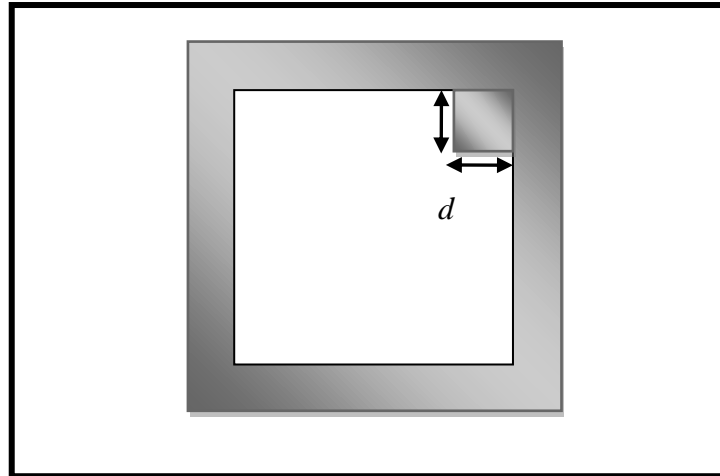
Figure 62 Square ring resonator with a perturbation stub

3.6.6 Calculation of S_{21} for Square Ring Resonator

Ring resonator with orthogonal feed line is shown in **Figure 63**. The closed-loop ring resonator with total length of $l = n\lambda_g$ is fed by dual orthogonal feed lines, where n is the mode number and λ_g is the guided wavelength. The ring resonator is supplied by the input and output feed lines acts a shunt circuit, which consists of the top and down sections of $l_1 = \frac{3n\lambda_g}{4}$ and $l_2 = \frac{n\lambda_g}{4}$, respectively. The $ABCD$ matrices of the top and down sections of the lossless ring circuit are given by:
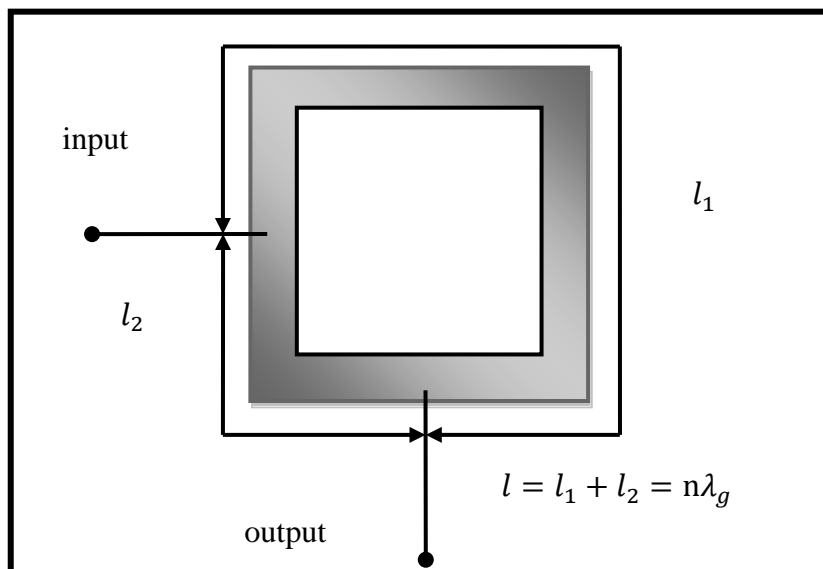
Figure 63 Configuration of the ring resonator supplied by dual orthogonal feed lines

$$\begin{bmatrix} A & B \\ C & D \end{bmatrix}_{upper} = \begin{bmatrix} \cos \beta l_1 & jZ_o \sin \beta l_1 \\ jY_o \sin \beta l_1 & \cos \beta l_1 \end{bmatrix} \tag{3.47a}$$

and

$$\begin{bmatrix} A & B \\ C & D \end{bmatrix}_{lower} = \begin{bmatrix} \cos \beta l_2 & jZ_o \sin \beta l_2 \\ jY_o \sin \beta l_2 & \cos \beta l_2 \end{bmatrix} \tag{3.47b}$$

where β is the propagation constant and $Z_o = \frac{1}{Y_o}$ is the characteristic impedance of the ring resonator. The Y parameters of the top and down sections are realized from (3.47a) and (3.47b) and are given by:

$$\begin{bmatrix} Y_{11} & Y_{12} \\ Y_{21} & Y_{22} \end{bmatrix}_j = \begin{bmatrix} D_j/B_j & (B_j C_j - A_j D_j)/B_j \\ -1/B_j & A_j/B_j \end{bmatrix} \tag{3.48}$$

where $j =$ up or down is for up or down sections. Moreover, the overall Y parameter of the whole circuit is expressed as:

$$\begin{bmatrix} Y_{11} & Y_{12} \\ Y_{21} & Y_{22} \end{bmatrix} = \begin{bmatrix} Y_{11} & Y_{12} \\ Y_{21} & Y_{22} \end{bmatrix}_{upper} + \begin{bmatrix} Y_{11} & Y_{12} \\ Y_{21} & Y_{22} \end{bmatrix}_{lower} =$$
$$\begin{bmatrix} -jY_o(\cot \beta l_1 + \cot \beta l_2) & jY_o(\csc \beta l_1 + \csc \beta l_2) \\ jY_o(\csc \beta l_1 + \csc \beta l_2) & -jY_o(\cot \beta l_1 + \cot \beta l_2) \end{bmatrix} \tag{3.49}$$

Furthermore, S_{21} of the ring circuit can be obtained from (3.49) and is expressed as [103]:

$$S_{21} = \frac{-2Y_{21}Y_o}{(Y_{11} + Y_o)(Y_{22} + Y_o) - Y_{21}Y_{12}}$$
$$= \frac{-j2(\csc \frac{3n\pi}{2} + \csc \frac{n\pi}{2})}{[1 - j(\cot \frac{3n\pi}{2} + \cot \frac{n\pi}{2})]^2 + [(\csc \frac{3n\pi}{2} + \csc \frac{n\pi}{2})]^2} \tag{3.50}$$

For odd-mode excitation:

$$|S_{21}| = 0, \qquad n = 1, 3, 5 \tag{3.51a}$$

and for even-mode excitation:

$$|S_{21}| = 1, \qquad n = 2, 4, 6, \tag{3.51b}$$

The evaluated results in (3.51) clarify that the ring resonator supplied by dual orthogonal fed lines can exclude the odd-mode resonant frequencies and run only at even-mode resonant frequencies [90,104-106].

3.6.7 Equivalent Lumped Elements G, L, C and Unloaded quality factor of Square Ring Resonators

Figure 64 presents the topology of a closed-loop microstrip square ring resonator. The equations of the ring which are written in simple manner as:

$$L_o = \frac{n\lambda_g}{4}$$

$$f_o = \frac{nc}{4L_o\sqrt{\varepsilon_{eff}}} \qquad\qquad (4.52)$$

where n is the mode number , λ_g is the guided-wavelength, L_o is the external side length of the square ring resonator, c is the speed of light in free space, f_o is the resonant frequency and ε_{eff} is effective relative dielectric constant. From this structure, if the width of the ring is narrow, the ring might have similar dispersion properties as a transmission line resonator. Hence, the ring resonator can be a closed loop transmission line and analyzed by transmission-line model [89, 106].
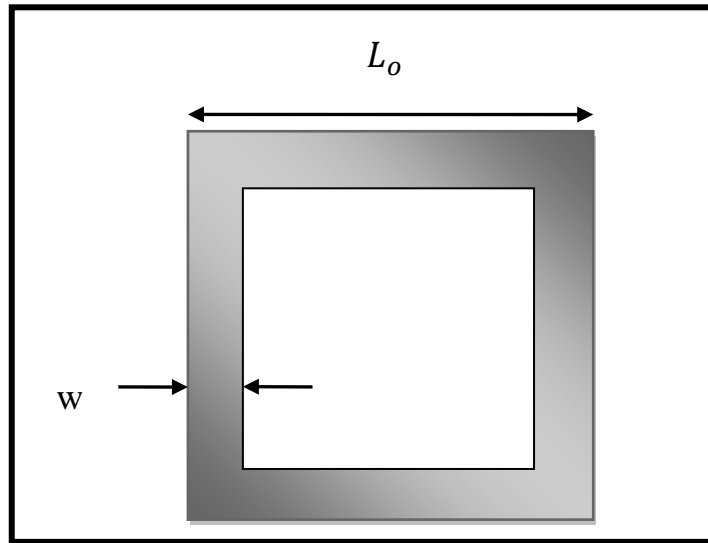
Figure 64 A closed- square loop microstrip ring resonator

Figure 65 (a) shows the single port network of the ring and its equivalent circuit. From Figure **65** (a), the equivalent input impedance of the ring is difficult to be derived from single port network. **Figure 65** (b) shows another configuration using two-port network with an open circuit at port 2 ($i_2 = 0$) to model the single-port network and evaluate the equivalent input impedance through $ABCD$ and Y parameter matrix operations [106]. As seen in **Figure 65** (b), the total length $l = n\lambda_g = 4L_o$ for the fundamental mode n =1 is divided by input and output ports

on arbitrary positions of the ring with two sections l_1 and l_2. The dual sections compose a parallel circuit. For this parallel circuit, a transmission line $ABCD$ matrix is utilized to find each section parameters. The $ABCD$ matrix of the individual transmission line lengths l_1 and l_2 is given as follows:

$$\begin{bmatrix} A & B \\ C & D \end{bmatrix}_{1,2} = \begin{bmatrix} cosh(\gamma l_{1,2}) & Z_O \, sinh(\gamma l_{1,2}) \\ Y_O \, sinh(\gamma l_{1,2}) & cosh(\gamma l_{1,2}) \end{bmatrix} , \quad \gamma = \alpha + j\beta \quad (3.53)$$

where subscripts 1 and 2 are corresponding to the transmission lines l_1 and l_2, respectively, $Z_O = \frac{1}{Y_O}$ is the characteristic impedance of the microstrip ring resonator, α is the attenuation constant, γ is the complex propagation constant and β is the phase constant [89, 106].
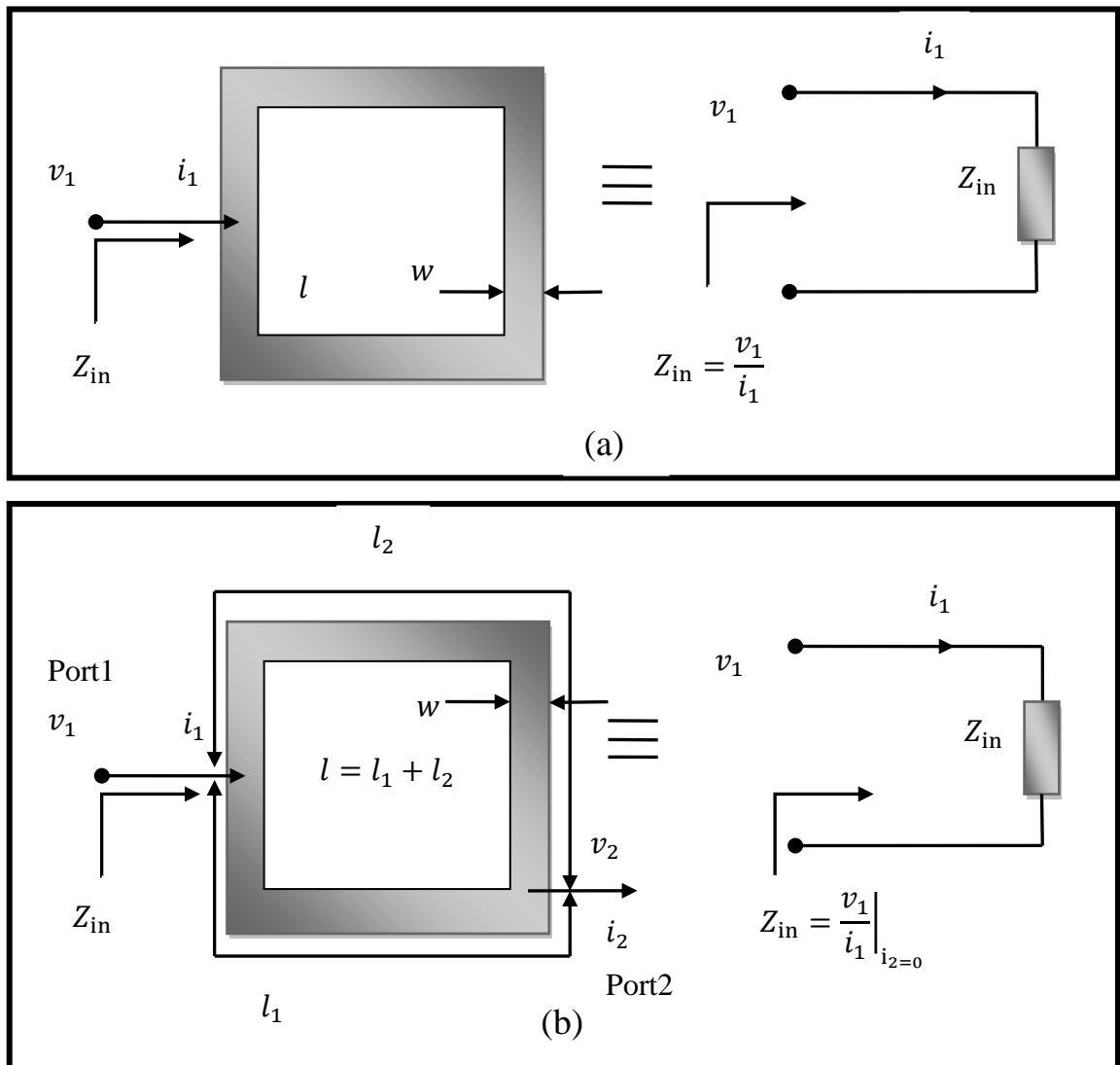
Figure 65 The input impedance of (a) One-port network and (b) Two-port network of the closed-loop ring resonator

The total Y parameters converted from $ABCD$ matrix in (3.53) for the parallel circuit are shown as:

$$\begin{bmatrix} Y_{11} & Y_{12} \\ Y_{21} & Y_{22} \end{bmatrix} = \begin{bmatrix} Y_o[coth(\gamma l_1) + coth(\gamma l_2)] & -Y_o[csch(\gamma l_1) + csch(\gamma l_2)] \\ -Y_o[csch(\gamma l_1) + csch(\gamma l_2)] & Y_o[coth(\gamma l_1) + coth(\gamma l_2)] \end{bmatrix} \quad (3.54)$$

By adjusting i_2 to zero, the input impedance Z_{in} of the closed-loop ring in **Figure 65** (b) can be determined as:

$$Z_{in} = \left.\frac{v_1}{i_1}\right|_{i_2=0} = \frac{Y_{22}}{Y_{22}Y_{11} - Y_{12}Y_{21}} \quad (3.55)$$

Letting $l_g = {}^l/_2 = \frac{\lambda_g}{2}$, Z_{in} can be rearranged as:

$$Z_{in} = \frac{Z_o}{2} \frac{1 + j\,tanh(\alpha l_g)\,tan(\beta l_g)}{tanh(\alpha l_g) + j\,tan(\beta l_g)} \quad (3.56)$$

Practically, transmission lines have very low loss and the attenuation term can be assumed that $\alpha l_g \ll 1$ and then $tanh(\alpha l_g) \approx \alpha l_g$. Assuming βl_g term and letting the angular frequency $\omega = \omega_o + \Delta\omega$, where ω_o is the resonant angular frequency and $\Delta\omega$ is small, then:

$$\beta l_g = \frac{\omega_o l_g}{v_p} + \frac{\Delta\omega l_g}{v_p} \quad (3.57)$$

where v_p is the phase velocity of the transmission line. When a resonance occurs, $\omega = \omega_o$ and $l_g = \frac{\lambda_g}{2} = \frac{\pi v_p}{\omega_o}$ .Thus, Equation (3.57) can be rearranged as:

$$\beta l_g = \pi + \frac{\pi\Delta\omega}{\omega_o} \quad (3.58a)$$

and

$$tanh(\beta l_g) \cong \frac{\pi\Delta\omega}{\omega_o} \quad (3.58b)$$

By these results, the input impedance Z_{in} can be approximated as:

$$Z_{in} \cong \frac{Z_o}{2} \frac{1 + j\alpha l_g \frac{\pi\Delta\omega}{\omega_o}}{\alpha l_g + j\frac{\pi\Delta\omega}{\omega_o}} \quad (3.59)$$

Since $\alpha l_g \frac{\pi\Delta\omega}{\omega_o} << 1$, Z_{in} can be rewritten as:

$$Z_{in} = \frac{\left(\frac{Z_o}{2\alpha l_g}\right)}{1 + j\frac{\pi\Delta\omega}{\alpha l_g \omega_o}} \tag{3.60}$$

For a general parallel *GLC* circuit, the input impedance is:

$$Z_{in} = \frac{1}{G + 2j\Delta\omega C} \tag{3.61}$$

It is found from (3.60) and (3.61), the input impedance of the square-loop ring resonator has similar form as that of a parallel *GLC* circuit. So, the conductance of the equivalent circuit of the ring is:

$$G = \frac{2\alpha l_g}{Z_o} = \frac{\alpha \lambda_g}{Z_o} \tag{3.62a}$$

and the capacitance of the equivalent circuit of the ring is:

$$C = \frac{\pi}{Z_o \omega_o} \tag{3.62b}$$

While the inductance of this equivalent circuit is derived from

$\omega_o = \frac{1}{\sqrt{L\,C}}$, and is given by:

$$L = \frac{1}{\omega_o^2 C} \tag{3.62c}$$

where *G, C,* and *L* stand for the equivalent conductance, capacitance, and inductance of the square-loop ring resonator. **Figure 66** illustrates the equivalent lumped element circuit of the ring in terms of *G, C,* and *L*. In addition, the unloaded *Q* of the ring resonator can be evaluated by [89]:

$$Q_u = \frac{\omega_o C}{G} = \frac{\pi}{\alpha \lambda_g} \tag{3.63}$$
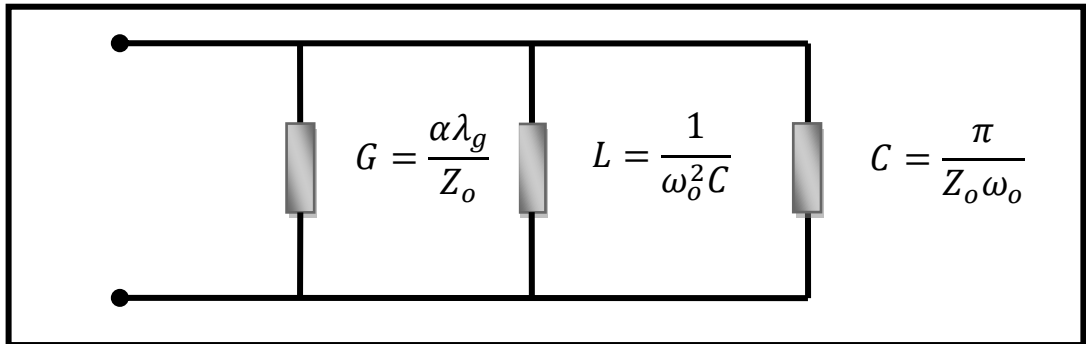
Figure 66 Equivalent elements *G, C,* and *L* of the closed-loop ring resonator

3.7 Notch (Bandstop) Filter

Bandstop filters or band-reject filters reject signals within a frequency band bounded by a lower and an upper limit and allow transmission at frequencies out of this band. The ideal bandstop filter amplitude response in frequency domain is given in **Figure 67** [81,107].
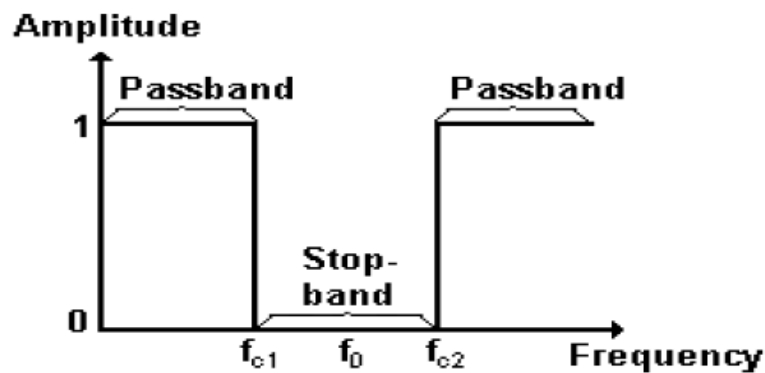
Figure 67 The ideal bandstop filter amplitude response

In **Figure 67**, f_{c1} and f_{c2} are the lower and upper corner frequencies and f_0 is the center frequency of the ideal bandstop filter. In ideal bandstop filter, attenuation in passband is zero, attenuation in stopband is infinite, and transition from passband to stopband is infinitely sharp. Such an ideal filter (brick wall filter) characteristics is not possible to obtain in practice. Practical filter responses have smoother passband to stopband transitions. Passband insertion losses are desired to be as small as possible and stopband attenuations are desired to be as high as possible. Ideal characteristics can be approximated using approximating functions like Butterworth, Chebyshev, Elliptic etc. within an acceptable tolerance.

bandstop amplitude responses using these functions are given in **Figure 68** .
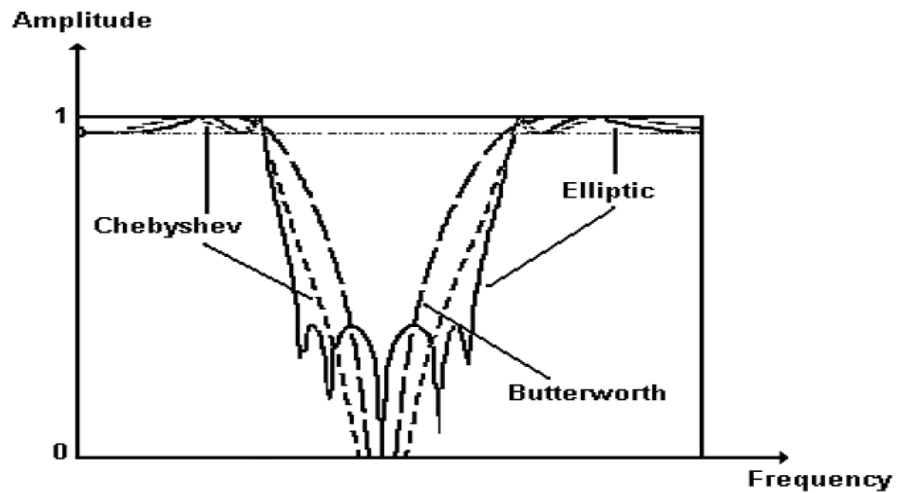
Figure 68 Approximations for Ideal Bandstop Filter

A bandstop filter (BSF) with a narrow stopband is called a notch filter. Notch filters basically reject or 'notch' out a specific frequency. So ideally they are like allpass filters except an abrupt attenuation at a specific frequency. Typical response of a notch filter and its important characteristics are shown in **Figure 69.**
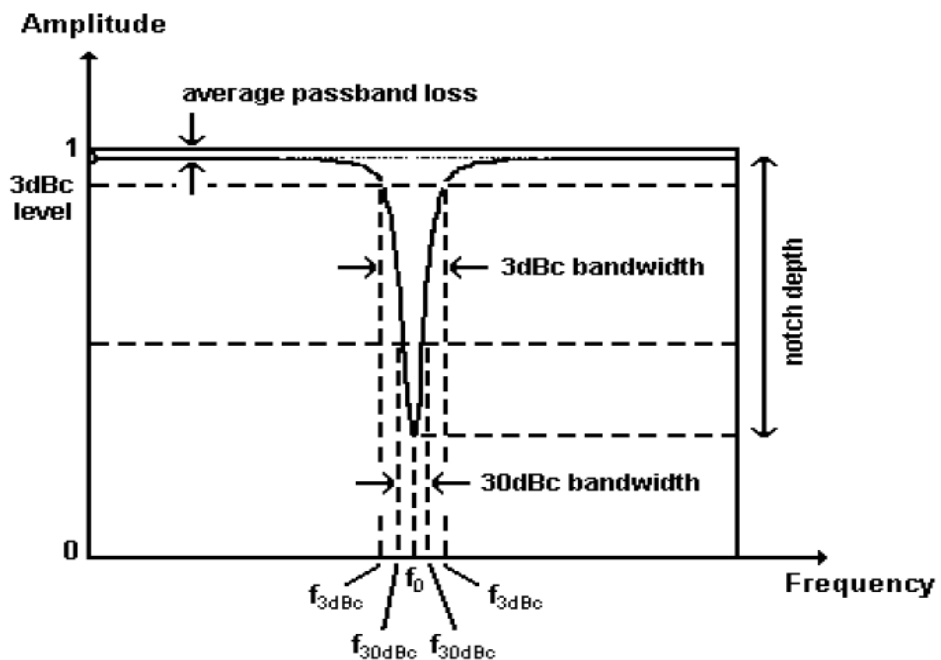
Figure 69 Typical response of a notch filter

The performance of notch filter can be evaluated by following parameters:

- Stop band attenuation level at center frequency
- Notch frequency bandwidth for given attenuation level
- Insertion loss at passband region

CHAPTER 4

DESIGN AND SIMULATION RESULTS FOR FRACTAL BANDPASS FILTERS

4.1 Introduction

This chapter is devoted to the design and simulation of miniaturized microstrip bandpass filters, realized by using Moore, Sierpinski and Hilbert fractal geometries.

The aim of this chapter is to design and simulate a series of miniaturized fractal single-mode and dual mode bandpass filters to be used in many wireless communication applications with different frequency requirements such as (2.4GHz). Furthermore, the effects of edge spacing, additional stub length and another parameters on some resulting fractal filter responses have been discussed and evaluated.

All filter designs presented in this chapter, have been modeled and simulated using available AWR2009 EM simulator package, which performs electromagnetic calculations using the method of moment (MoM) in addition to full-wave based electromagnetic simulator Sonnet software package [108,109].

A bandpass filter requirements usually include the desired center frequency, bandwidth percentage, maximum insertion loss in the passband, and some essential rejection levels in the stopbands. There will also be a specification on the minimum return loss in the passband. The guided wave length (λ_g) is calculated by[1,89,110]:

$$\lambda_g = \frac{c}{f_0 \sqrt{\varepsilon_{eff}}} \tag{4.1}$$

Where λ_g is guided wavelength, c light velocity, ε_r relative dielectric constant, f_0 center frequency and ε_{eff} effective dielectric constant which can be calculated as[1]:

$$\varepsilon_{eff} = \frac{\varepsilon_r + 1}{2} + \frac{\varepsilon_r - 1}{2} \left(1 + \frac{10}{u}\right)^{-ab} \tag{4.2}$$

where $u = w/h$, and

$$a = 1 + \frac{1}{49} \ln\left(\frac{u^4 + \left(\frac{u}{52}\right)^2}{u^4 + 0.432}\right) + \frac{1}{18.7} \ln\left[1 + \left(\frac{u}{18.1}\right)^3\right] \qquad (4.3)$$

$$b = 0.564 \left(\frac{\varepsilon_r - 0.9}{\varepsilon_r + 0.9}\right)^{0.053} \qquad (4.4)$$

The accuracy of this model is better than 0.2% for $\varepsilon_r \leq 128$ and $0.01 \leq u \leq 100$. However, in the present work, effective dielectric constant has been calculated using the approximated equation [111]:

$$\varepsilon_{eff} = \frac{\varepsilon_r + 1}{2} \qquad (4.5)$$

The degree of coupling for space filling structures depends on width to gap ratio of fractal curve strips, which affects resonant frequency of output response[48]. On the other hand, the edge spacing between two resonators and tap position length, can be properly tuned to maximize return loss and minimize insertion loss to optimize frequency response of the filter [112,113]. However, extensive details about this subject are to be presented later in this chapter.

As a drawback, in a real planar resonator, higher levels of fractal iteration imply lower value of microstrip width, thus raising the dissipative losses with a corresponding drop of the quality factor [113,114].

The procedure steps for designing fractal filters using AWR2009 or Sonnet electromagnetic modeling and simulation can be generalized as in Figure **70** and **Figure 71** according to adopted fractal geometry.

AWR2009 and Sonnet simulators are based on method of moment and full wave principle (modified method of moment) respectively, such that they evaluate the filter response by dividing first the resonators in small divisions (mesh), less or more fitted according to the desired accuracy, and then solving a set of linear equations derived from an integral equation. Each filter has been run under specific frequency range and chosen frequency step. Suitable boundary conditions are assigned, and then meshing is carried out on the model to get final refined mesh. In meshing, it is well-known that a finer mesh (more divisions) will give a more precise solution. However, a finer mesh will also require more time for the computer to solve the study. Therefore, it is necessary to decide the proper balance between computation time and an acceptable level of accuracy. The stationary solver (including parametric sweeps) uses a linear solver algorithm for solution determination. The execution has

been performed using Intel(R) Core(TM) i5-3770 @2.67 GHz CPU. Moreover, AWR2009 projects can be exporeted to Sonnet simulator using EXPORT command.
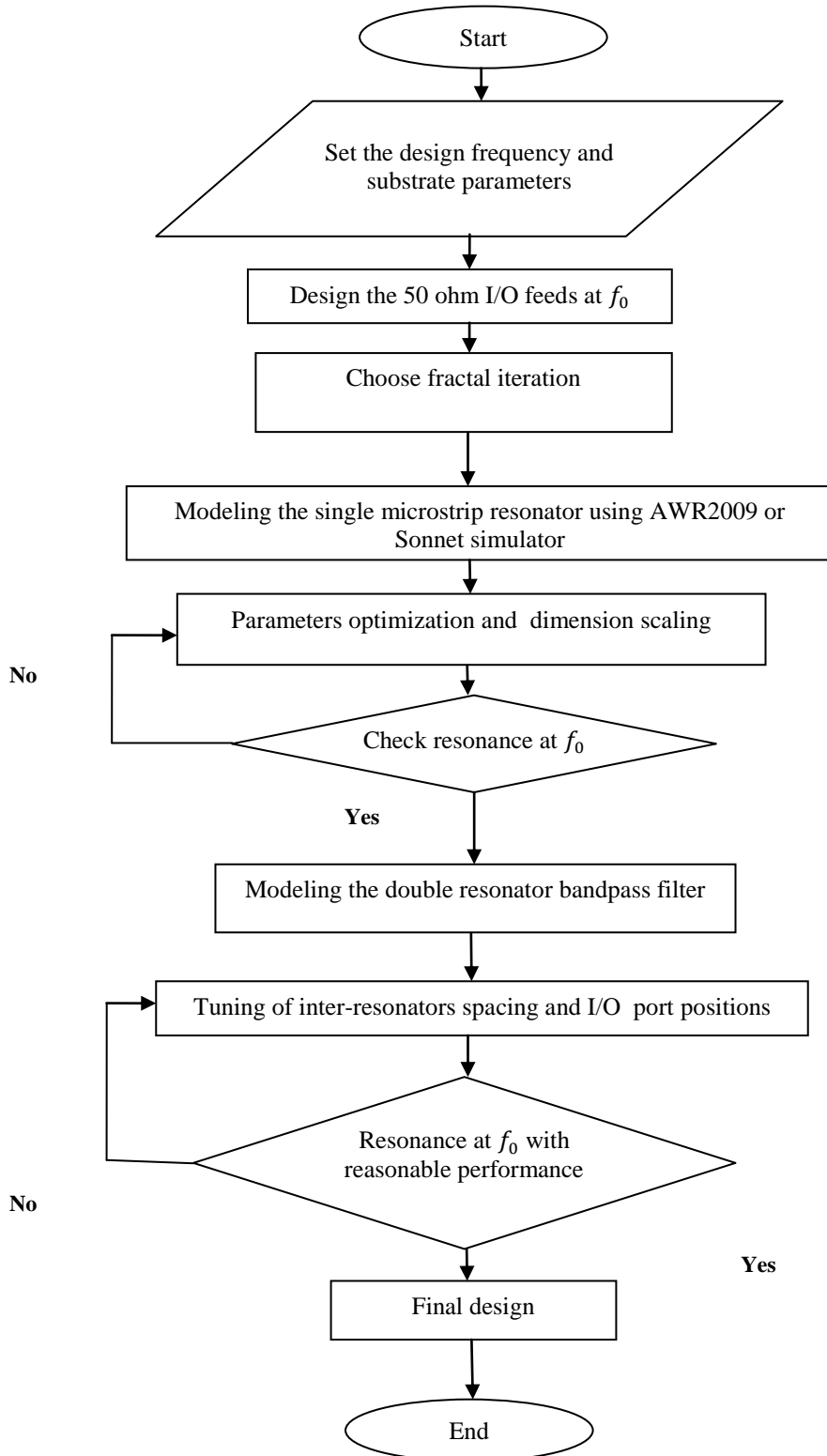
Figure 70   Flowchart for Moore, Hilbert and Peano BPF designs
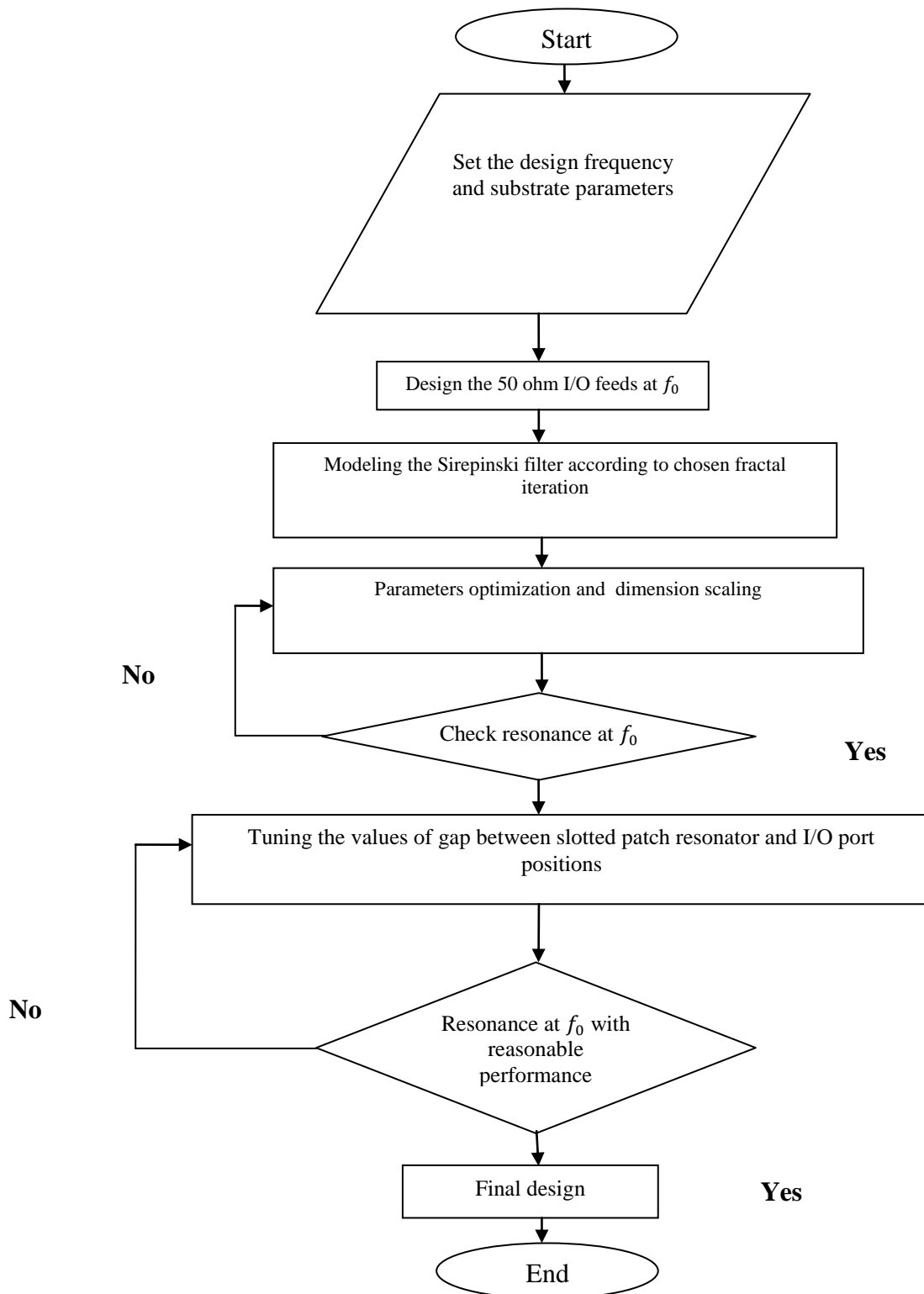
Figure 71 Flowchart for Sierpinski BPF designs

All designed filters in this chapter are based on the first five publications in the "PUBLICATIONS RELATED TO Ph.D THESIS" list in the end of this thesis.

4.2 Design and Simulation Results of Moore Microstrip BPFs

Filter designs using two open-loop ring resonators with non-symmetric tapping feed lines have been created to fabricate compact bandpass filters with high selectivity. The new features for the proposed filters are high levels of miniaturizations and selectivity by applying fractal geometry on the two open-loop resonators. Moore fractal geometry has been selected for this reason because it has substantial space-filling property in addition to the symmetrical open loop structure at each iteration level. The required steps of Moore fractal bandpass filter designs using EM simulator have been illustrated in **Figure 70**.

Firstly, dual edge-coupled Moore resonators based on 2nd iteration level have been implemented at a frequency of 2.4 GHz as in **Figure 72**. The structures of this filter have been etched using RT/Duroid substrate with a relative dielectric constant of 10.8 , substrate thickness of 1.27 mm and conductor metal thickness of 35 μm by using the standard mask etching technique. The resultant filter dimensions have been found to be 12.9×6.1 mm^2 with w= 0.4 mm, g =1.5 mm, q =0.5 mm, x =1.3 mm and y =1.5 mm. The coupling gap between the two resonators (d) is of 0.7 mm while I/O feeder lengths are 1.75 mm.

These procedural steps have been repeated with a microstrip bandpass filter based on the 3rd iteration of Moore fractal resonators, designed at the same frequency and using the same substrate specifications. **Figure 73** explains the configuration of this microstrip bandpass filter. This filter possesses total dimensions of 9.68× 4.64 mm^2 with w= 0.405 mm, g =0.2 mm, q =0.45 mm, x =0.2 mm, y =0.2 and d =0.4 mm. The 50 ohm I/O feeder lengths are 1.1 mm.

Filter topologies, shown in **Figures 72** and **73**, have been modeled and analyzed using EM Sonnet Simulator. The resultant simulated responses of return loss, S11, and transmission, S21, for these filters are illustrated in **Figures 74** and **75** respectively. It is apparent that the resultant bandpass filters based on 2nd and 3rd iteration of Moore fractal geometries present a quasi-elliptic transmission response

with transmission zeros that are somehow symmetrically postioned around the design frequency near the passband edges. It is obvious from these simulation results that the performance response does not support harmonics that normally accompany the bandpass filter response.

Relating to this issue, some adjustments in the filter structure can excite these harmonics to generate multiband bandpass response. However, this subject is out of the scope of this study to construct miniaturized bandpass filter. Furthermore, the higher harmonics levels implemented by the 3rd iteration fractal based filter is less than those of the filter based on the 2nd iteration. This dissimilarity in the out of band levels(the upper stopbands) is mainly attributed to the positions of the tapping positions and the coupling gap between the two resonators of the two filter structures. This confirms the results reported in   [89,115], since these factors influence the electromagnetic couplings between the two resonators. The percentages of fractional bandwidths for 2nd and 3rd iteration Moore BPFs are of 5% and 3.75% which are in theory within narrow band ranges.
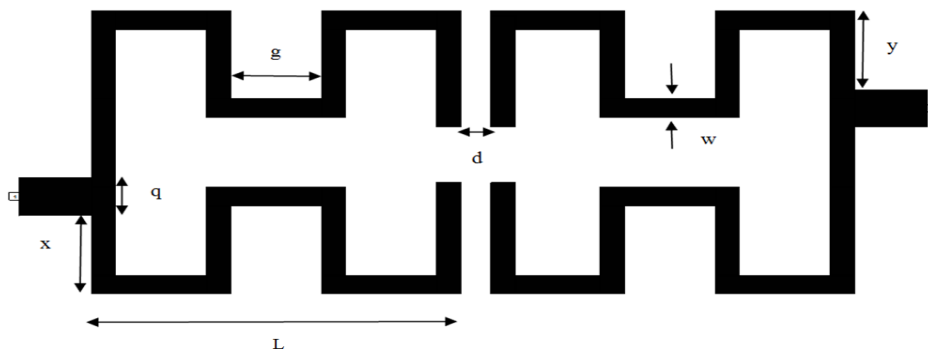
Figure 72 The modeled layout of 2nd iteration Moore fractal BPF at w =0.4 mm and g=1.5 mm
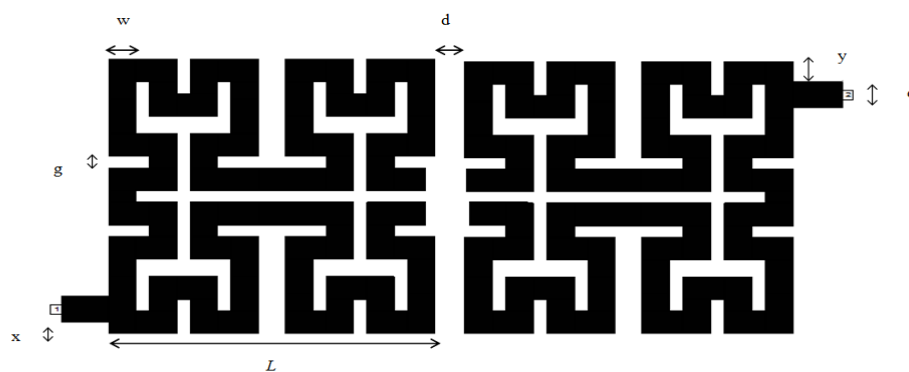
Figure 73 The modeled layout of 3rd iteration Moore fractal BPF at w =0.4 mm and g=0.2 mm
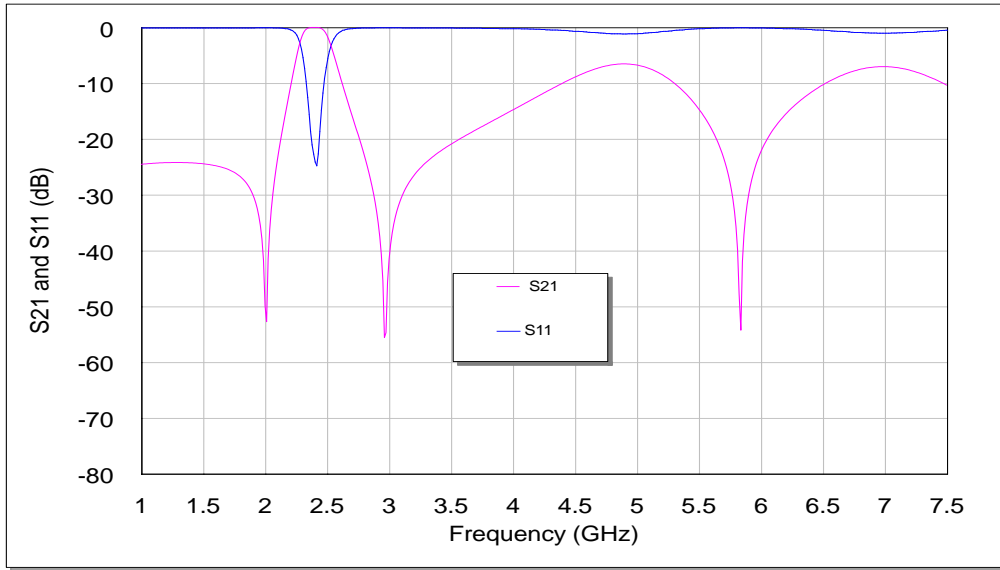
Figure 74 The return loss and transmission responses of 2nd iteration Moore BPF designed for 2.4 GHz
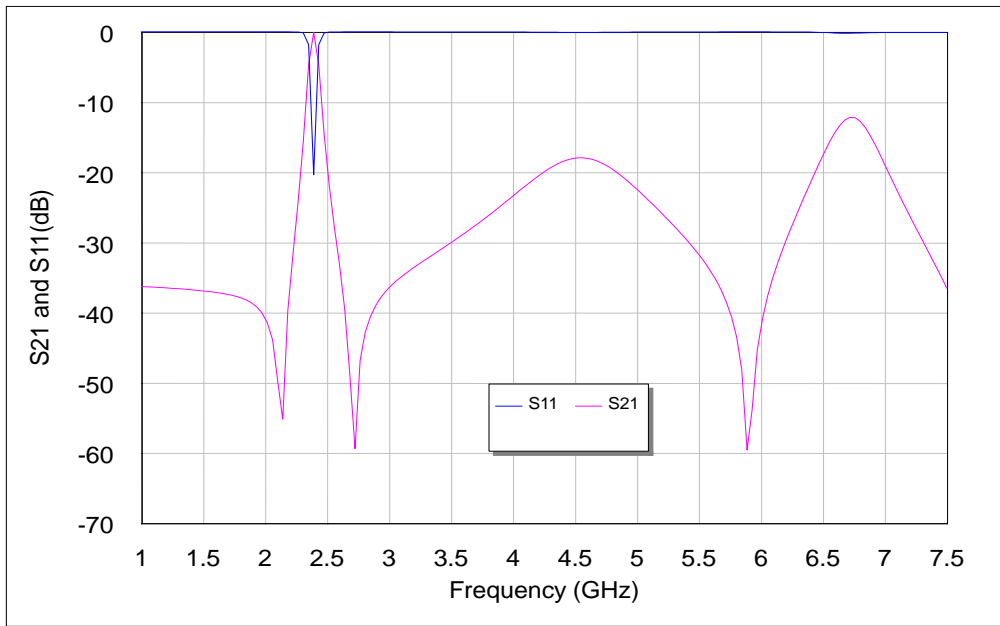
Figure 75 The return loss and transmission responses of 3rd iteration Moore BPF designed for 2.4 GHz

Table 4 gives an idea about the modeled Moore filter dimensions and main result parameters of BPF responses as designed for 2.4 GHz applications. These parameters contain dimensions of proposed filters, insertion loss, return loss and bandwidth.

A critical problem in the miniaturization of passive resonators and filters originates from the reality that resonating structures have to involve definite size relative to the guided wavelength, λ_g, which is evaluated, at the design frequency, by equation (4.1).

From equation (4.5), the effective dielectric constant ε_e = 5.4 and guided wavelength λ_g = 53.79 mm have been determined at frequency f = 2.4 GHz. According on these computations, the overall dimensions in terms of λ_g are to be of

$(0.24\lambda_g$ x $0.11\lambda_g)$ and $(0.18\lambda_g$ x $0.086\lambda_g)$ for 2nd and 3rd Moore bandpass filters respectively.

The size lessening percentages of 3rd iteration Moore BPF with respect to the 2nd iteration one is about 43%.

Parameter	2nd Iteration	3rd Iteration
Side Length (L), mm	6.1	4.64
Occupied Area, mm^2	78.69	44.9152
Return loss , S$_{11}$ (dB)	-23.9	-20.5
Insertion Loss (dB)	-0.1	-0.155
Bandwidth(MHz)	120	90

Table 4 The Dimensions and Electrical Specifications of Moore BPFs

It is significance to point out that these filters can be modeled for other operating frequencies according to given system requirements by using dimensions modifications as notified in design flow chart of **Figure 70** using appropriate w and g values that manage the side length, L, of fractal resonators. For example, resonance at 1.7 GHz design frequency has been acquired by selecting w = 0.5 mm

and g = 0.3 mm that make L = 6.1 mm for 3rd iteration Moore BPF under same substrate specifications.

Based on the specified specifications, the filter bandwidth could be controled under same iteration level and design frequency. This is performed by estimating the w/g ratio in such a manner to vary L to some extent (not quite different) using suitable scaling. For instance, 40 MHz bandwidth has been obtained via the EM simulator by opting w = 0.5 mm and g =1.3 mm which produces L =5.9 mm for 2nd iteration Moore BPF under same frequency, 2.4 GHz, and substrate requirements.

The design frequency and bandwidth tunings in this study have been also approved for fractal resonators reported in [24,116]. The coupling gap between the two resonators, d, as in **Figures 72** and **73** and Input /Output feeder locations can be absolutely adjusted to reduce insertion loss and increase return loss so as to improve frequency response of the filter as much as possible .

The implemented fractal filters have noteworthy lower insertion loss and greater return loss magnitudes as compared with Hilbert and Minkowski-like fractal BPFs depicted in [41] and [42] respectively under same design frequency and substrate specifications. In addition, these two pole fractal bandpass filters are more minaturized than dual-mode Minkowski and Koch-like pre-fractal BPFs depicted in [42] and [117] respectively designed at the similar resonant frequency and using a substrate with the similar specifications. However, it is estimated that, further size reduction can be achieved for the filter structure related to the 4th iteration of the proposed fractal generation process in the case of no practical constraints.

With the intention of geting close into the nature of current distributions of the proposed filters, simulation graphs for the surface current distributions at two operational frequencies, 2.4 GHz (the center frequency) and 2.7 GHz (in the stopband region), are described in **Figures 76** and **77** respectively. In these figures, the red color points to the uppermost coupling effect while the blue color means the least one. As it can be observed, the current distributions at 2.4 GHz and 2.7 GHz are highly different and they are dimensioning themselves as 2nd and 3rd iteration Moore fractal geometries.The highest surface current densities can be seen at the center frequency, which indicates that low losses are exist and the desired resonant frequency is within upper excitation condition. In contrast, the minimum current densities can be perceived at 2.7 GHz in rejectband region . In this case, weakest

coupling can be seen, which is given by the truth that Moore BPFs are not enough being induced and, therefore, offer a physically powerful rejection in an otherwise passband structure.

Also, the maximum current densities are quite focused in only one resonator of each Moore BPFs corresponding to 2nd and 3rd iteration at both frequencies. This might clarify the suppression of higher harmonics in out of band regions.

(a)

(b)
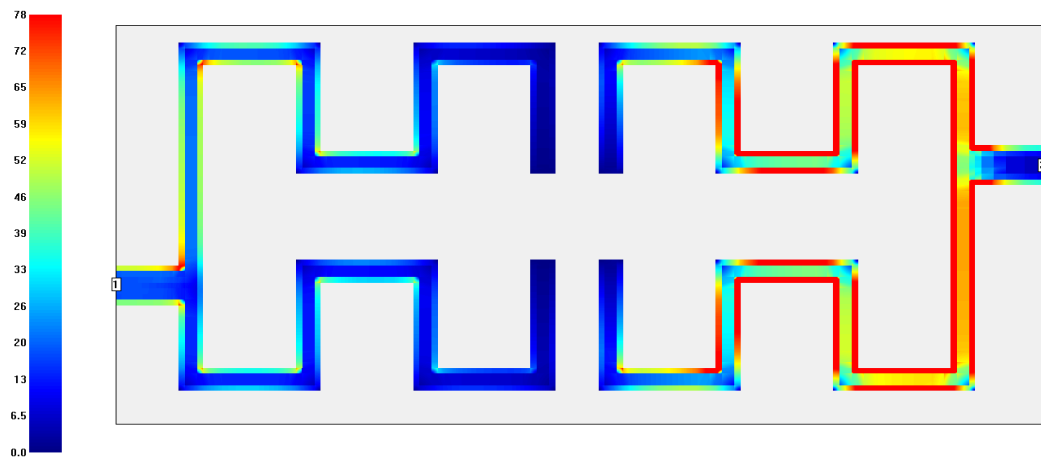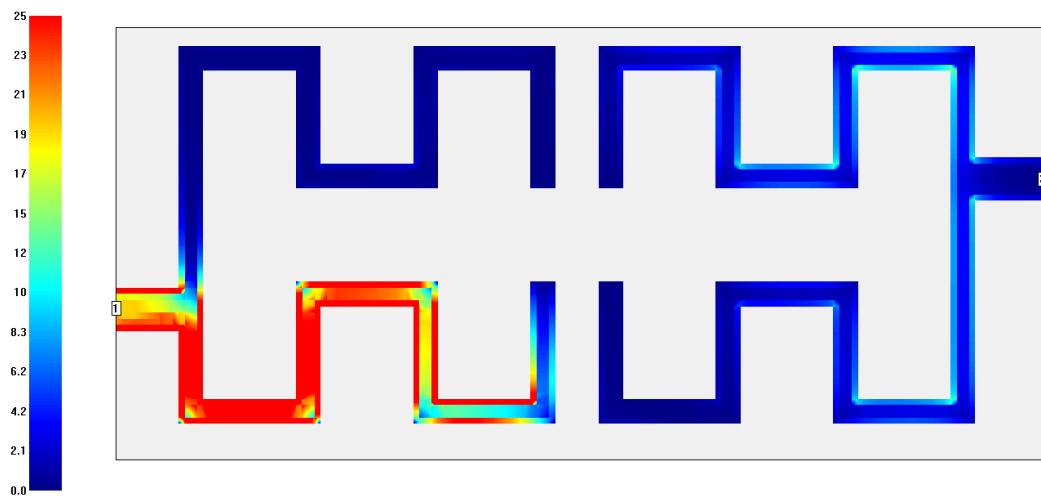
Figure 76 Simulted current density distributions of the 2nd iteration Moore microstrip BPF (a) at 2.4 GHz and (b) at 2.7 GHz

(a)

(b)
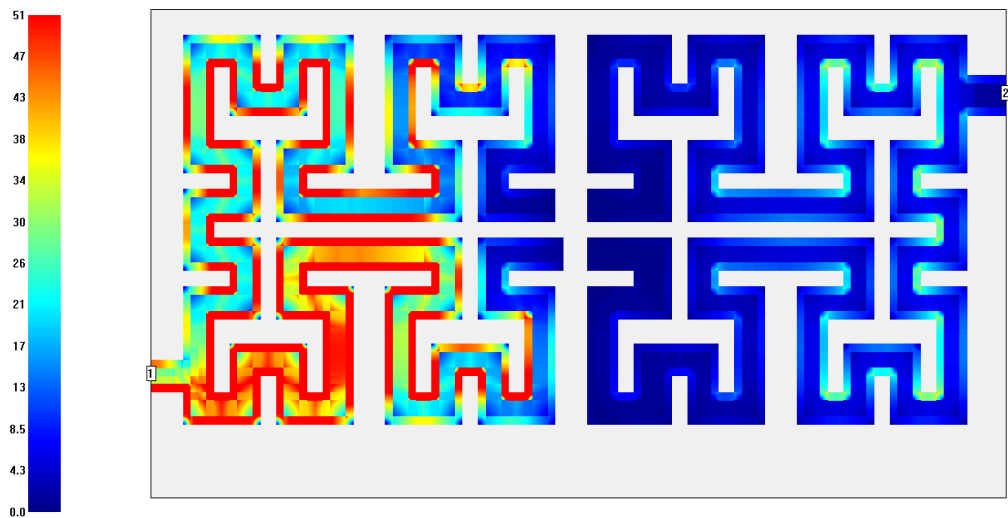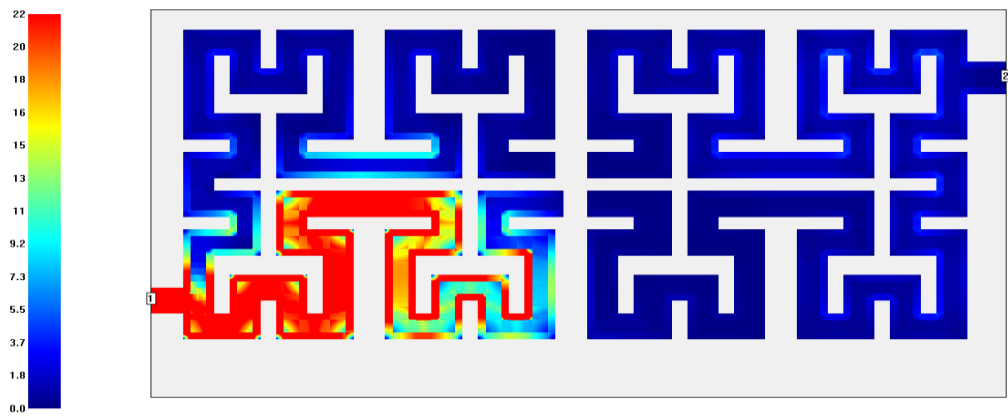
Figure 77 Simulted current density distributions of the 3rd iteration Moore microstrip BPF (a) at 2.4 GHz and (b) at 2.7 GHZ

The photographs of manufactured filter prototypes based on the 2nd and 3rd iteration Moore fractal geometries are illustrated in **Figures 78** and **79** respectively. The output performances of these fabricated filters have been evaluated using HP8720C vector network analyzer.

Figure 78 Graph of produced 2nd iteration Moore fractal BPF

85
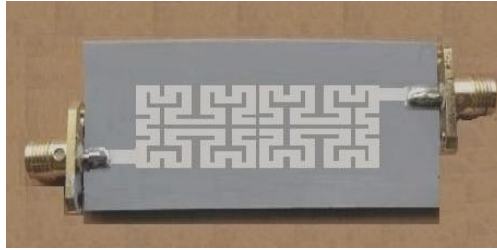
Figure 79 Graph of produced 3rd iteration Moore fractal BPF

Figures 80 and **81** show measured and simulated out-of-band S21 responses of 2nd and 3rd iteration fractal filters respectively, while measured and simulated return loss S11 responses for same filters are shown in **Figures 82** and **83** respectively. In the measured and simulated results, only single pole comes into view in the passband despite the filters are of 2nd order. This is because the output responses are shown through a large swept frequency range, and the passband only takes up a tiny section of the shown frequency range. If the results are viewed thtough a narrow swept frequency range, additional facts all through the passband, including the two poles, will start to come into sight. The experimental return loss values are 15.5 dB and 17 dB for 2nd and 3rd iteration Moore fractal BPFs respectively while the experimental insertion loss values are better than 1 dB for both fractal filters. Consequently, the measured and simulated results are a little different. This small discrepancy might be related to tolerances in the substrate requirements and in manufacture process, where the gap between the two resonators and the tapping feed line locations have huge effect on the overall coupling required to obtain the desired filter response. However these results have high-quality of conformity.
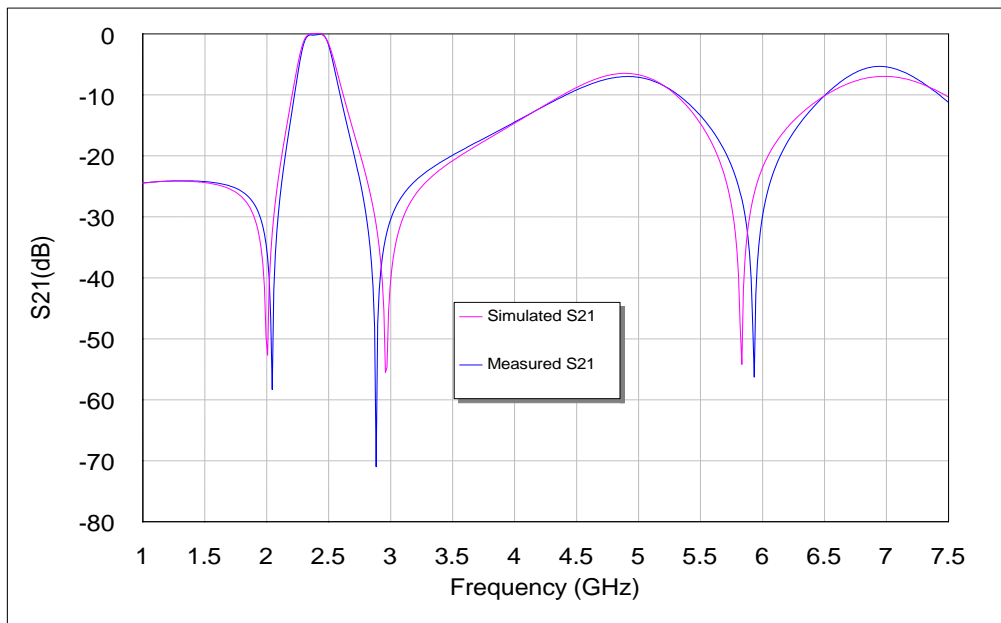
Figure 80 Simulated and measured out-of-band S21responses of the proposed filter based on 2nd iteration Moore curve geometry
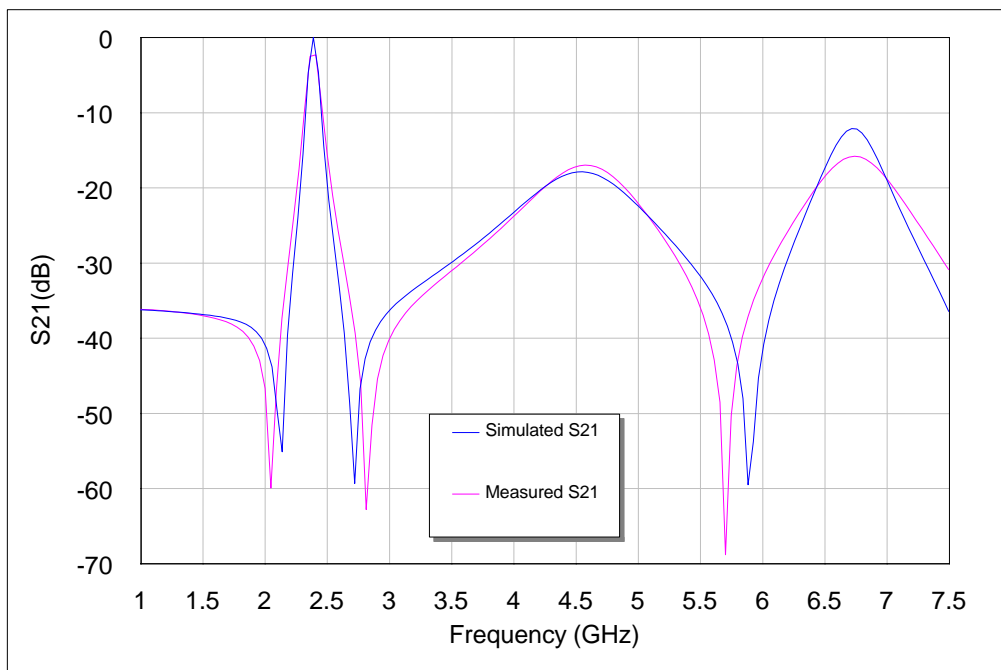
Figure 81 Simulated and measured out-of-band S21 responses of the proposed filter based on 3rd iteration Moore curve geometry
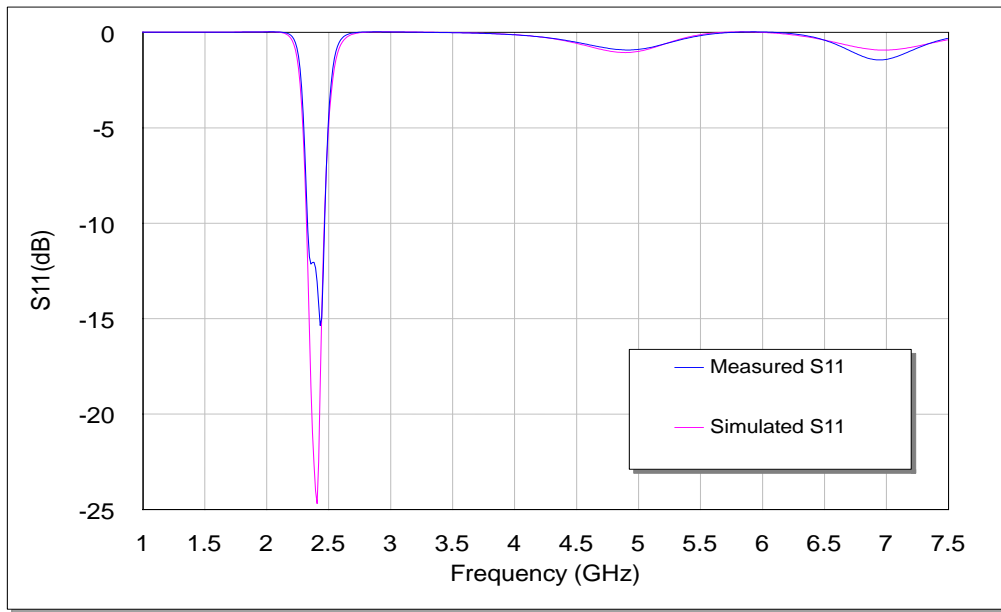
Figure 82 Simulated and measured S11 responses of the proposed filter based on 2nd iteration Moore curve geometry
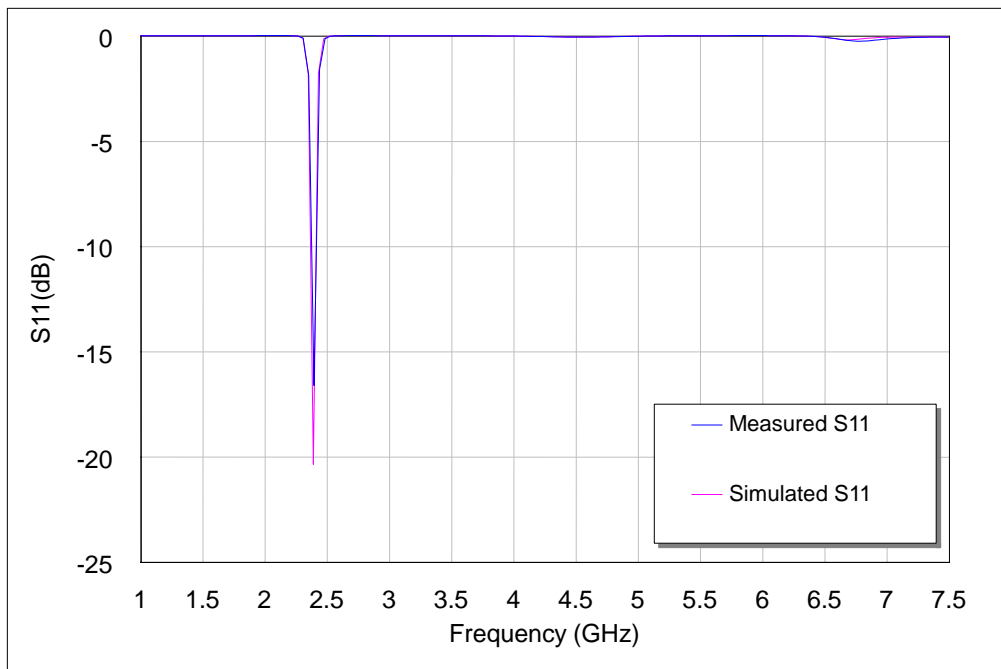
Figure 83 Simulated and measured S11 responses of the proposed filter based on 3rd iteration Moore curve geometry

The degree of coupling effect depends on width strip and spacing between strips values of Moore fractal curve, which affects the performance of output frequency response due to changing in overall strip length and hence the side length of fractal shape .

Figures 84 and **85** verify the effects of changing w and g on these filters. The variation of these parameters is not only varying the resonant frequency and insertion loss, but also shifting the locations of the transmission zeros that control the attenuation levels for these filters.
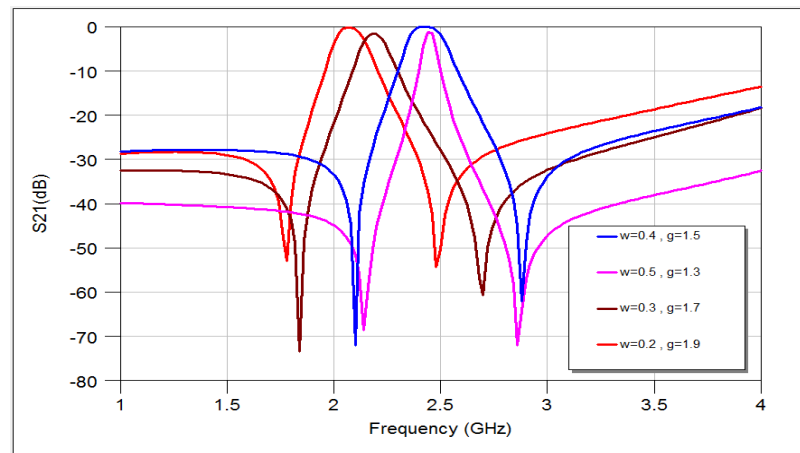
Figure 84 The transmission responses of the resulting 2nd iteration fractal microstrip bandpass filter of different w and g values
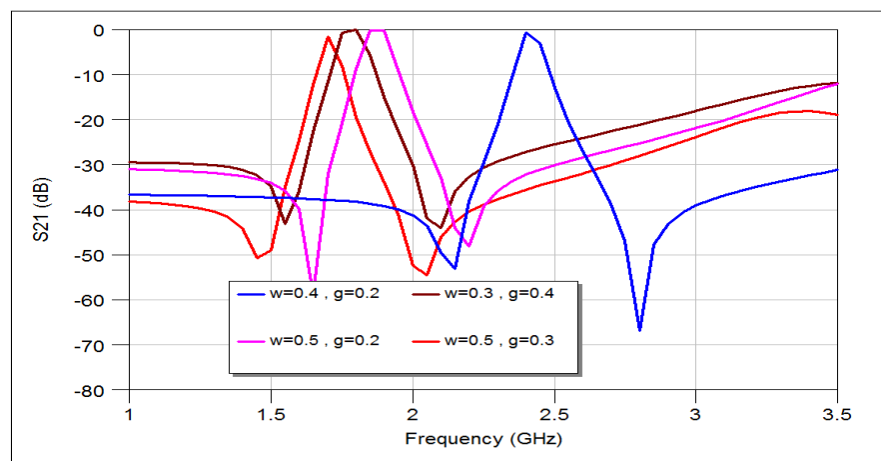
Figure 85 The transmission responses of the resulting 3rd iteration fractal microstrip bandpass filter of different w and g values

4.3 Design and Simulation Results of Sierpinski Bandpass Filters

All designed Sierpinski filters in this section are based on the second publication in the "PUBLICATIONS RELATED TO PhD THESIS" list in the end of this thesis which is published in 2012.However, after two years of this publication, an extensive parametric study on our proposed Sierpinski filters has been reported in the publication entitled with "*New Kinds of Fractal Iterated and Miniaturized Narrowband Bandpass Filters for Wireless Applications*" done by V.Soni and M. Kumar which is indexed in ieee Xplorer in 2014.

The initial pattern for the presented bandpass filter as a fractal is a square patch with a side length *L*. The inserted slotted structures are then based on Sierpinski carpet. This fractal geometry shown in **Figure 86**, is a uniform fractal which is a generalization of the Cantor set into two dimensions. The Sierpinski carpet is formed comparablely to the Sierpinski gasket, but it employs squares instead of triangles. The steps are, begin with a solid (filled) square **C(0)**. Divide this into 9 smaller similar squares. Eliminate the interior of the center square to get the first iteration, i.e., **C(1)**. Now subdivide each of the eight remaining solid squares into 9 similar squares and remove the center square from each to get **C(2)**. Stay in this manner with the construction to obtain a decreasing sequence of similar sets.

The Sierpinski carpet is the connection of all the sets in this sequence, that is, the set of points that continue after this construction is repeated infinitely. **Figure 86** shows the first four iterations. The squares in red represent some of the smaller similar squares used in the construction, which are then combined relatively to the black ones.

The ideal fractal structure is obtained by iterating infinite number of times. However, it has been concluded, in practice, that the number of generating iterations should be limited to only a few, before additional complexities arise [44].
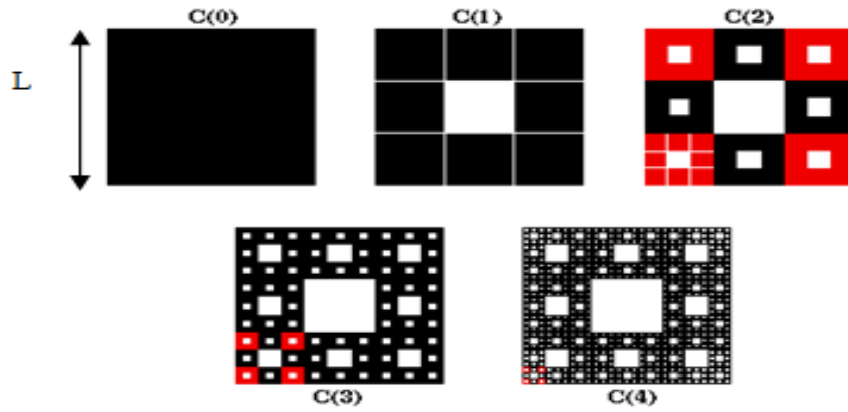
Figure 86 The generation process of the Sierpinski fractal geometry iterations from **C(0)** to **C(4)** where **C(0)** is zeroth iteration ,**C(1)** is the first iteration and so on.

Up to third iteration, i.e., **C(3)**, dual-mode single microstrip patch bandpass filter structures have been designed at $f = 5.33$ GHz. It has been presumed that, these filter structures have been etched using a substrate with a dielectric constant of $\varepsilon_r = 10.8$ and thickness of 1.27 mm. The side length of the square patch resonator, $L = 9$ mm, has been calculated from

$$L = 0.4\lambda_g \tag{4.7}$$

Generally in degenerate dual-mode case, the bandpass filter response can be gained through the induction of the two degenerate modes by input output feed lines and setting the coupling between the two modes by inserting appropriate form of perturbation within the resonators. In this design, small perturbations are applied to each dual-mode resonator, at locations that are assumed at an angle 45^0 offset from its two orthogonal modes. These perturbations are in the shape of a small square patch with a side length *d*, added to the upper right corner of the conventional square patch as illustrated in **Figure 87**, and in other subsequent iterations resonators of **Figures 89,91,93**. For coupling requirements of the orthogonal modes, the perturbations could also have forms other than this shape. But since the proposed resonating structures are described by their diagonal symmetry, this shape of perturbation is the most fitting to satisfy the required coupling [42,81,88]. The dimensions of the perturbations of each filter must be scaled for the required filter

performance, since the behaivor and the strength of the coupling between the two degenerate modes of the dual-mode resonator are primarily evaluated by the perturbation's size and shape.

A dual-mode filter structure based on the conventional square patch resonator, and three filter structures based on resonators having the shapes of the first three iterations of **Figure 86**, have been modeled and analyzed at operating frequency of 5.33 GHz using a full-wave based electromagnetic simulator from Sonnet Software Inc. These filter structures are shown in **Figures 87,89,91** and **93** respectively. The corresponding simulation results of return loss S_{11} and transmission S_{21} responses of these filters are plotted in **Figures 88,90,92** and **94** respectively. Comparing the insertion losses, S_{21}^0, which are peaks of transmission responses and bandwidths at -3dB in **Figures 90,92** and **94** with those of **Figure 88** , it is seen that the bandpass filters with iterations offer better performance than conventional dual-mode square patch resonator. This way, they have narrower bandwidth and lower insertion loss as compared to conventional filter of **Figure 87**. It is also worth pointing out that the fractal filters iteration levels **C(1)** to **C(3)** have less symmetrical transmission zeros as compared to conventional resonator. **Table 5** explains the resultant simulated parameters for designed filters.
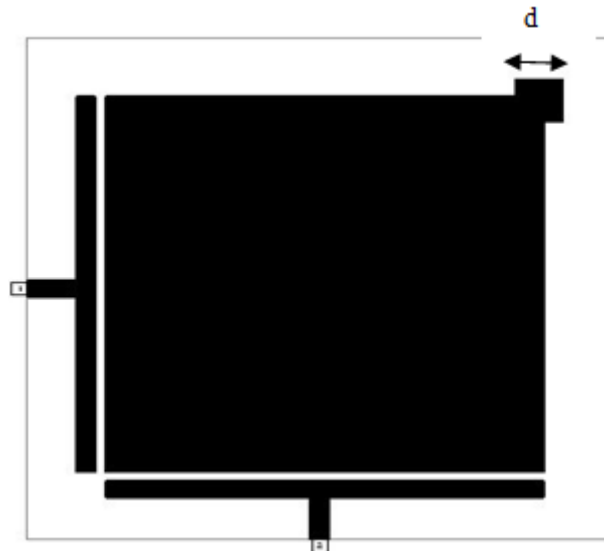
Figure 87 The layout of the modeled conventional dual-mode square patch microstrip resonator at d =1mm

As shown in **Figures 95,96** and **97**, increasing d, the side length of small perturbation square patch at the right top corners in **Figures 89,91** and **93** causes S21 first to move rapidly upward toward the ideal 0dB point and then split into two visible peaks. Ideally there would be no coupling between the two modes at d = 0 mm.

It is seen from these figures that the splitting of frequency between the two modes and the coupling effect are increased as the perturbation size d, is increased.

Simulation graphs show that the modeled bandpass filters possess good performance curves. As it can be seen, all filter responses exhibit dual transmission zeros that are located around the design frequency. The offered filter designs can readily be changed to other frequencies required for other wireless communication systems. In this case, the resulting new filter will be of greater or lower in size according to the frequency requirements of the specified applications.
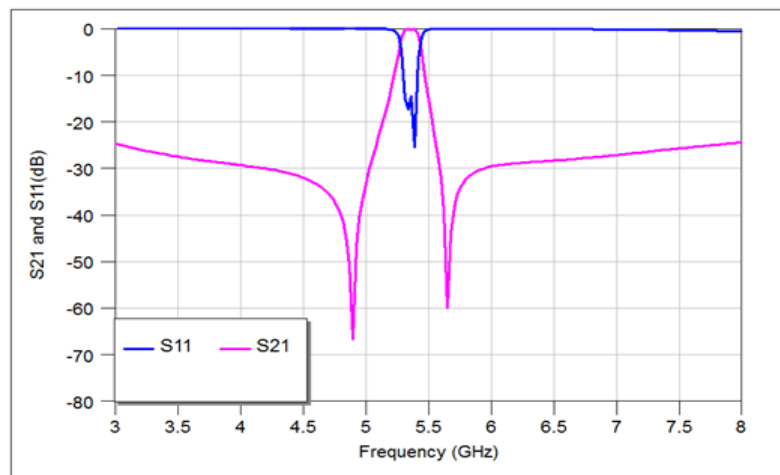
Figure 88 Return loss, S11, and transmission , S21 , responses of the conventional square patch microstrip bandpass filter shown in **Figure 87**
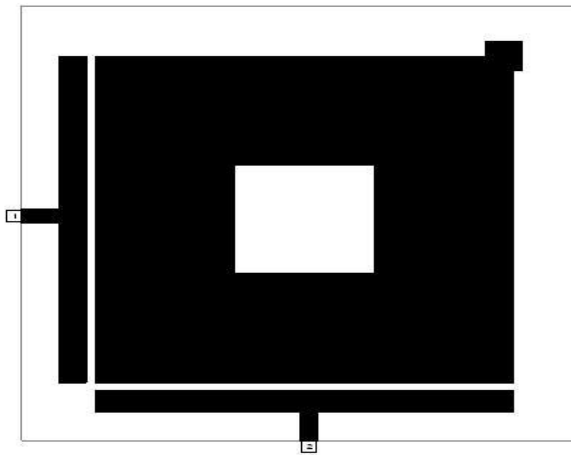
Figure 89 The layout of the modeled first iteration dual-mode Sierpinski patch microstrip resonator at d =0.8 mm
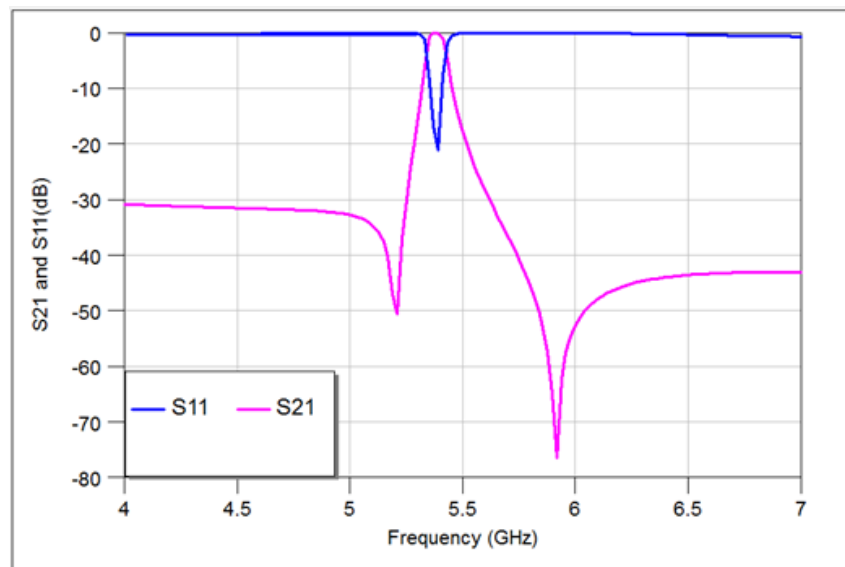
Figure 90 Return loss, S11, and transmission , S21, responses of the first iteration Sierpinski patch microstrip resonator filter shown in **Figure 89**

It is envisaged that the proposed fractal shape resonator may become a good-looking structure for developing minaiturized and good performance bandpass filters for modern wireless networks.
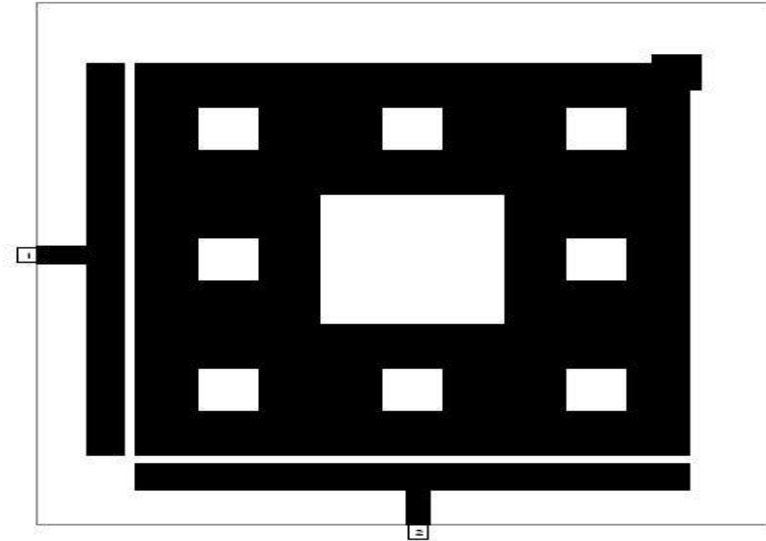
Figure 91 The layout of the modeled second iteration dual-mode Sierpinski patch microstrip resonator at d = 0.8 mm.
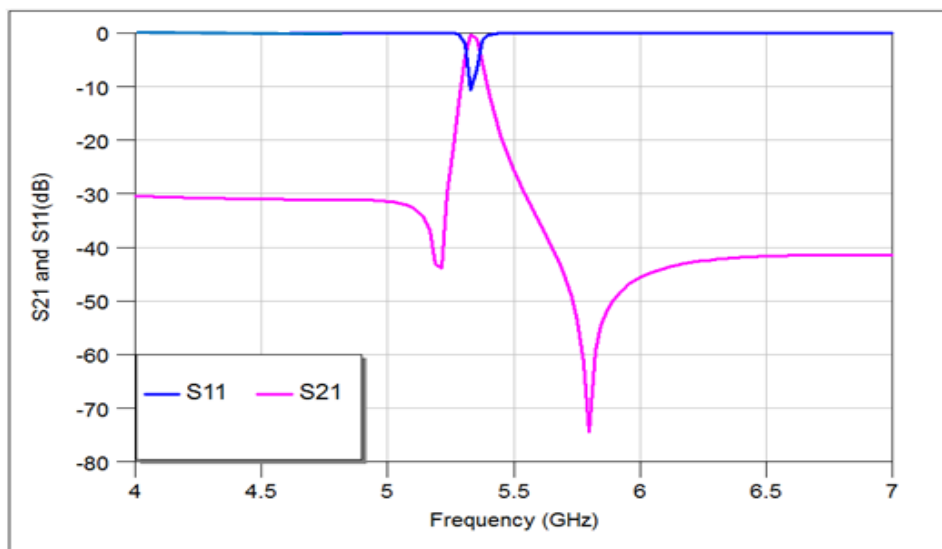
Figure 92 Return loss, S11, and transmission , S21, responses of the second iteration Sierpinski patch microstrip resonator filter shown in **Figure 91**

The proposed technique can be considered as a flexible design tool for compact microstrip bandpass filter for various wireless communication systems.
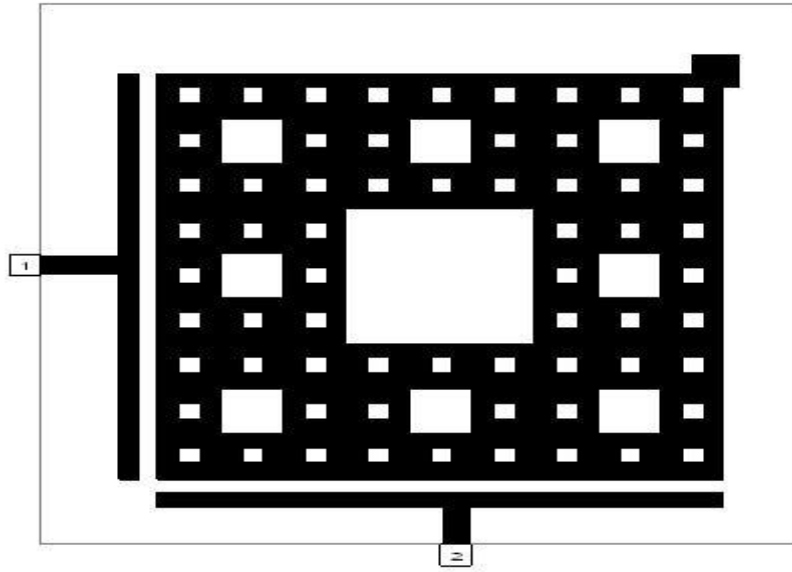
Figure 93 The layout of the modeled third iteration dual-mode Sierpinski patch microstrip resonator at d =0.7 mm
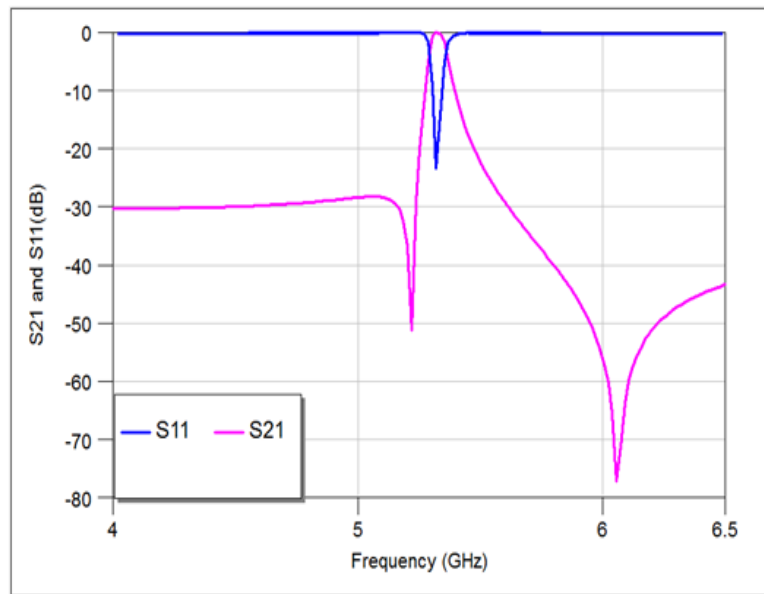
Figure 94 Return loss, S11, and transmission, S21, responses of the third iteration Sierpinski patch microstrip resonator filter shown in **Figure 93**

Type Parameter	C(0)	C(1)	C(2)	C(3)
Return Loss (dB),S11	-25.4	-21.2	-10.7	-23.3
Insertion Loss (dB),$S21^{0}$	-0.13	-0.0649	-0.098	-0.028
Actual Bandwidth at-3dB (MHz)	160	60	50	75

Table 5 Summary of The Simulated Parameters of The Modeled Filters
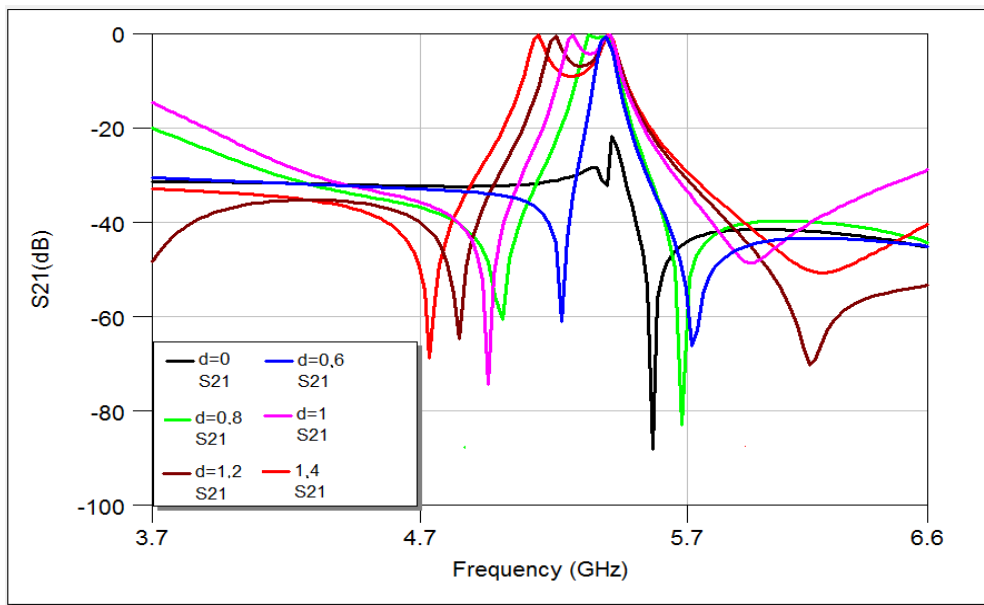
Figure 95 Simulated transmission responses, S21, of the first iteration Sierpinski fractal bandpass filter as a function of d in units of mm
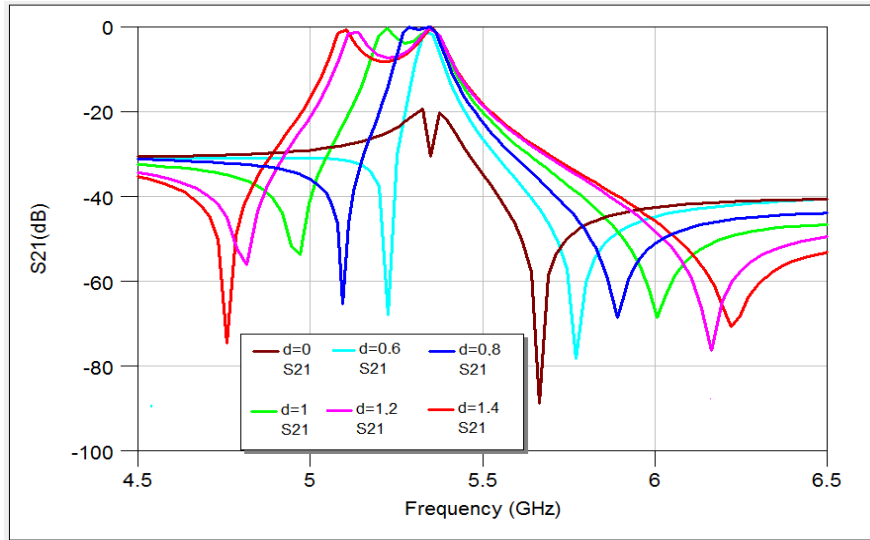
Figure 96 Simulated transmission responses, S21, of the second iteration Sierpinski fractal bandpass filter as a function of d in units of mm.
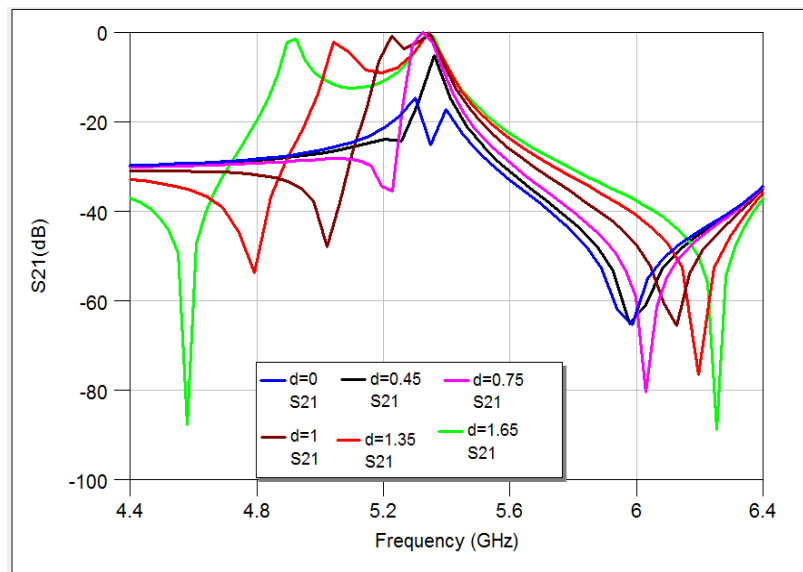
Figure 97 Simulated transmission responses, S21, of the third iteration Sierpinski fractal bandpass filter as a function of d in units of mm.

4.4 Design and Simulation Results of Stepped Impedance Hilbert Fractal Bandpass Filters

Step impedance resonators (SIR) is a non-uniform transmission line, which were used in the filter design either for miniaturization purposes, or shift the spurious passband to the higher frequency, or to suppress the harmonic frequencies [119].The

SIR employed in this section was shown in **Figure 98**, it is made of two transmission line sections with two different characteristic impedances Z_1 and Z_2 with corresponding electrical lengths **x** and **y**, respectively. The input admittance that viewed from an open end can be calculated by[120] :

$$Y_{in} = \frac{2\, j\, Y_2\, (K\, K_1 + K_2)(K - K_1\, K_2)}{K(1 - K_1^2)(1 - K_2^2) - 2(1 - K^2)K_1\, K_2} \qquad (4.8)$$

Where $K_1 = \tan(x/2)$, $K_2 = \tan(y)$ and $K = Z_2 / Z_1$.
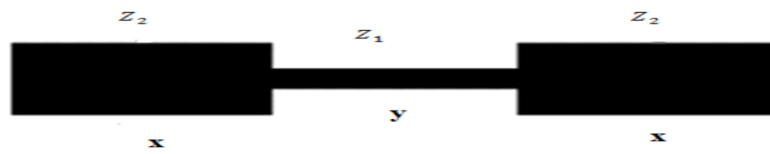
Figure 98 Schematic of the employed two-sections SIR

Stepped impedance filter configurations based on 1st and 2nd iteration Hilbert fractal geometries depicted in **Figures 99** and **100** consist of two resonators with asymmetric feed lines tapping the resonators. The coupling between the two open ends of the resonators takes place through the gap capacitance represented by the spacing d. Each resonator represents a single pole resonant circuit. Then the resulting two resonator bandpass filters will have two poles. The filters presented in this section over perform those reported in [89,115] respectively. In the present study, to design more compact bandpass filter, two miniaturization techniques have been applied to the hairpin resonators. The first is the application of fractal geometry and the second is the use of the SIR technique.
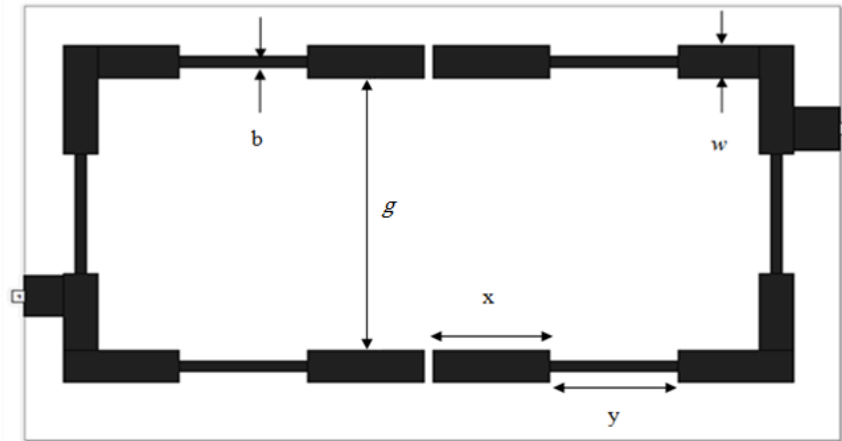
Figure 99 The modeled layout of 1st iteration two Hilbert resonators with SIR BPF
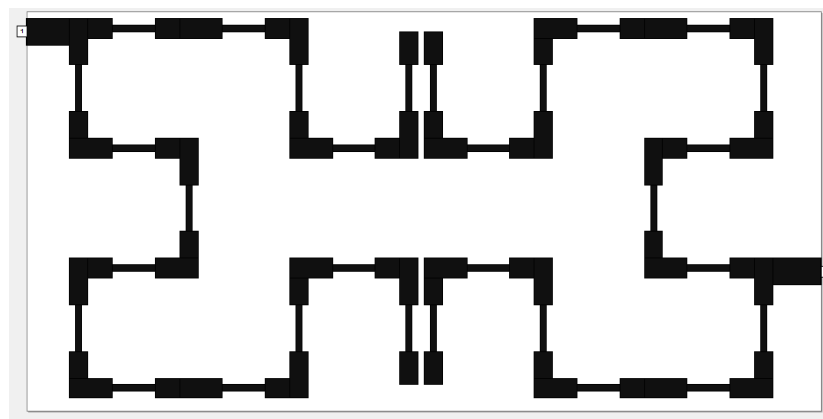
Figure 100 The modeled layout of 2nd iteration two Hilbert resonators with SIR BPF

In addition to the dimensional scaling of the modeled resonator, to reach to design frequency, other parameters play an important role as optimization factors in filter performance. These parameters are the spacing between the adjacent resonators and I/O feed line tap positionss. Parametric study to explore the effects of values of these parameters on the resulting filter performance, will lead to minimum insertion loss and maximum return loss at the design frequency. In this study, we have used 1st iteration bandpass filter as explanation example for adopted optimization process as it can be seen from **Table 6** and **Table 7**.

Parameters	d=0 mm	d=0.13mm	d=0.33mm	d=0.53mm
S_{11} (dB)	....	-12.71	-4.196	-0.316
Insertion Loss(dB)	....	-0.33	-2.079	-10.591
Band Rejection levels(dB)	....	--90.07, -70.557	-78.863, -88.868	-87.678, -95.353

Table 6 Summary of The Simulated Parameters of The Modeled Filters

Parameters	S_{11} (dB)	Insertion Loss (dB)	Band Rejection levels(dB)
P=q=0 mm	-0.755	-7.95	-74.331, -77.271
P=q=3.8 mm	....	....	....
P=q=1.4 mm	-1.748	-4.81	-78.672, -73.793
P=2 mm and q=2.2 mm	-3.29	-2.66	-72.315, -73.324
P=2.8 mm and q=3 mm	-12.71	-0.33	-90.07, -70.557

Table 7 Summary of Simulation Result Parameters of 1st Iteration Stepped Impedance Hilbert BPF with Respect to p and q Values

Filter structures, presented in **Figures 99** and **100**, have been modeled and analyzed at an operating frequency, in the ISM band, of 2.4 GHz using AWR2009 simulator. These filter structures have supposed to be etched using a substrate with relative dielectric constant of 9.6 and 0.508 mm in thickness. The resulting filter dimensions based on first iteration of Hilbert fractal geometry have been found to be 18.29×9.79 mm^2 with w= 0.9 mm ,g =7.5 mm , b =0.3 mm ,x =3 mm and y =3.11 mm. On the other hand, The dimensions of the fractal filter based on second iteration are found to be 11.5× 5.7 mm^2 with w= 0.3 mm , =0.8 mm , b =0.1 mm , x =0.7 mm and y =0.7 mm except in the up and bottom terminals nearby edge spacing coupling where y reduced to 0.4 mm to resonate at the design frequency.The resonators are directly coupled to the I/O through 50 Ω microstrip feed lines with asymmetric tap positions. The performance of the modelled filters, in terms of the return loss S11

and the transmission S21 responses, has been evaluated within swept frequency range from 1 to 5 GHz in order to monitor the filter out-of-band response and the level of the possible second harmonics.

A parametric study has been conducted to explore the most effective filter parameters on the filter responses. These parameters include the coupling gap spacing and the I/O feed line tap positions.

Figures 101 and **102** show the resulting S11 and S21 responses corresponding to different values of the spacing (d) between the two resonators, for the 1st iteration Hilbert fractal based filters. **Table 6** shows the results of the modeled Hilbert filter with edge spacing as a parameter with d=0 mm, 0.13 mm, 0.33 mm and 0.53 mm. It is clear, in both figures and **Table 6**; there is non-desired output frequency response in the case of d=0 mm, while its effect is more noticeable on the transmission zeros, return loss, insertion loss on the frequency responses of d=0.13, 0.33 and 0.53 mm. However, the results imply that the gap spacing affects the position of the transmission zero on the right side of the passband slightly more than that of the left of the passband. An optimal response can be found at d=0.13 mm since it has lowest insertion loss and highest return loss.
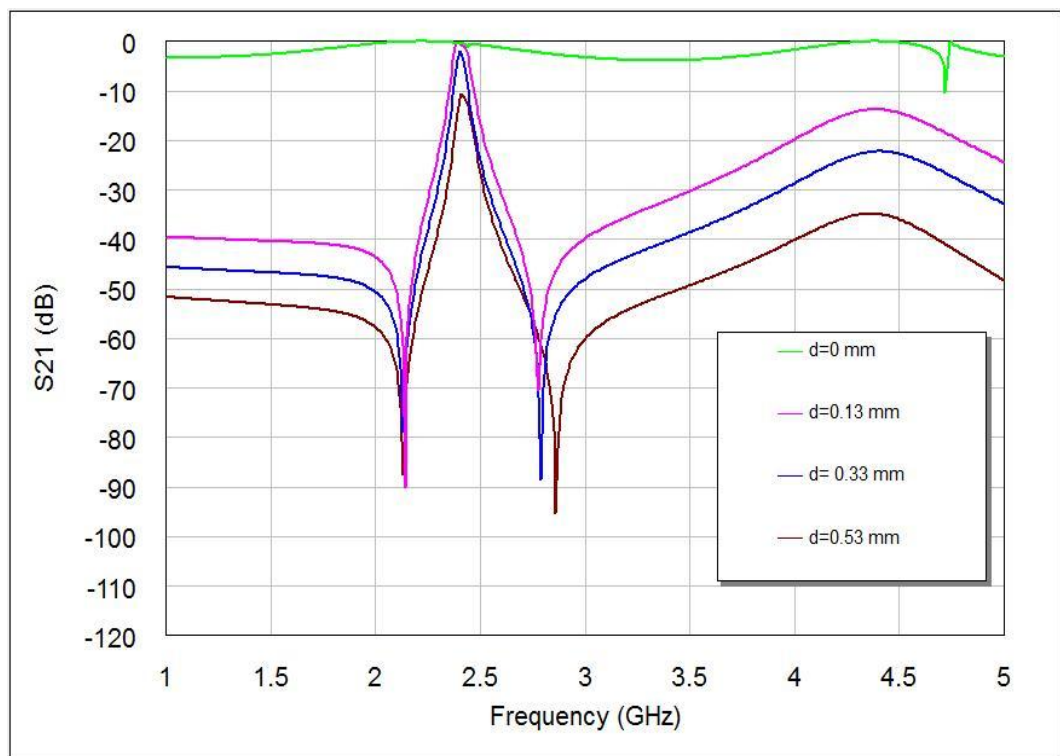
Figure 101 The transmission responses of the resulting first iteration Hilbert microstrip filter with respect to different edge spacing values, d(in mm)
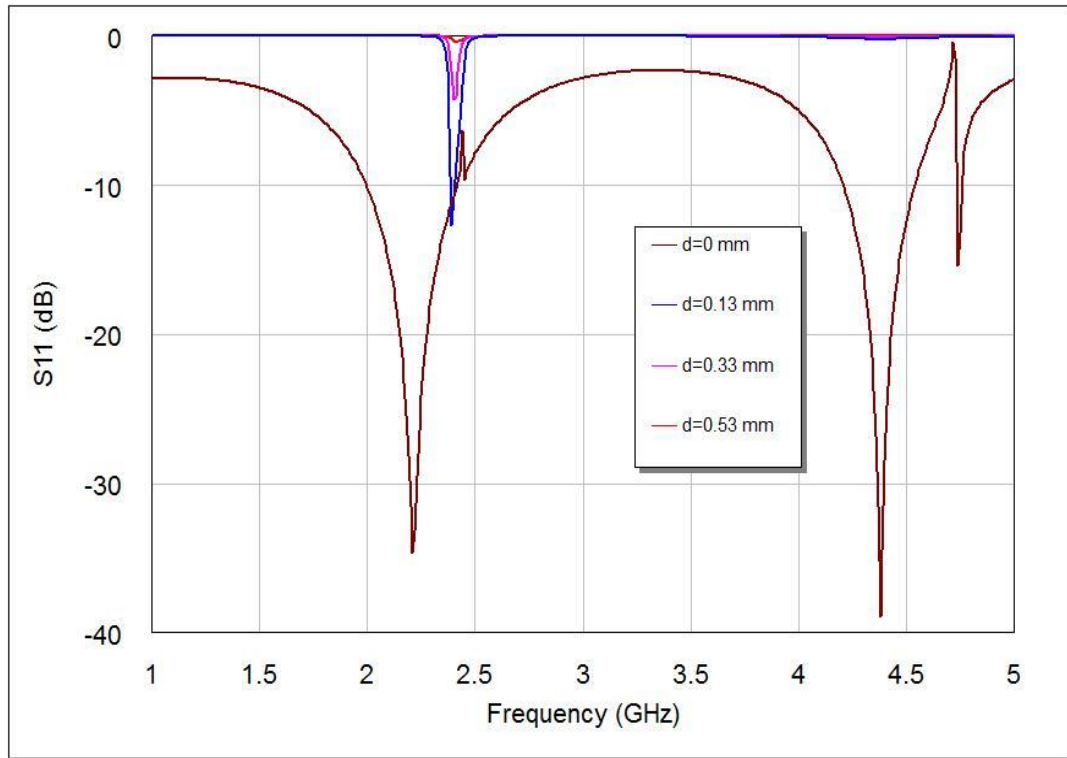
Figure 102 The return loss responses of the resulting first iteration Hilbert microstrip filter with respect to different edge spacing values, d(in mm)

The effects of varying the I/O feed line tap position on the filter responses have been demonstrated in **Figure 103** and explained in **Table 7**. It is worthwhile to observe that I/O feed line tap positions have a considerable effect on the locations of the transmission zeros at both sides of the passband. This will affect the sharpness and skirt characteristics of the resulting response. By proper tuning of the I/O feed line tap positions, the selectivity of the proposed filters can be enhanced to a large extent. However, as the results imply, this could be achieved for feed line positions at p =2.8 mm and q=3 mm. The results also reveal that the variation of the I/O feed line tap positions has big effects on the locations of transmission zeros of the bandpass filter based on the first iteration Hilbert geometry and certainly on of the filter based on the second iteration fractal geometry.
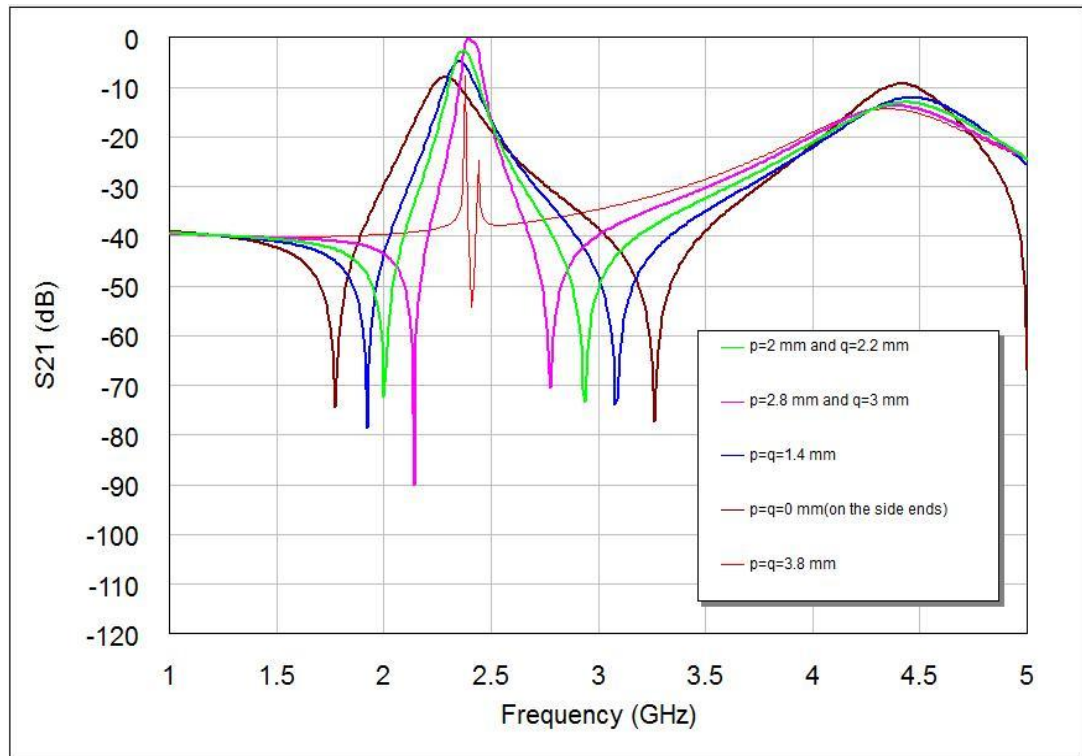
Figure 103 The transmission responses of the resulting first iteration Hilbert
microstrip filter with respect to different I/O port positions, p and q(in mm)

By using the principles of previous parametric studies, optimal simulation results of
return loss, S11, and transmission, S21, responses of modeled filters are shown in
Figures 104 and **105**. It is clear, that the resulting bandpass filters based on the 1st
to 2nd iteration Hilbert fractal geometry offer quasi-elliptic responses with
transmission zeros that are asymmetrically located around the deign frequency. It is
worth pointing from **Table 8** that 1st iteration Hilbert fractal BPF offers lower
bandwidth, slightly higher return loss and higher insertion loss as compared to 2nd
iteration one.

Figures 104 and **105** show the out-of-band responses of the filters depicted in
Figures 99 and **100** respectively. It is clear from thses figures, that the performance
response has 2nd harmonic suppression in out-of-band regions.
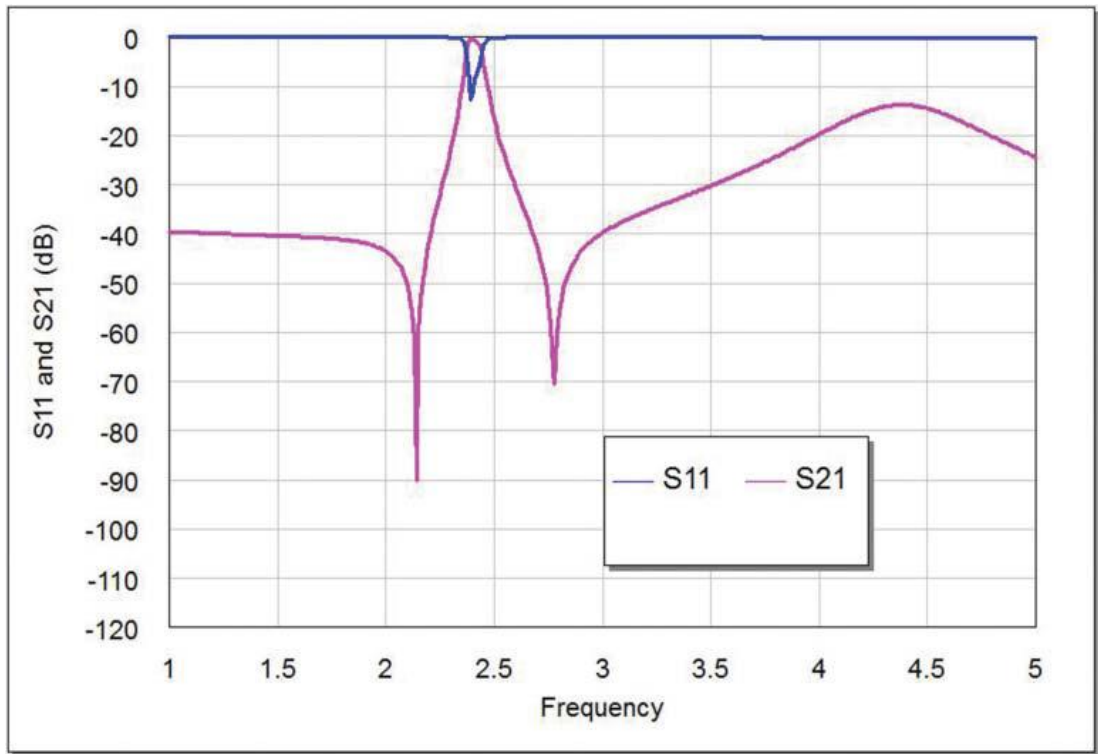
Figure 104 The return loss and transmission responses of BPF depicted in **Figure 99**, designed for 2.4 GHz
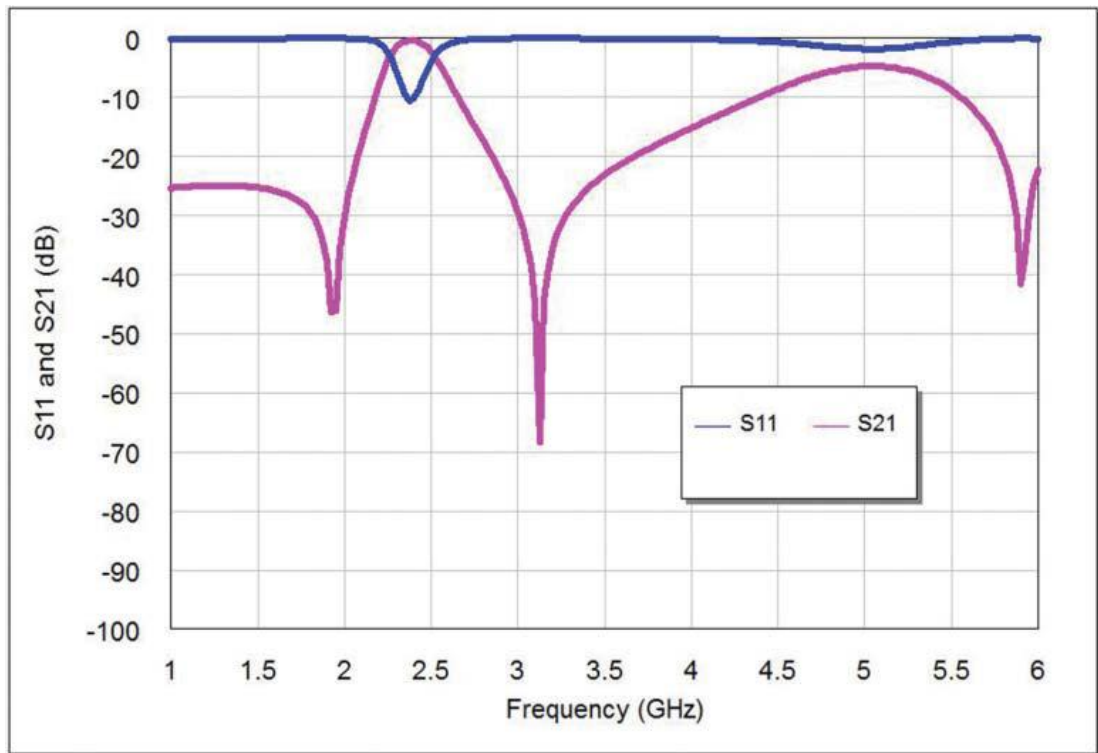
Figure 105 The return loss and transmission responses of BPF depicted in **Figure 100**, designed for 2.4 GHz

Table 8 shows results of the modeled filter dimensions as designed for 2.4 GHz application with corresponding filter performance parameters. The previous filter designs can be applied for other operating frequencies by varying the filter dimensions up or down depending on the required resonant frequencies. In this case, the resulting filters might be of larger or smaller in sizes according to the frequency requirements of the specific applications.

Table 8 shows bandwidths of 70 MHz and 240 MHz for proposed stepped impedance Hilbert filters. These bandwidths represent in-band frequency difference at -3 dB in passband region around 2.4 GHz. It is clear that as fractal iteration increases as value of microstrip width decreases, thus increasing the dissipative losses with a corresponding degradation of rejection levels [51] as it can be concluded from **Table 8** and output responses of proposed filters. These results agree with the findings reported in [113].

Parameter	1st Iteration	2nd Iteration
Side Length, mm	9.79	5.7
Occupied Area, mm^2	179.06	65.55
Band Rejection levels(dB)	-90.07 (left)	-46.345 (left)
	-70.557 (right)	-68.257 (right)
S_{11} (dB)	-12.71	-10.5
Insertion Loss(dB)	-0.33	-0.42
Bandwidth(MHz)	70	240

Table 8 Summary of The Calculated and Simulated Results of The Modeled Filters

4.5 Design and Simulation Results of Hilbert-zz Microstrip Bandpass Filter

A space-filling curve (SFC) may be adjusted over a flat or curved surface, and due to the angles between segments, the physical length of the curve is always greater than that of any straight line that can be fitted in the surface. A space filling curve is a curve that is large in terms of total strip length but small in terms of the area in which the curve can be included.

Figure 106 shows some specific types of reported Hilbert space filling curves which are called Hilbert zz set. The dimension of a fractal provides a detail of how much a space it fills. It is a measure of the weight of the irregularities when viewed at miniaturized scales. By the way, it can be implied from these fractal configurations, the new set has greater physical lengths as compared to Hilbert fractal shapes and hence more miniaturization possibilities for designing RF and Microwave microstrip filters [121,122].
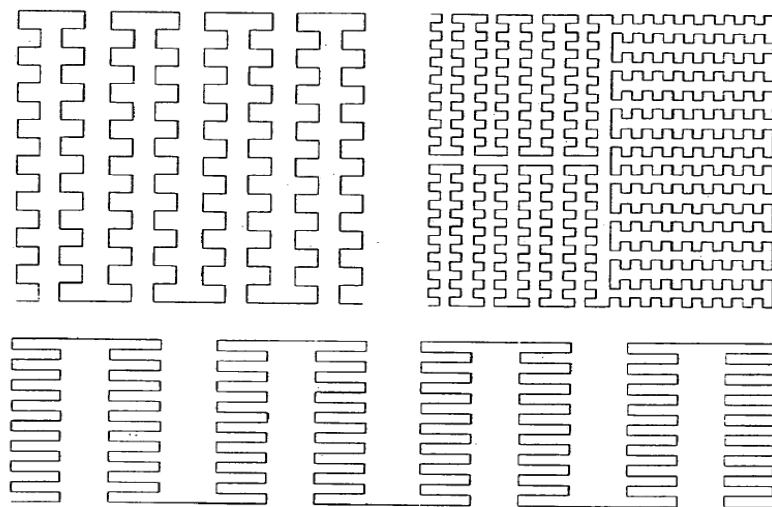
Figure 106 Hilbert zz space filling curves

A single resonator based on Hilbert-zz fractal geometry, has been designed at a frequency of 2.4 GHz. It has been supposed that the filter structure has been etched using a substrate with a relative dielectric constant of 9 and a substrate thickness of 1.27 mm. The resulting resonator dimensions have been found to be 3.34x 3 mm^2 and a trace width of about 0.1 mm and gap between strip of about 0.09 mm. The output response offered by this resonator is useless to be introduced here. The same resonator with depicted dimensions and substrate specifications has been used to build a two-resonator microstrip bandpass filter. The topology of this filter is shown in **Figure 107**. The overall dimensions of this filter are of 6.74x 3 mm^2. To enhance a suitable capacitive coupling between the resonators, stubs have been added to each resonator. These stubs will increase the overall length of the resonators making it resonates at a lower frequency. It has been found that this stub provides a suitable means to make the resonator resonates at the design frequency when modeling it in

the Sonnet EM simulator. In this case, the field solver will compute the same resonant frequency for both resonators.

The total strip length and side length of Hilbert-zz resonator of **Figure 107** without additional stub can be calculated by following equations:

$$L=264f+7g \tag{4.9}$$

$$S=4(2f+g)+3g \tag{4.10}$$

where $f =2w+g$, is initial drawn strip during modeling .On the other hand, the total curve length in the case of existing coupling stub can be calculated by :

$$L=264f+7g+S+r \tag{4.11}$$
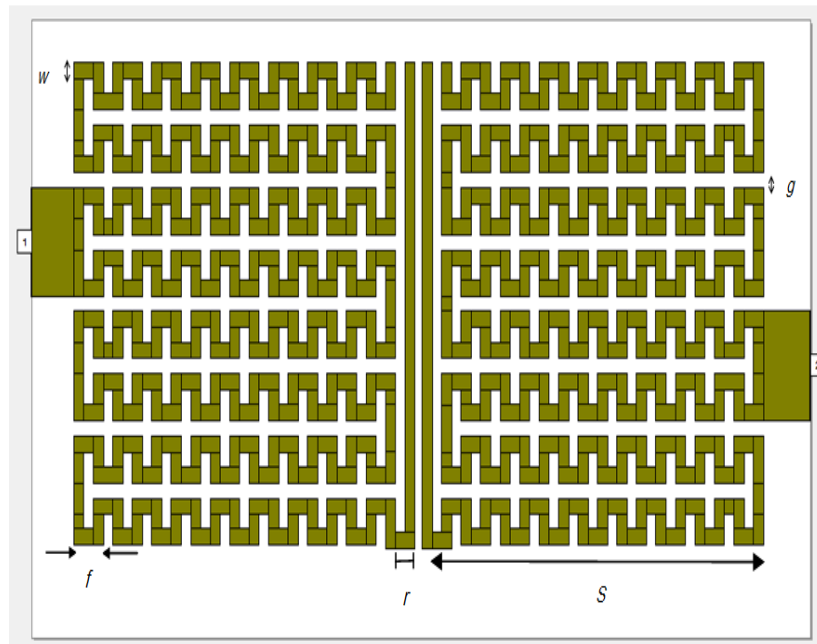
Figure 107 The modeled layout of   Hilbert zz resonators BPF

where r is connecting segment between Hilbert-zz resonator and coupling stub. It is found that the bandpass filter based on Hilbert-zz fractal resonators offers a higher degree of miniaturization, as compared to 2nd and 3rd iteration of Hilbert fractal resonators due to its higher packaging capabilities. Also, this filter possesses a noticeable compactness over the conventional half-wavelength resonator filter.

Filter structure, depicted in **Figure 107**, have been modeled and analyzed at an operating frequency, in the ISM band, of 2.4 GHz using Sonnet electromagnetic

simulator. The simulation responses of return loss, S11, and transmission, S21, responses of this filter are shown in **Figure 108**. In this figure, pass region has been designed at a center frequency of 2.4 GHz with bandwidth of 90 MHz , - 10.4 dB return loss and -0.42 dB insertion loss .
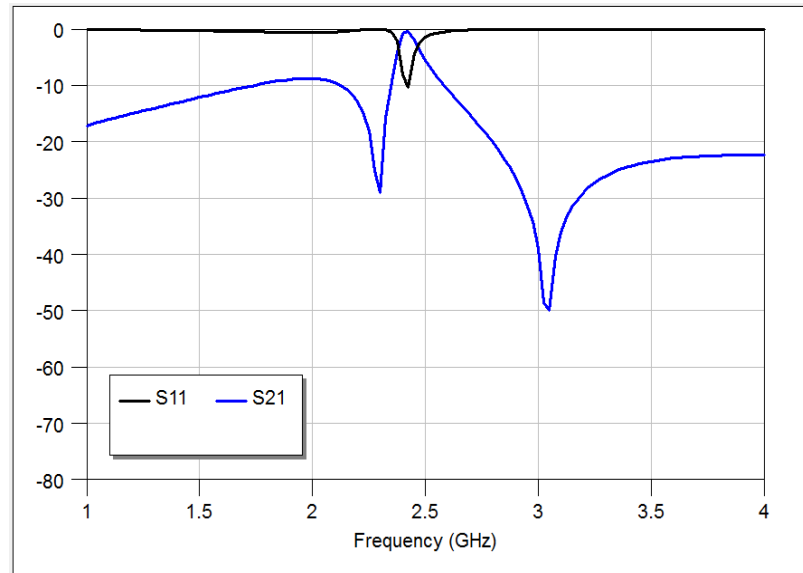
Figure 108 The return loss and transmission responses of Hilbert zz fractal BPF designed for 2.4 GHz

This filter offers a good quasi-elliptic transmission response with transmission zeros that are asymmetrically located around 2.4 GHz.

The I/O ports positions and edge spacing are important parameters that motivate the resulting multi-resonator filter performance. **Figures 109-110** show the resulting filter responses corresponding to different values of the coupling stub length. It is clear, from these figures; the variation in stub lengths affects the resonant frequency, as well as its effect on the transmission zeros. It is also pointing that return loss values have been changed to a level of about from -10.413 dB to -0.202 dB and the insertion loss values differ from -0.404dB to -13.222 dB that are with respect to d values from d $=3$ mm down to d $=0$ mm .

Figure 111 shows the out-of-band responses of the microstrip Hilbert-zz filter. It can be concluded from this figure, the output response has no tendency to support higher harmonics which conventionally accompany the bandpass filter performances. **Figure 112** displays the scattering parameter for S11 and S21 simulation results of Hilbert-zz filter.
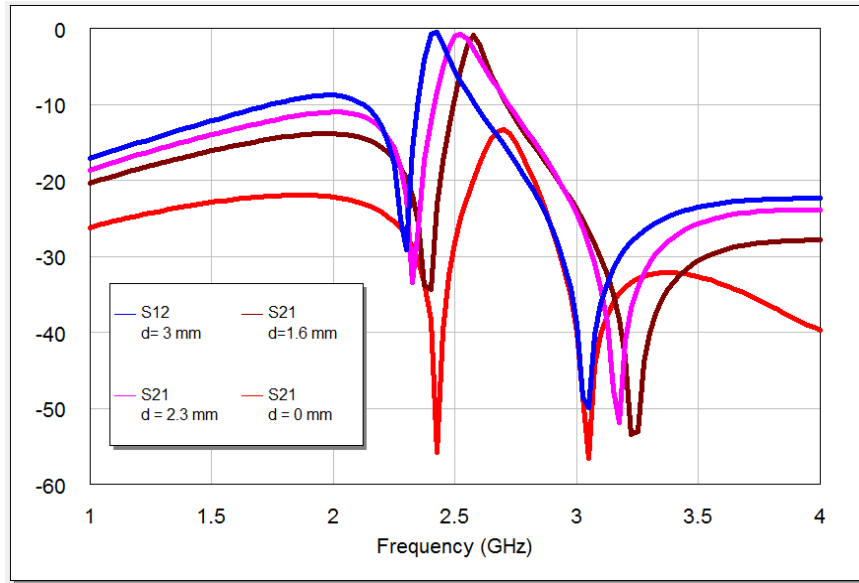
Figure 109 The transmission responses (S21) of the filter structure based on Hilbert zz curve with respect to different stub lengths
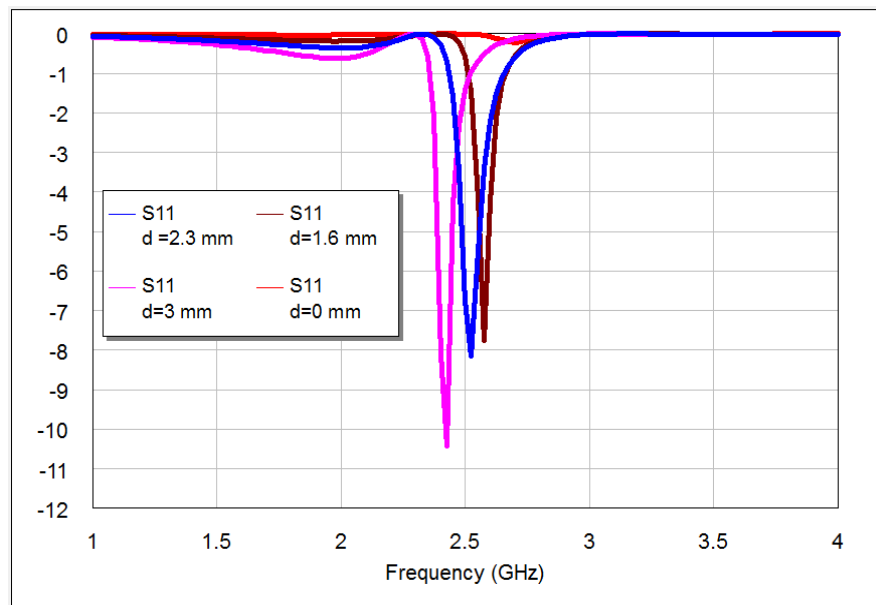
Figure 110 The return loss responses (S11) of the filter structure based on Hilbert zz curve with respect to different stub lengths
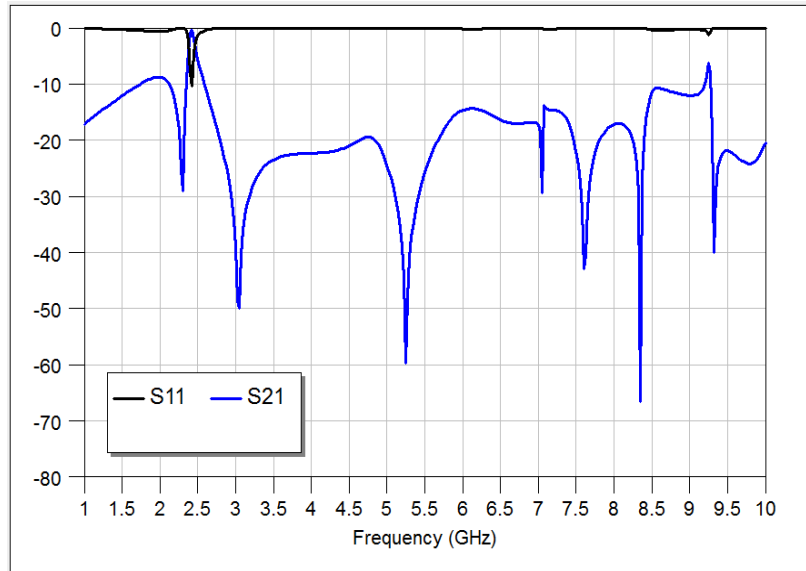
Figure 111 The out of band responses of the filter structure based on Hilbert zz
curve with coupling stub
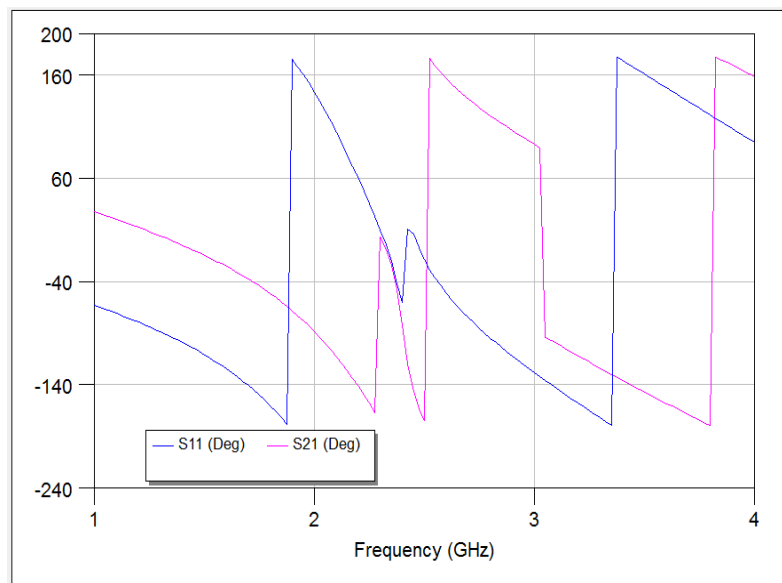
Figure 112 The phase responses of the resulting Hilbert zz fractal two-resonator
microstrip BPF

Figures 113-114 demonstrate the surface current patterns on the conducting surface
of both resonators at the design frequency where red color indicates higher coupling
effect while blue indicates lower coupling effect. It clear from these figures that only
at the design frequency the effective modes are induced and coupled to each other
leading to the required filter performance, whereas at the other frequency, no modes
are excited as expected. In these figures, the same color visualization is used as an

indication for the current densities. It is clear that highest current densities occur at the resonant frequency.
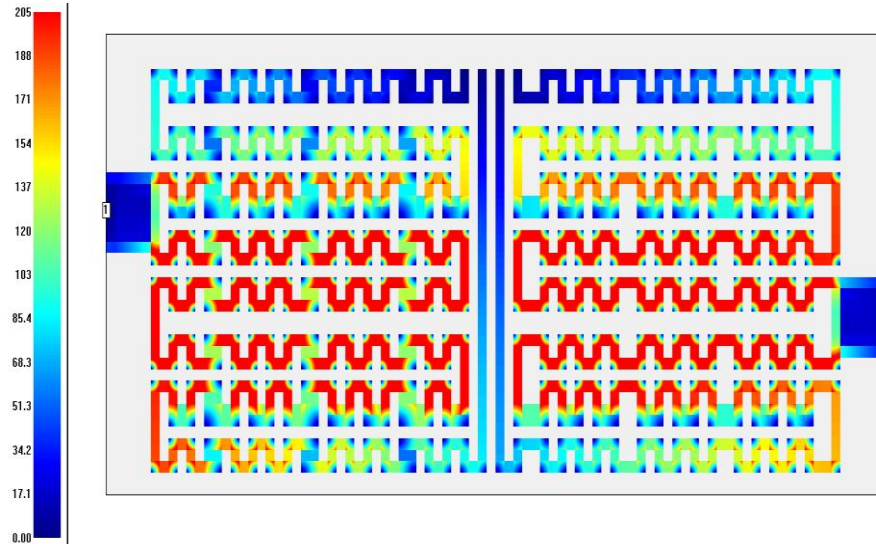
Figure 113 Current density distribution at the conducting surface of stubbed Hilbert-zz bandpass filter simulated at a resonant frequency of 2.4 GHz
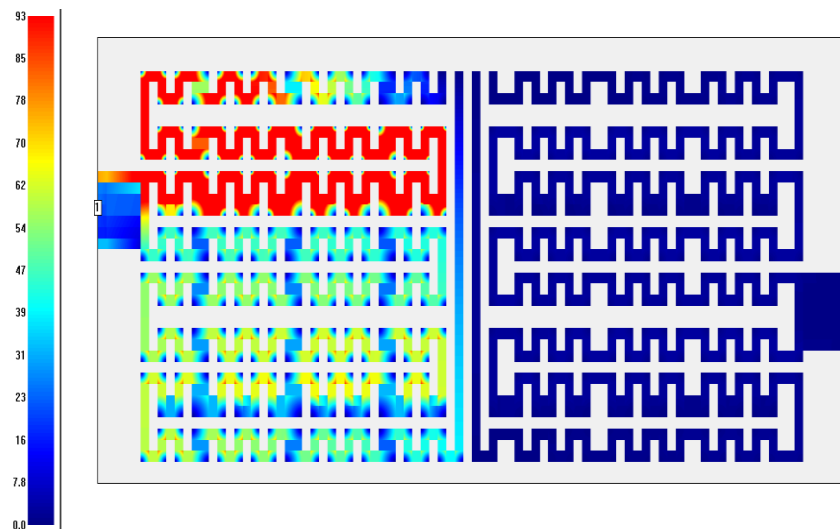
Figure 114 Current density distribution at the conducting surface of stubbed Hilbert-zz bandpass filter simulated at a resonant frequency of 3 GHz

4.6 Two Pole Dual Peano Bandpass Filter

Dual resonator based on 1st iteration Peano fractal geometry, has been designed at resonant band frequencies of 2.25 GHz and 4.825 GHz as in **Figure 115**. It has

been supposed that the modeled filter configuration has been etched using a substrate with a relative dielectric constant of 10.8 and a substrate thickness of 1.27 mm. The resulting resonator dimensions have been found to be 7.4 mm × 15 mm, with $w = 0.6$ mm , $g = 2.8$ mm , r = 7.5 mm, q = 0.2 mm and k = 0.7 mm while the edge spacing between two Peano resonators is 0.2 mm. The input/output feed positions and spacing between the resonators are effective parameters that can adjust the filter performance.
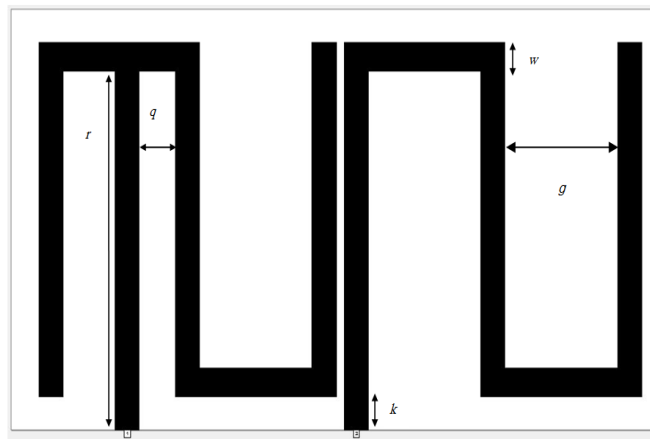
Figure 115 The modeled microstrip bandpass filter with two resonators based on 1st iteration Peano curve geometry

The corresponding frequency responses of S11 and S21 are shown in **Figure 116** .It is clear, from this graph, that the resulting bandpass filters based on the 1st   iterations Peano fractal geometry offer good quasi-elliptic transmission responses with transmission zeros that are located around the design frequency for each band at 2.25 GHz and 4.825 GHz . At the same time, there is good isolation between the two passbands. Four attenuation poles in the stopband can be observed as follows: 1.125 GHz, 2.85 GHz, 3.45 GHz and 5.675 GHz. **Table 9** shows the electrical specification parameters of the modeled filter.
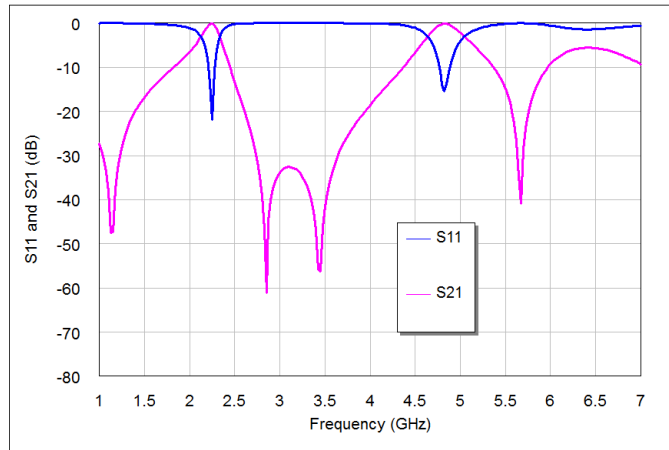
Figure 116 The return loss and transmission responses of the resulting 1st iteration fractal two-resonator microstrip bandpass filter

Figure 117 shows the phase response for S11 and S12 with respect to different frequencies.It is worth pointing that S21 phase responses offer higher frequency jumps as compared with S11 phase response. Moreover, the intersections between S11 and S21 responses can be recognized at operating band frequencies.
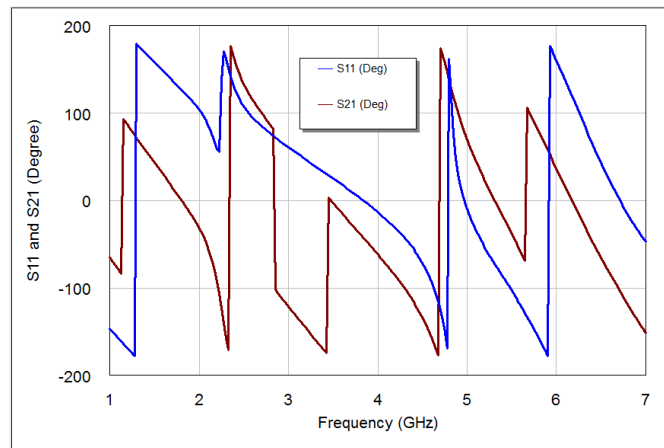
Figure 117 The phase responses of the resulting 1st iteration fractal two-resonator microstrip bandpass filter

In addition to *w* and *g* values, I/O ports positions have remarkable effect in the resulting filter performance. **Figures 118-119** show the resulting S11 and S21 responses corresponding to input port positions, q=0.2 mm, 0.5 mm, 0.8 mm and 1.2 mm. It is very obvious, in both figures the variation of q slightly affects the resonant

frequency, while its effect is much more noticeable on magnitudes of the transmission zeros, return loss and insertion loss. This parameter can be used to minimize insertion loss and maximize return loss according to q settings.

To understand which part of filter is being utilized at each operating band frequency, the surface current distributions are presented as in **Figures 120-121**.These responses have been investigated using sonnet simulator, where red color indicates the highest coupling effect while blue color indicates the lowest one. It can be observed from these figures, that surface currents are scaling themselves as first iteration Peano fractal geometry.

Band \ Parameter	1st band	2nd band
Resonant Frequency(GHz)	2.25	4.825
Return Loss, S_{11} (dB)	-21.84	-15.51
Insertion Loss (dB),$S21^0$	-0.146	-0.139
Bandwidth(GHz)	0.20	0.41

Table 9 Summary of The Simulated Result Parameter of The Modeled Peano BPF
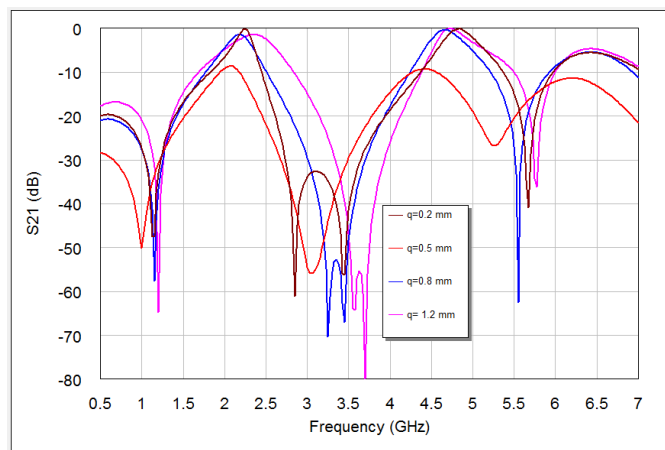
Figure 118 Influence of q values on S21 responses
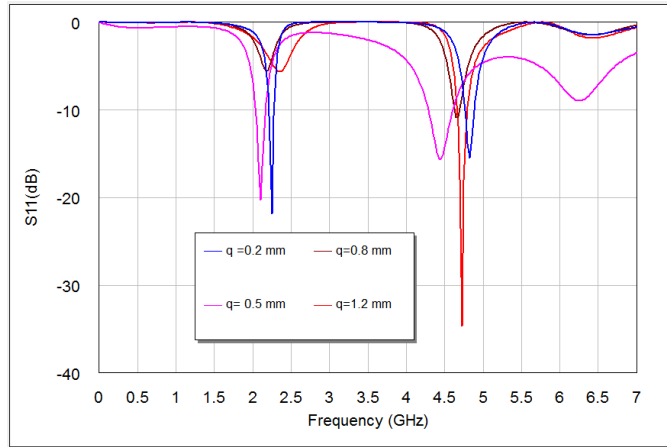
Figure 119 Influence of q values on S11 responses
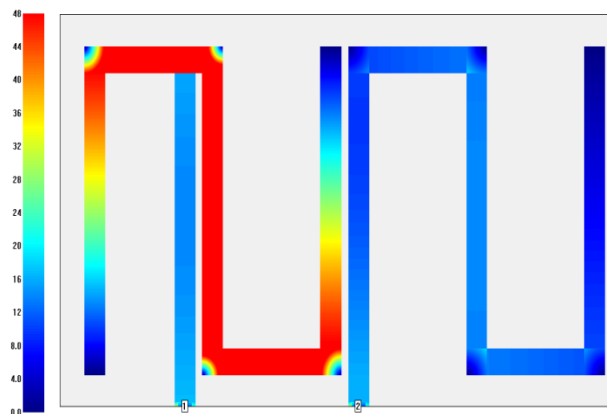
Figure 120 Current density distribution at the conducting surface of the 1st iteration Peano bandpass filter simulated at a resonant frequency of 2.25 GHz
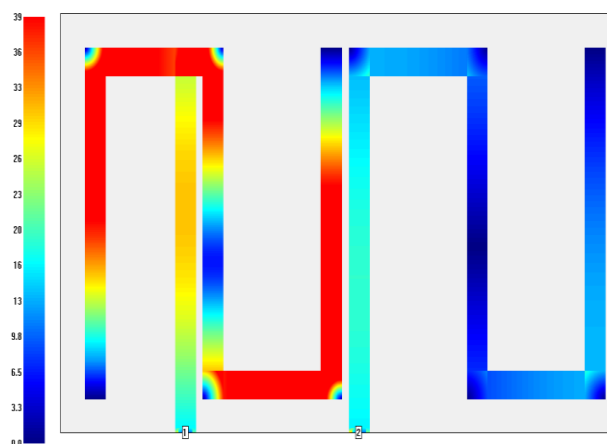
Figure 121 Current density distribution at the conducting surface of the 1st iteration Peano bandpass filter simulated at a resonant frequency of 4.825 GHz

CHAPTER 5

DESIGN AND SIMULATION RESULTS FOR MICROSTRIP WIDE BANDPASS AND NARROW BANDSTOP FILTERS

5.1 Introduction

New designs of Wide Bandpass Filter (WBPF) and Narrow Bandstop Filter (NBSF) based on Hilbert fractal resonators have been modeled using Sonnet simulator. The output frequency responses of the these filters have been examined to study the corresponding wide bandpass and narrow bandstop performances at the frequency around 2GHz. Additionally, the phase dispersion and surface current density details about proposed filters have been presented and analyzed. The proposed technique offers a new alternative to construct low-cost high-performance filter devices, suitable for a wide range of wireless communication systems.

All designed Hilbert filters in this section are based on the sixth publication in the "PUBLICATIONS RELATED TO PhD THESIS" list in the end of this thesis.

5.2 WBPF and NBSF Based on Hilbert Fractal Geometry

In this chapter, the design of microstrip Hilbert fractal based filters has been done by placing two resonators next to each other in specified distance. Each resonator is physical component that stores both magnetic and electric energy in a frequency-dependent way. At fundamental frequency, the magnetic and electric current distributions in the resonator are equally stored.

Hilbert fractal based resonators are well popular in planar filters application, for they have more compact sizes, reasonable loss, better power handling features and more miniaturization as compared with meander structure or split ring resonators [24,59].

Accordingly, WBPF consists of two microstrip resonators as in **Figure 122**, each resonator is based on 2nd iteration of Hilbert fractal geometry. By the way, Hilbert resonator represents a single pole resonant circuit. So, the resulting two resonator bandpass filters will have two poles(2nd order filter) regardless the iteration number of the fractal geometry. It has been assumed that the proposed filter structure has been etched using RT/Duroid substrate 6010LM with a relative dielectric constant of 10.8, substrate thickness of 1.27 mm and metallization thickness of 35 μm. Two 50 ohm feed lines as input and output (I/O) ports are placed in left up and right bottom corners of the filter. The width and length of these feeders are about 1.3 mm and 1.5 mm respectively.
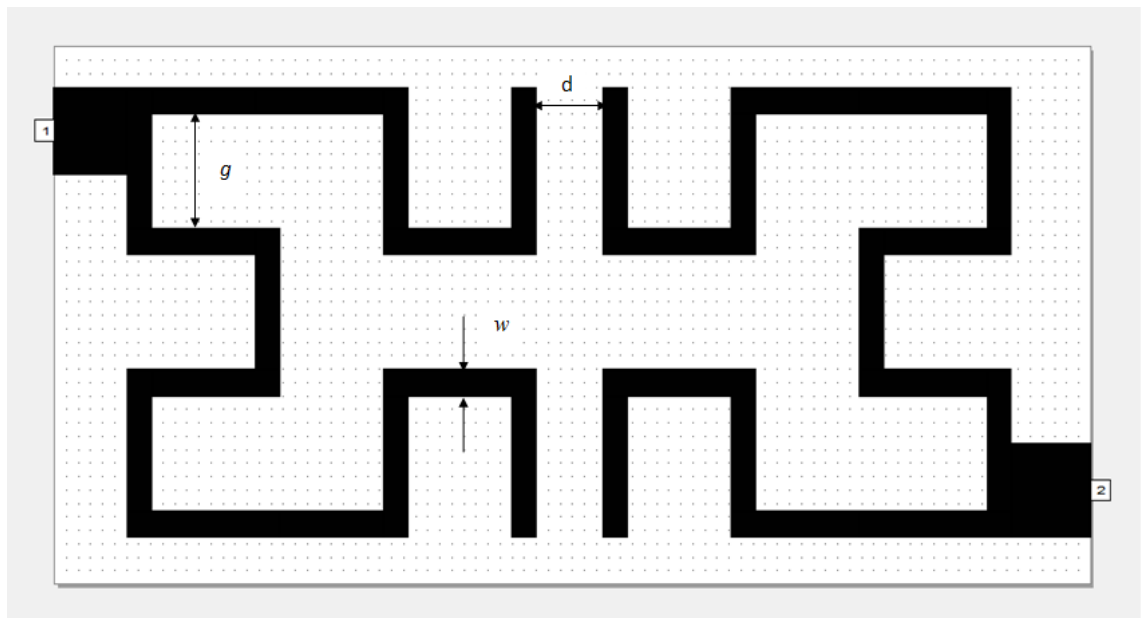
Figure 122 The modeled layout of 2nd iteration two Hilbert resonators WBPF

The proposed filter has overall dimensions of 13.5 x 6.7 mm^2 with a trace width of about 0.4mm, gap between strips of about 1.7 mm and edge spacing between the two resonators, d = 0.1 mm. The dimensions of this microstrip filter using electromagnetic modeling and simulation have been chosen by arbitrary trails and suitable scaling according to selected frequency of wireless communication systems. The layout of the proposed microstrip filter and dimension scaling method are essentially based on that presented in [89]. WBPF design has been simulated and evaluated using a full-wave based electromagnetic simulator Sonnet software package.

Sonnet simulator are based on the modified method of moment, such that they evaluate the filter response by dividing first the resonators in small grid divisions(mesh), adjusted according to the desired accuracy, and then solving a set of linear equations derived from an integral equation.The grid division here has been chosen to be 1 mm. The filter has been run under frequency range from 1 GHz to 3.5 GHz with frequency step of 0.025 GHz. Suitable boundary conditions are assigned, then meshing is carried out on the model to get final refined mesh. In meshing, it is well-known that more and smaller divisions will give a more exact solution. However, these smaller divisions will also require more time for the computer processor to solve the study. Therefore, it is necessary to choose the suitable balance between computation time and an acceptable level of accuracy. Using computer devices with four or more core processors can reduce the time of execution in the case of finer mesh. The stationary solver (including parametric sweeps) uses a linear solver algorithm for solution determination.

The simulation results of return loss and transmission responses for WBPF are shown in **Figure 123**. In this figure, pass-band has two resonances at 2 and 2.2 GHz with a bandwidth of 0.52 GHz, - 28 dB return loss and -0.125 dB insertion loss, can be observed clearly.
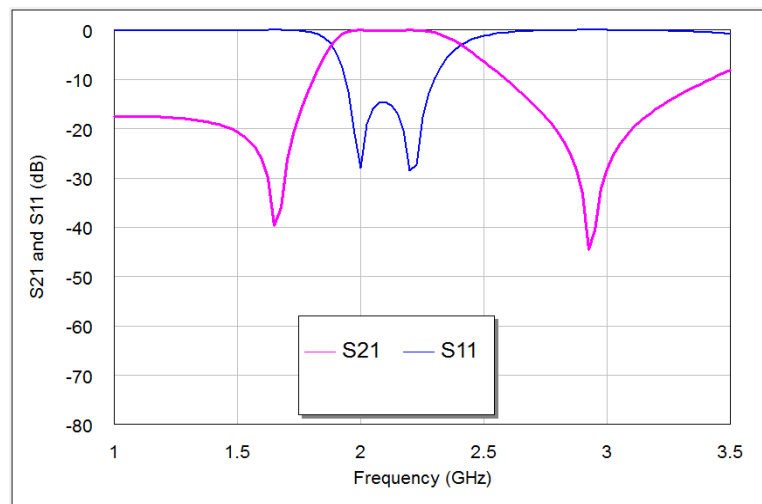
Figure 123 The return loss and transmission responses of the 2nd iteration   two Hilbert resonators WBPF

The same resonators with depicted dimensions substrate specifications and simulator setting has been used to build NBSF, but with coupling edge spacing between the

two resonators, d = 0 mm. The topology of this filter is shown in **Figure 124** with overall dimensions of 13.4 x 6.7 mm^2. The filter is simulated under frequency range from 1 GHz to 3 GHz with frequency step of 0.025 GHz.
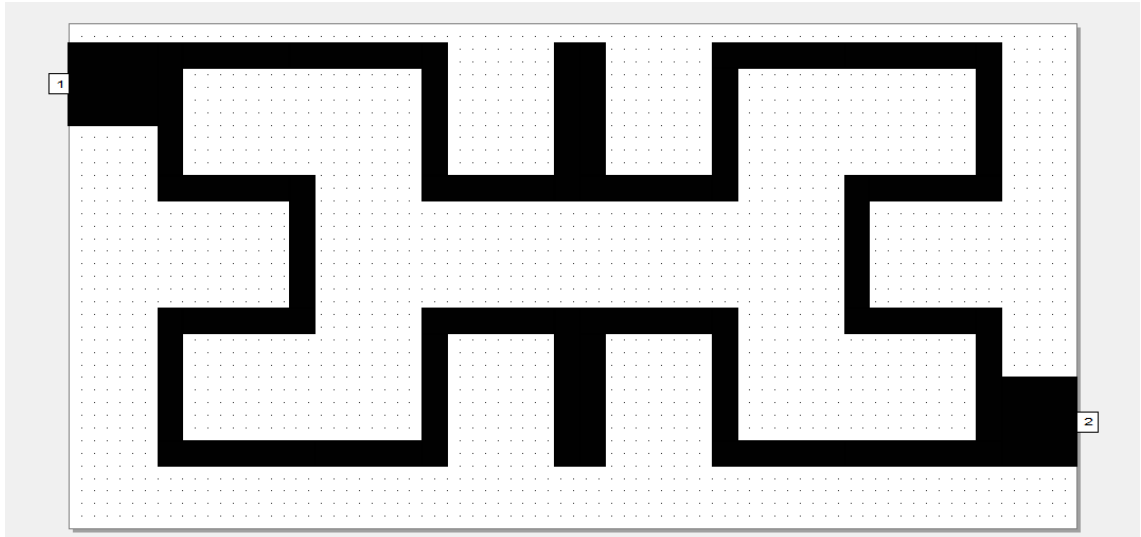
Figure 124 The modeled layout of 2nd iteration two Hilbert resonators NBSF

The corresponding results of return loss and transmission responses are shown in **Figure 125**.It has seen from this figure that the center frequency is 2.37 GHz and rejection band is 20 MHz, while the return loss and insertion loss values are -0.1873 dB and 13.746 dB respectively. This NBSF can be used in broadband communication systems that are sensitive to fixed frequency interferences.
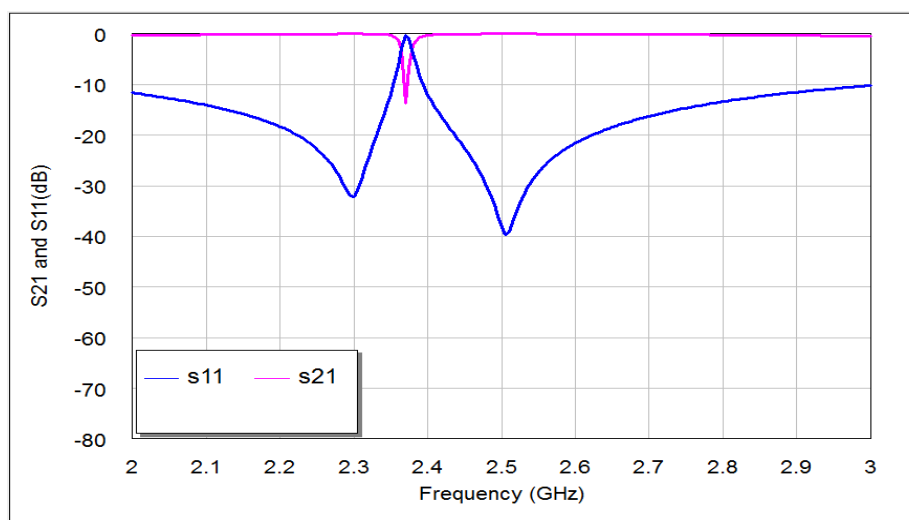
Figure 125 The return loss and transmission responses of the 2nd iteration two Hilbert resonators NBSF

It can be concluded from **Figures 123** and **125** that the simulation results of return loss, S11, and transmission, S21, responses of these filters offer good frequency responses with adequate performance. By the way, two transmission zeros (for WBPF) and reflection zeros (for NBSF) have been appeared in output frequency responses of proposed filters at finite frequencies near the pass-band and reject-band regions as depicted from **Figure 123** and **Figure 125** respectively .These responses are known as quasi-elliptic frequency responses for the designed filters. However, these responses and their consequent transmission and reflection zeros could be, to a certain extent, adjusted through the variation of edge coupling gap between Hilbert resonators and/or the input/output coupling used. For WBPF, two transmission zeros are located around resonant frequencies at 1.65 GHz and 2.9 GHz with S21 magnitudes of -39.73dB and -44.742dB, respectively while NBSF exhibits two reflection zeros of -32.176 dB and -38.227 dB at 2.3 GHz and 2.5 GHz , respectively.

In general, all passive resonating devices must have definite size in terms of the guided wavelength (λ_g) which can be calculated according equations (4.1).

Based on above equations, the overall dimensions in terms of λ_g are found to be of ($0.23\lambda_g$ x $0.11\lambda_g$) and ($0.257\lambda_g$ x $0.13\lambda_g$) for WBPF and NBSF respectively.

Besides the resonator dimensions, to reach to design frequency, there is also another vital parameter plays an important role in the resulting multi-resonator filter performance [116], this is the spacing between the adjacent resonators (d). Its effect obviously appears in the return loss and insertion loss magnitudes more than resonance.Moreover; this factor characterizes interaction of two resonators which is used mostly in resonator filter theory. This gap is also known as capacitive coupling and it couples these resonators electrically. On the other hand, the direct coupled resonators (at d=0 mm) are interacted magnetically and it represents inductive coupling.

Parametric study to investigate the effects of this parameter on the resulting filter performance, will lead to reach to minimum insertion loss and maximum return loss at the design frequency as well as the intended type of filter as pass or reject band.

In this study, we have used Hilbert microstrip resonators based on 2nd iteration level as a clarification example for adopting the optimization process as it can be seen from **Figures 126-127** and **Table 10**. **Figures 126-127** show the resulting S11 and S21 responses corresponding to different values of the spacing between the two resonators for the 2nd iteration of Hilbert fractal based filters. **Table 10** shows the results of the modeled Hilbert filters with edge spacing as a parameter with d=0 mm, 0.1 mm, 0.3 mm and 0.5 mm. It is clear, in both figures and **Table 10**; the variation in the spacing slightly affects the resonant frequency, while its effect is more noticeable on the transmission zeroes, return loss, insertion loss, bandwidth as well as the class of filter.
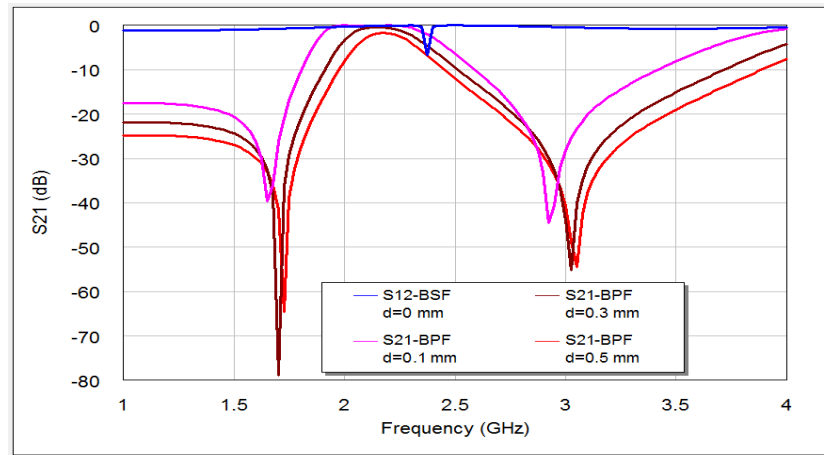
Figure 126 The transmission responses of the resulting 2nd iteration Hilbert microstrip filter with respect to different edge spacing values, d, (in mm)
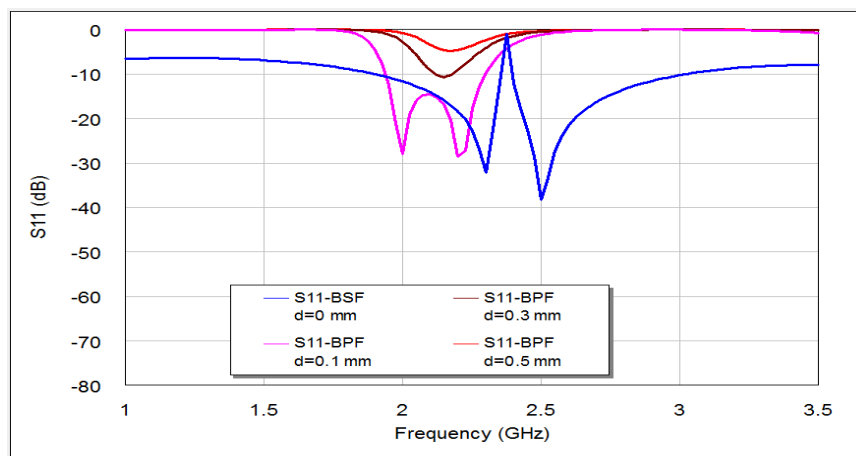
Figure 127 The return loss responses of the resulting 2nd iteration Hilbert microstrip filter with respect to different edge spacing values, d, (in mm).

	d=0 mm (BSF)	d=0.1mm (BPF)	d=0.3mm (BPF)	d=0.5mm (BPF)
Resonance Frequencies, GHz	2.37	2,2.2	2.1384	2.1655
Return Loss (dB)	-0.1873	-28	-10.57	-4.812
Insertion Loss(dB)	-13.746	-0.125	-0.4	-2.158
Actual Bandwidth (at -3dB)	20 MHz	520 MHz	331 MHz	170 MHz
Trans. or Reflect. Zeros(dB)	-32.176, -38.227	-39.73, -44.742	-78.895, -55.157	-64.604, -54.414

Table 10 Summary of The Simulated Parameters of Hilbert Filters with Respect to d Values

The BSF response can be obtained with d=0 mm as compared to BPF responses with other d cases. This is because of increased inductance of the filter structure without coupling gap case, consequently producing BSF response. Also, the simulation results involve that the gap spacing affects the position of the transmission zero on the right side of the passband slightly more than that of the left of the passband as in edge spacing values, 0.1 mm, 0.3 mm and 0.5 mm. The optimal responses of S11 and S21 for WBPF can be found in d = 0.1 mm case.

Figures 128-129 show the phase scattering parameters for S11 and S12 responses within the swept frequency range from 1 to 4 GHz and within output phase angle range from -200 to 200 degree. These responses include some frequency jumps which are the significant properties of quasi-elliptic filters. Accordingly, the intersection between S11 and S21 responses can be recognized easily, especially nearby resonant frequency.However, the S11 scattering response for NBSF configuration offers lowest jumping rate than other scattering responses of proposed filters where obvious phase decay can be identified easily, especially after 2.37 GHz center frequency.
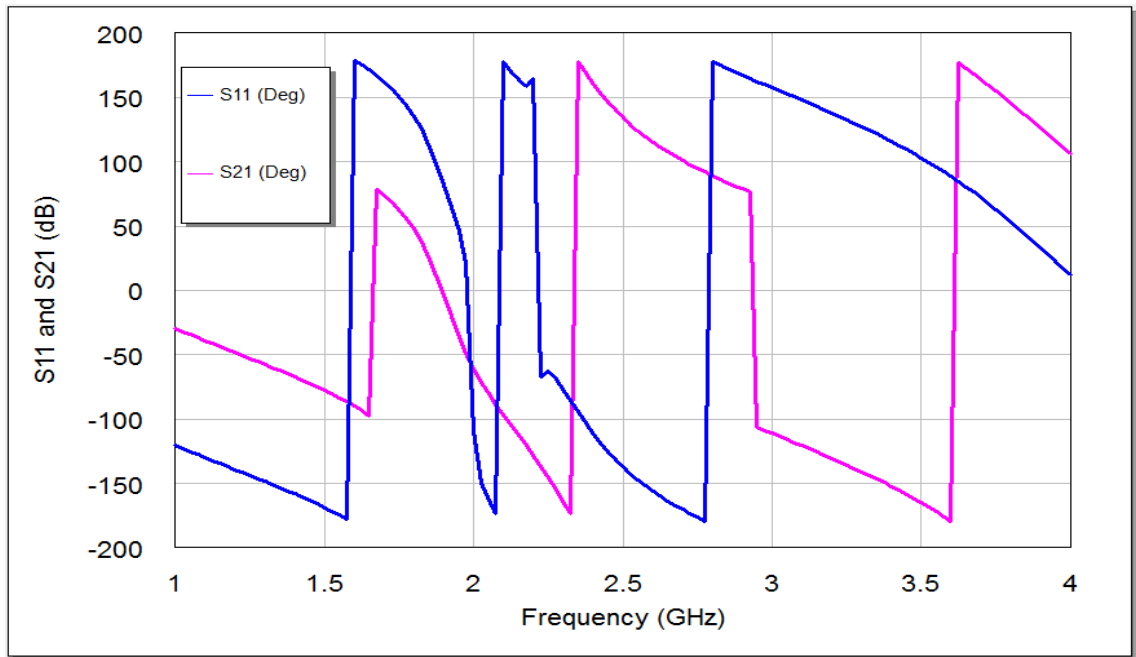
Figure 128 The phase responses of the resulting WBPF
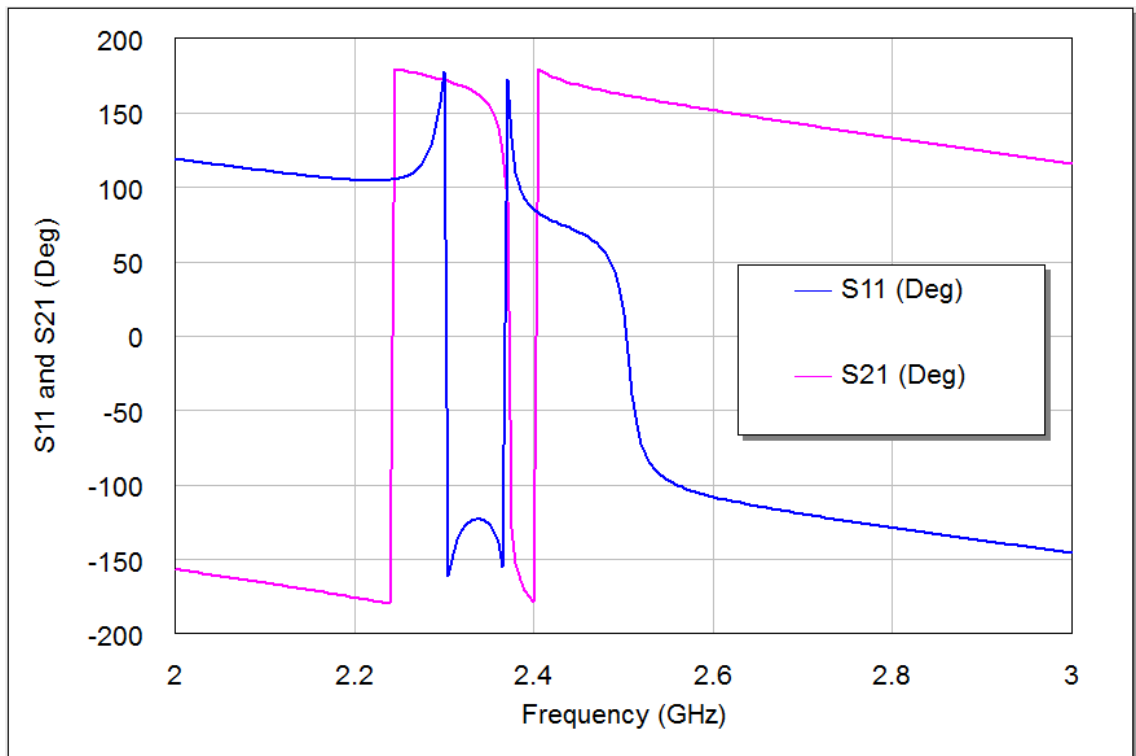
Figure 129 The phase responses of the resulting NBSF

To recognize which part of filter is being utilized (highest and lowest coupling regions) at each operating frequency, the surface current distributions are presented

as in **Figures 130-133** .These plots show surface current intensity graphs obtained by Sonnet simulator on the conducting surface of both Hilbert resonators. The surface current distributions are scaling themselves as second iteration Hilbert fractal geometry for each resonator .It is very clear from these figures that the current distributions differ from frequency to another where the red color indicates maximum coupling effect while blue color indicate the least one. The maximum surface current densities can be seen at the resonant frequencies for both WBPF and NBSF structures, which is due to the fact that the quasi-static resonance is being fully excited. Whereas the lowest current intensities can be observed at 3 GHz in the stop - band region for WBPF and pass-band region for NBSF at the same frequency. In this case, weakest coupling can be seen, which is given by the fact that the designed filter are not being excited at 3 GHz.
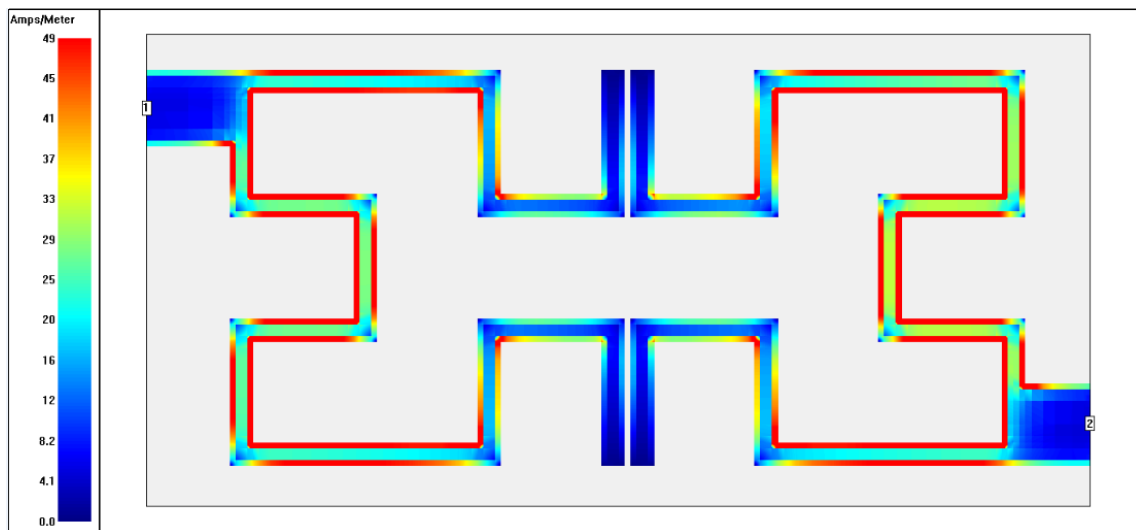
Figure 130 Current density distribution at the conducting surface of the 2nd iteration Hilbert WBPF simulated at an operating frequency of 2 GHz
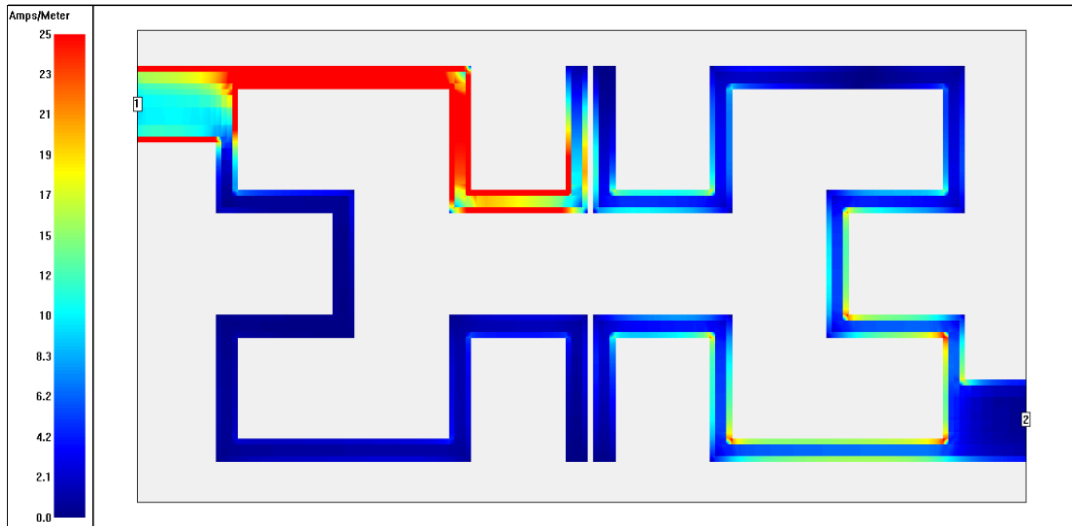
Figure 131 Current density distribution at the conducting surface of the 2nd iteration Hilbert WBPF simulated at an operating frequency of 3 GHz
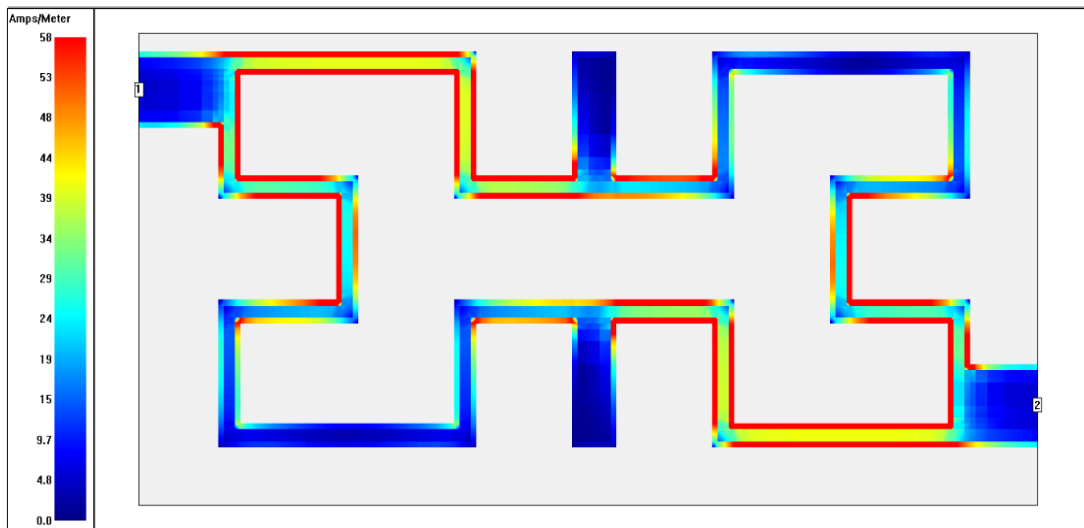
Figure 132 Current density distribution at the conducting surface of the 2nd iteration Hilbert NBSF simulated at an operating frequency of 2.37 GHz
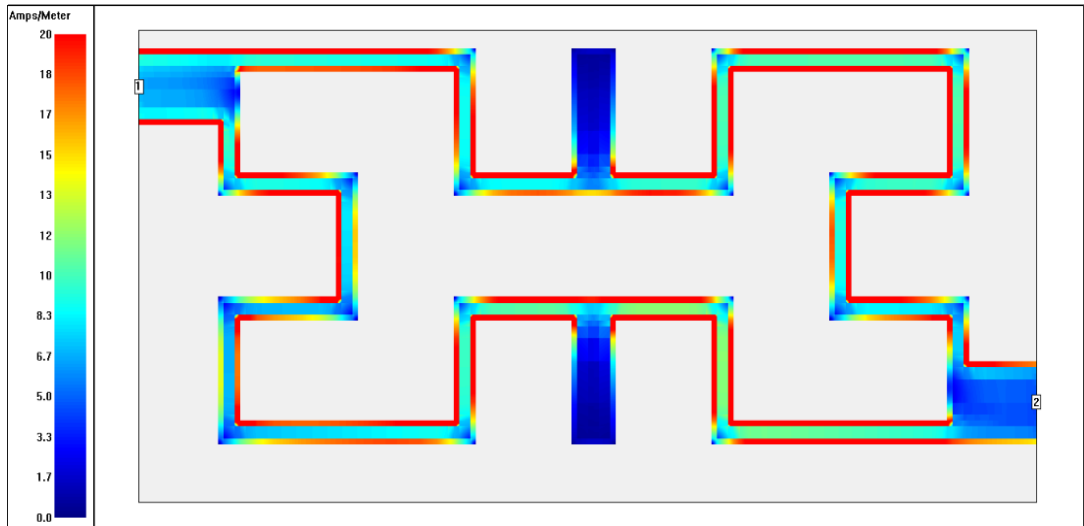
Figure 133 Current density distribution at the conducting surface of the 2nd iteration Hilbert NBSF simulated at an operating frequency of 3 GHz

CHAPTER 6

CONCLUSIONS AND SUGGESTIONS FOR FUTURE WORK

6.1 Conclusions

In this dissertation, new fractal bandpass and bandstop filters have been proposed for wireless communication applications. In the first section of this dissertation, single band and dual band fractal BPFs were proposed and evaluated. The aim of this section is to design and simulate a series of miniaturized fractal single-mode based on Moore ,Hilbert, Hilbert-zz and Peano fractal geometries to be used in many wireless communication applications within ISM band (2.4GHz) while Sierpinski fractal geometries have been investigated to design dual mode(two-pole) bandpass filters at resonant frequency (5.33 GHz). The other section of this dissertation is related to new designs of WBPF and NBSF based on Hilbert fractal curves. The research highlights can be summarized as follows:

1. New microstrip bandpass filter designs based on the 2nd and 3rd iteration levels of Moore space-filling curves have been presented as compact filters with satisfactory frequency responses and eliminated higher harmonics . These filters have been organized for ISM band applications at a resonant frequency of 2.4 GHz using a substrate with a dielectric coefficient of 10.8, dielectric thickness of 1.27 mm and metallization thickness of 35 μm. Under similar design frequency and substrate specifications, the proposed Moore microstrip filters have significant minor insertion loss and greater return loss values as compared with Minkowski-like and Hilbert fractal BPFs reported in [41] and [42] respectively. Furthermore , Moore bandpass filters are more compact than dual-mode Minkowski and Koch-like pre-fractal BPFs reported in [42] and [117] respectively. However, it is guessed that, more miniaturization level can be obtained for the filter configuration

corresponding to the 4th iteration of the proposed fractal generation method, if there are no practical restrictions.

2. Narrowband, compact and easily fabricated microstrip bandpass filter designs based on Sierpinski fractal geometry have been introduced in this thesis. They are constructed from dual-mode (two poles) square slotted microstrip resonator from 1st to 3rd iteration of Sierpinski fractal geometries. These microstrip fractal filters have the improvements of possessing much narrower and sharper frequency responses than those of the single pole resonator and typical square patch filter. The resulting filter structures from successive fractal iterations show a notably small insertion loss, and sharper response of about 1% fractional bandwidth as compared with the microstrip square patch filter of 3% fractional bandwidth designed at resonant frequency of 5.33 GHz using a dielectric coefficient of 10.8, dielectric thickness of 1.27 mm and metallization thickness of 35 μm. Also ,under same material specifications, these filters have lower insertion losses as compared with square ring resonator BPFs with open end stub reported in [123] operating at 5.8 GHz and dual band dual mode Sierpinski BPFs stated in [124] around the first band operating band frequencies of 5.4 GHz .

3. New properties of fractal design scheme has been achieved to build compact microstrip bandpass filter .This filter composes of dual edge coupled resonators, each resonator is based on specific type of Hilbert space-filling curve which is called Hilbert-zz fractal geometry. The inserted coupling stub for each resonator enhances the electromagnetic coupling for microstrip filter designed for ISM band wireless application using a dielectric constant of 9 and dielectric thickness of 1.27 mm. This fractal filter offers a good quasi-elliptic transmission response with transmission zeros that are asymmetrically located around 2.4 GHz with suppressed harmonics in out of band regions of frequency responses .It is found that the bandpass filter based on Hilbert-zz fractal resonators offers a higher degree of miniaturization, as compared to 2nd and 3rd iteration of the conventional Hilbert fractal resonators due to its higher packaging

capabilities. Also, this filter possesses a noticeable compactness over the conventional half-wavelength resonator filter [41].

4. Novel microstrip bandpass filter designs using step impedance resonator (SIR) transmission line and Hilbert fractal geometries have been explained in this thesis. The proposed filters have been built from dual edge coupled resonators; each resonator is based on applying step impedance resonator generator on 1st and 2nd iteration levels of Hilbert fractal resonators on each segment for each fractal iteration. The proposed filters have been modeled for the ISM band applications at center frequency of 2.4 GHz and using a substrate having a dielectric constant of 9.6 and a thickness of 0.508 mm. SIR approach inserted more reduction level to compacted Hilbert resonators by space filling property. The new filter designs have small sizes and low insertion loss as well as higher harmonics elimination which are very gorgeous features required for microwave circuit applications.Accordingly, these microstrip filters have more levels of compactness as compared to reported filters in [113] .

5. A new dual band microstrip bandpass filter with quasi elliptic response has been presented. The proposed filter structure have been composed of dual coupled resonators which are based on first iteration of Peano fractal curves using a substrate having a dielectric constant of 10.8 and a thickness of 1.27 mm. Numerical simulations using AWR2009 show that the proposed filter offers good quasi-elliptic transmission responses with transmission zeros that are located around the design frequency for each band at 2.25 GHz and 4.825 GHz . At the same time, there is good isolation between the two passbands. Four attenuation poles in the stopband can be observed as follows: 1.125 GHz, 2.85 GHz, 3.45 GHz and 5.675 GHz. It may be expected that the new fractal bandpass filter is a very good-looking structure for developing multiband miniaturized components with recent development in wireless communications.

6. For Moore, Hilbert-zz and stepped impedance Hilbert resonators, the coupling spacing between dual resonators and Input /Output port positions, can be properly tuned to increase return loss and decrease insertion loss as far as possible to improve frequency response of these

filters while the effective coupling depends on width strip and spacing between strips values of space filling curves.

7. WBPF and NBSF designs are designed as good quality and miniaturized 2nd order filters. The proposed microstrip fractal based filters consist of two resonators based on 2nd iteration of Hilbert fractal geometry using a substrate having a dielectric constant of 10.8 and a thickness of 1.27 mm. WBPF has been designed at resonant frequencies of 2 and 2.2 GHz with a bandwidth of 0.52 GHz in pass-band region, while NBSF has a center frequency of 2.37 GHz with 20 MHz bandwidth in the stop-band region. It has been found the coupling edge spacing (d) affects the filter performances obviously, in addition to circuit type as pass or reject band. The proposed designs offer high performance and simple fabrication for the implementation of fractal microstrip filters, which can be modified to be suitable for a wide variety of communication systems.

6.2 Suggestions for Future Work

Recent wireless technologies have quickly grown to locate their way into commercial and industrial applications. Many wireless communication systems, such as the global position system (GPS), global system for mobile (GSM), and Bluetooth system, industrial scientific medical (ISM band) have been demonstrated and applied.

Microwave filtering techniques are essential objects for controlling the spectrum of signals and tackling interferences issues in many wireless communication systems. Nowadays the physical volumes of RF and microwave front ends are dominated. Since the trend for future wireless systems is toward smaller and lighter filters size, there has been an ascending need for compact microwave and RF filters with interesting performences. Some of the suggestion that can be recommended on this issue as follows:

1. Relating the work presented in this thesis, additional research work has to be carried out to investigate the feasibility of designing compact size dual-mode bandpass filter based on Moore fractal geometries and multiband dual mode Sierpinski bandpass filters.

2. In this work, filters of two orders were achieved in order to verify the proposed designs. In fact, some concepts proposed in this dissertation can also be used in high-order filters to achieve higher selectivity .

3. Combing Moore fractal curves with SIR technique to produce more miniaturized filters with suppressed higher harmonics in out of band regions.

4. The ability of Moore and Sierpinski fractal shapes to construct as 3D objects, which can be used to build conformal fractal filters and resonators of higher performance in different frequency applications.

5. All microstrip filter designs have been investigated using EM software packages represented by AWR2009 and Sonnet simulators. The output responses by these simulators are well-known by designers that they have high convergence to measured results as it can be noted from Moore bandpass filter structures. However, experimental verifications for remaining modeled filters are still needed.

REFERENCES

1. **Hong J. S. and Lancaster M. J., (2001),** "*Microstrip Filters for RF/Microwave Application*", John Wiley & Son.

2. **Giannattasio G., Erfanian J., Wong K. D., Wills P., Nguyen H., Croda T., Rauscher K., Fernando X., Pavlidou N., (2009) ,** "*A Guide to the Wireless Engineering Body of Knowledge*" ,John Wiley & Sons.

3. **Matthaei G. L., Young L., and Jones E. M. T., (1964),** "*Microwave Filters, Impedance-Matching Networks and Coupling Structures*", New York: McGraw-Hill.

4. **Skwirzynski J. K., (1965),** "*Design Theory and Data for Electrical Filters*", London: Van Nostrand.

5. **Zverev A. I., (1967),** "*Handbook of Filter Synthesis*", New York: John Wiley.

6. **Howe J. H., (1974),** "*Stripline Circuit Design*", Dedham, MA: Artech House.

7. **Rhodes J. D., (1976)**, "*Theory of Electrical Filters*", New York: John Wiley.

8. **Malherbe J. A. G., (1979)**, "*Microwave Transmission Line Filters*", Dedham, MA: Artech House.

9. **Bahl I. J., Bhartia P., (1988)**, "*Microwave Solid State Circuit Design*", New York: John Wiley.

10. **Chang K.,** (1989), "*Handbook of Microwave and Optical Components*", Vol. 1, New York: John Wiley.

11. **Rhea R. W., (1994)**, "*HF Filter Design and Computer Simulation*", Atlanta, GA: Noble Publishing.

12. **Kajfez D., Guillon D., (1986)**, "*Dielectric Resonators*", Artech House, Norwood, MA.

13. **Kobayashe Y., Minegishi M., (1988)**, "*A Low Loss Bandpass Filter Using Electrically Coupled High-Q $TM_{01\delta}$ Dielectric Rod Resonators,*" IEEE Transaction on Microwave Theory and Techniques, vol. MTT-36, pp. 1727–1739.

14. **Madrangeas V., Aubourg M., Guillon P., Vigneron S., Theron B., (1992)**, "*Analysis and Realization of L-Band Dielectric Resonator Microwave Filter,*" IEEE Transaction on Microwave Theory and Techniques, vol. 40, pp. 120–127.

15. **Usyal S., (1997)**, "*Coplanar Waveguide Edge Coupled Bandpass Filters with finite ground planes,*" Electronics Letters, vol. 33, no. 5, pp. 375–376.

16. **Lin F.-L., Chiu C.-W., Wu R.-B., (1995),** "*Coplanar Waveguide Bandpass Filter-A Ribbon-of-Brick-Wall Design,*" IEEE Transaction on Microwave Theory and Techniques, vol. 43, no. 7, pp. 1589–1596.

17. **Weller T. M., (2000)**, "*Edge-coupled coplanar waveguide bandpass filter design,*" IEEE Transaction on Microwave Theory and Techniques, vol. 48, no. 12, pp.2453–2458.

18. **Tsujiguchi T., Matsumoto H., Nishikawa T., (1998)**, "*A Miniaturized End-Coupled Bandpass Filter Using λ/4 Hairpin Coplanar Resonators,*" in International IEEE MTT-S sypousim, vol. 2, pp. 829–832.

19. **Zhou J., Lancaster M. J., Huang F., (2004)**, *"Coplanar Quarter Wavelength Quasi Elliptic Filters without Bond Wire Bridges,"* IEEE Transaction on Microwave Theory and Techniques, vol. 52, no. 4, pp. 1150–1156.

20. **Tsujiguchi T., Matsumoto H., Nishikawa T.,(2001)**, *"A miniaturized Double Surface CPW Bandpass Filter Improved Spurious Responses,"* IEEE Transaction on Microwave Theory and Techniques, vol. 49, no. 5, pp. 879–885.

21. **Gao J., Zhu L., (2004)**, *"Asymmetric Parallel Coupled CPW Stages for Harmonic Suppressed λ/4 Bandpass Filters,"* Electronics Letters, vol. 40, no. 18, pp. 1122–1123.

22. **Bagad V. S., (2009)**, *"Microwave Engineering"*, Technical Publications Pune.

23. **Leonid A. B., Smolskiy S.M., Kochemasov V. N., (2012)**, *"Handbook of RF, Microwave, and Millimeter-wave Components"*, Artech House.

24. **Barra M., (2004)**, *"Miniaturized Superconducting Planar Filters for Telecommunication Applications"*, PhD Thesis, University of Napoli, Italy.

25. **Reppel M. , Mage J.C., (2000)** , *"Superconducting Microstrip Bandpass Filter on LaAlO$_3$ with High Out of Band Rejection"*, IEEE Microwave and Guided letters, Vol. 10, pp. 180-182.

26. **Hong J. S., Lancaster M. J., Jedamzik D., Greed R. B., (1999)**, *"On the Development of Superconducting Microstrip Filters for Mobile Communications Applications"*, IEEE Transactions on Microwave Theory and Techniques, Vol. 47, pp. 1656-1663.

27. **Huang F., (2003)**, *"Ultra Compact Superconducting Narrow Band Filters Using Single and Twin Spiral Resonators"*, IEEE Transactions on Microwave Theory and Techniques, vol. 51, pp. 487-491.

28. **Kwak J. S., Lee J. H., Hong J.P., Han S. K., Kim W. S. , Char K. R., (2003)**, "*Narrow Pass Band High Temperature Superconducting Filters of Highly Compact Sizes for Personal Communication Service Applications*", IEEE Transactions on Applied Superconductivity, vol. 13, pp. 17-19.

29. **Matthaei G. L., (2003)**, "*Narrow Band, Fixed Tuned And Tunable Bandpass Filters With Zig-Zag Hairpin Comb Resonators*", IEEE Transactions On Microwave Theory and Techniques, vol. 51, pp 1214/1219.

30. **Futatsumori S., Furuno M., Hikage T., Nojima T. , Akasegawa A., Nakanishi T. , Yamanaka K., (2009)** , "*Precise Measurement of IMD Behavior in 5GHz HTS Resonators and Evaluation of Nonlinear Microwave Characteristics*", IEEE Transactions on Applied Superconductivity, vol.19, no. 3, pp. 3595-3599.

31. **Ohshima S., Ohsaka M., Lee J. H., Takeuchi S., Kinouchi H., Ono S., Takano Y., Nakamura T., Yokoo M., , Saito A., (2009)** , "*Development of High-Speed Mechanical Tuning System for HTS Filters*", IEEE Transactions on Applied Superconductivity, vol. 19, no. 3, pp. 903-906 .

32. **Reppel M., (2000)**, "Novel HTS Microstrip Resonator Configurations for Microwave Bandpass Filters", PhD Thesis, Bergish University, Wuppertal, Germany.

33. **Suma M. N., Suhas K., (2009),** "*Performance Analysis and Process Parameters of Novel LTCC Filters*", International Journal of Recent Trends in Engineering, vol.1, no. 3, pp. 346-349.

34. **F.-L. Jenq, K.-K. Chong, H.-D. Yen, C.-C. Liu , (2009)**, "*Design of A Compact Dual-Mode Ring Resonator Bandpass Filter with Harmonic Suppression*", Journal of the Chinese Institute of Engineers, vol. 32, no. 5, pp. 741-744.

35. **Dong Y., (2009)**, "*Planar Realization of Q-Band Triple-Mode Filter Using High Order Resonances*", Microwave and Optical Technology Letters, vol. 51, no. 3, pp. 600-603.

36. **Zhu L., Wecowski P. M., Wunew K., (1999)** , "*Planar Dual-Mode Filter Using Cross-Slotted Patch Resonator for Simultaneous Size and Loss Reduction*", IEEE Transactions on Microwave Theory and Techniques, vol. 47, no. 5, pp. 650-654.

37. **Menzel W., Zhu L., Wu K., Bogelsack F., (2003)**, "*On the design of novel Compact Broadband Planar Filters,*" IEEE Transactions on Microwave Theory and Techniques, vol. 51, no.2, pp. 364-370.

38. **Zhu L., Sun S., Menzel W., (2005)**, "*Ultra-wideband (UWB) bandpass filters using multiple-mode resonator,*" IEEE Microwave Wireless Components Letters, vol. 15, no. 11, pp. 796- 798.

39. **Chiou Y.-C., Kuo J.-T. , Cheng E., (2006)**, "*Broadband Quasichebyshev Bandpass Filters with Multimode Stepped Impedance Resonators (SIRs),*" IEEE Transaction on Microwave Theory and Techniques, vol.54, no.8, pp. 3352-3358.

40. **Mandelbrot B. B., (1983)**, "*The Fractal Geometry of Nature*", W. H. Freeman and Company.

41. **Mezaal Y. S., (2009)**, "*A New Microstrip Bandpass Filter Design Based on Hilbert Fractal Geometry for Modern Wireless Communication Applications*", International Journal on advanced Computing Techniques (IJACT), vol.1, no. 2, pp.35-39.

42. **Ali J. K., (2008)**, "*A New Miniaturized Fractal Bandpass Filter Based on Dual-Mode Microstrip Square Ring Resonator*", Proceeding of the 5th International Multi-Conference on Signals, Systems and Devices, IEEE SSD '08, pp. 1-5, Amman, Jordan.

43. **Peitgen H.-O., Jürgens H., Saupe D., (2004),** "*Chaos and Fractal*", *New Frontiers of Science*, Springer.

44. **Falconer K., (2003),** "*Fractal Geometry; Mathematical Foundations and Applications*", 2nd Edition, John Wiley and Sons.

45. **Bin Ja'afer A. S., (2005)**, "*Sierpinski Gasket Patch and Monopole Fractal Antenna*", MSc Thesis, University Technology Malaysia.

46. **Werner D. H., Gangul S., (2003)**, "*An Overview' of Fractal Antenna Engineering Research*", IEEE Antennas and Propagation Magazine, vol.45, no.1, pp. 38-57.

47. **Ahmed E. S., (2012)**, "*Dual-Mode Dual-Band Microstrip Bandpass Filter Based on Fourth Iteration T-square Fractal and Shorting Pin*", radio engineering journal, vol.1, no.2, pp. 617-623.

48. **Barra M., Collado C., Mateu J. , Callaghan J. M.,(2005)** ,"*Miniaturization of Superconducting Filters Using Hilbert Fractal Curves*", IEEE Transactions on Applied Superconductivity, vol. 15, no.3, pp. 3841-3846.

49. **Segan H., (1994)**, "*Space-Filling Curves*", Springer-Verlag, New York.

50. **Ali J.K., Mezaal Y.S., (2009)**, "*A New Miniature Peano Fractal-Based Bandpass Filter Design with 2nd Harmonic Suppression*", 3rd IEEE International Symposium on Microwave, Antenna, Propagation, and EMC Technologies for Wireless Communications, MAPE 2009, pp.1019-1022, 27-29, Beijing, China.

51. **Ali J. K. , Mezaal Y. S., (2009)**, *A New Miniature Narrowband Microstrip Bandpass Filter Design Based on Peano Fractal Geometry*, Iraqi Journal of Applied Physics,vol. 5, pp.3-9 .

52. **Ali J. K., (2009)**, "*A New Microstrip-Fed Printed Slot Antenna Based on Moore Space-Filling Geometry*", Antennas & Propagation Conference, pp. 449-452, Loughborough.

53. **Hutchinson J., (1981)**, "*Fractals and self-similarity*", Indiana University Mathmatics Journal, vol.30, pp. 713-747.

54. **LANDER E. S. (2001)**, "**Initial sequencing and analysis of the human genome**", Nature, vol.409, pp. 2001, pp. 860-911.

55. **Olson H. F.,** (1967), "*Music, Physics and Engineering*", Dover Publications, New York.

56. **Hsu K. J., Hsu A. J.**, (1990), "*Fractal Geometry of Music*", National Academy of Science, vol. 87, pp. 938-941.

57. **Turcotte D. L., (1997)**, "*Fractals and Chaos in Geology and Geophysics*", Cambridge University Press.

58. **Ali J. K , Hussein N. N., (2009)** , "*A New Fractal Microstrip Bandpass Filter Design Based on Dual-Mode Square Ring Resonator for Wireless Communication Systems*", Iraqi Journal of Applied Physics, vol. 6, no.1, pp. 7-12.

59. **Jarry P., Beneat J., (2009)**, "Design and Realizations of Miniaturized fractal Microwave and RF Filters", John Wiley & Sons.

60. *www.fractus.com*. Data Download Date: 23.08.2014.

61. **Yordanov O. I. , Angelov I., Konotop V. V., Yurkevich I. V., (1999)**, "*Prospects of Fractal Filters and Reflectors*", in ISCAP'91, Seventh International Conference, pp. 698–700 .

62. **Liu J.-C. , Chien C.-H. , Lu P.-C. , Chen J.-Y. , Lin H.-J. , (2007)**, "*Cross-coupled Hilbert Spiral Resonator for Bandpass Filter Design and*

Applications", Microwave and Optical Technology Letters , vol.49, no.8 pp.1890-1894.

63. **Bengin V. C., Radonic V., Jokanovic B., (2006)** ,"*Complementary Split Ring Resonators Using Square Sierpinski Fractal Curves*", Proceedings of the 36th European Microwave Conference, pp.1333-1335.

64. **Kim I. K., Kingsley N., Morton M. A., Pinel S., Papapolymerou J., Tentzeris M. M., Laskar J. , Yook J.G. ,**(2006), "*Koch Fractal Shape Microstrip Bandpass Filters on High Resistivity Silicon for the Suppression of the 2nd Harmonic*", Journal of the Korean Electromagnetic Engineering Society, JKEES, vol. 6, no.4, pp.1-10.

65. **Xiao J.-K. , Chu Q.-X., (2007)**, "*Novel Microstrip Triangular Resonator Bandpass Filter with Transmission Zeros and Wide Bands Using Fractal-Shaped Defection*", Progress In Electromagnetic Research, vol.77, pp.343–356.

66. **Chen J., Weng Z.-B., Jiao Y.-C. , Zhang F.-S., (2007)**, "*Lowpass Filter Design of Hilbert Curve Ring Defected Ground Structure*", Progress in Electromagnetic Research, vol.70, pp.269–280.

67. **Yan D., Zhang K., (2010)**, "*HDGS Bandstop Filter Design by FGA*", IEEE Youth Conference on Information Computing and Telecommunications (YC-ICT), pp.5-8, Beijing, china.

68. **Ali J. K., Alsaedi H., (2012)**, "*Second Harmonic Reduction of Miniaturized Dual-mode Microstrip Bandpass Filters Using Fractal Shaped Open Stub Resonators*", PIERS Proceedings, pp. 1266-1269, Kuala Lumpur, Malaysia.

69. **Alqaisy M. A. , Ali J. K**, **Chakrabarty C. K. , Hock G. C. , (2013)**, " *Design of A Compact Dual-mode Dual-band Microstrip Bandpass Filter Based on Semi-fractal CSRR*" , Progress In Electromagnetics Research Symposium, pp.1-5, Stockholm, Sweden .

70. **Alqaisy M. , Chakrabraty C. , Ali J. K., Alhawari A. R. H. , (2014)**, "*A Miniature Fractal Based Dual Mode Dual Band Microstrip Bandpass Filter Design* ", International Journal of Microwave and Wireless Technologies, Available on CJO2014. DOI: http://dx.doi.org/10.1017/S1759078714000622.

71. **Collin R. E., (2001)**, "*Foundations for Microwave Engineering*", McGraw - Hill.

72. **Xiao J.-K., Chu Q.-X., Huang H.-F., (2008)**, "*Triangular Resonator Bandpass Filter with Tunable Operation*", Progress In Electromagnetic Research, vol. 2, pp. 167–176.

73. **Sebastian M. T., (2008)**, "*Dielectric Material for Wireless Communication*", Elsevier Ltd.

74. **Pozar D. M., (2005)**, "*Microwave Engineering*", John Wiley & Sons, New York.

75. **Edward T. C., Steer M. B., (2000)**, "*Foundations for Interconnect and Microstrip Design*", John Wiley and Sons.

76. **Atia A. E. , Williams A. E., (1972)**, "*Narrow Bandpass Waveguide Filters*" , IEEE Trans. Microwave Theory and Tech.,vol. 20, no. 4, pp. 258-265.

77. **Bell H. C., (2007)**, "*The Coupling Matrix in Lowpass Prototype Filters*", IEEE Microwave Magazine, vol. 8, no.2, pp. 70-76.

78. **López L. S., Weller T. M., (2004)**, "*A Low-Loss Quartz-Based Cross-Coupled Filter Integrated onto Low-Resistivity Silicon*", IEEE Transactions on Microwave Theory and Techniques, vol. 52, no.8, pp. 1809-1812.

79. **Matthaei G. L., L. Young, Jones E. M. T. (1980)**, "*Microwave Filters, Impedance-Matching Networks and Coupling Structures*", New York: McGraw-Hill.

80. **Kundu A. C., Awai I., Kajitani T., (1997)**, *"Theory on Rotated Excitation of A Circular Dual-Mode Resonator and Filter"*, IEEE MTT-S Digest, vol. 2, pp. 781-784.

81. **Hong J. S., (2011)**, "Microstrip Filters for RF/Microwave Application," 2nd edition, New York, Wiley.

82. **Wolff I., (1972)**, *"Microstrip Bandpass Filter Using Degenerate Modes of a Microstrip Ring Resonator,"* Electronics Letters, vol.8, no.12, pp. 302–303.

83. **Hong J. S., Lancaster M. J., (1995)**, *"Bandpass Characteristics of New Dual-Mode Microstrip Square Loop Resonators,"* Electronics Letters, vol. 31, no.11, pp.891–892.

84. **Hong J. S., Lancaster M. J., (1995)** " *Microstrip Bandpass Filter Using Degenerate Modes of a Novel Meander Loop Resonator"* , IEEE Microwave and Guided Wave Letters,vol. 5, no.11, pp. 371-372.

85. **Hong J. S., Lancaster M. J., (1997)**, *"Recent Advances in Microstrip Filters for Communications and Other Applications,"* in IEE Colloquium on Advances in Passive Microwave Components, London, pp. 2/1-2/6.

86. **Wheeler H. A., (1965)**, *"Transmission Line Properties of Parallel Strips Separated by a Dielectric Sheet,"* IEEE Transactions, MTT-13, pp.172–185.

87. **Gorur A., (2004)**, *"Description of Coupling Between Degenerate Modes of a Dual-Mode Microstrip Loop Resonator Using a Novel Perturbation Arrangement and Its Dual-Mode Bandpass Filter Applications "*, IEEE Transactions on Microwave Theory and Techniques, vol. 52, no. 2, pp. 671-677.

88. **Amari S., (2004)**, *"Comments on Description of Coupling Between Degenerate Modes of a Dual-Mode Microstrip Loop Resonator Using a Novel Perturbation Arrangement and Its Dual-Mode Bandpass Filter*

Applications", IEEE Transactions on Microwave Theory and Techniques, vol. 52, no. 9, p.p. 2190-2192.

89. **Chang K., Hsieh L., (2004)**, "*Microwave Ring Circuits and Related Structures*", 2nd Edition, John Wiley and Sons Ltd.

90. **Hsieh L., Chang K., (2003)**, "*High Efficiency Piezoelectric-Transducer-Tuned Feedback Microstrip Ring-Resonator Oscillators Operating at High Resonant Frequencies*", IEEE Transactions on Microwave Theory and Techniques, vol. MTT-28, pp. 1141-1145.

91. **Banciu M. G., (2003)**, "*Radio Frequency and Microwave Design Methods for Mobile Communications*", Ph.D Thesis, University of New South, Wales.

92. **Makimoto M., Yamashita S., (2000)**, "*Microwave Resonators and Filters for Wireless Communication*", Springer.

93. **Matsuo M., Yabuki H., Makimoto M., (2001)**, "*Dual-Mode Stepped Impedance Ring Resonator for Bandpass Filter Applications*", IEEE Transactions on Microwave Theory and Techniques, vol. 49, no. 7, pp. 1235-1240.

94. **Banciu M. G., Ramer R., (2000)**, "*Design of Microstrip Dual-Mode Filters Using Finite-Difference Time-Domain Method*", Proceedings of the Asia-Pacific Microwave Conference, vol. 1, pp. 975-978, Sydney.

95. **Hong J. S., Lancaster M. J., (1996)**, "*Couplings of Microstrip Square Open-Loop Resonators for Cross-Coupled Planar Microwave Filters*," IEEE Transactions on Microwave Theory and Techniques, vol. 44, no.12, pp. 2099-2109.

96. **Tan B. T., Chew S. T., Leong M. S. , Ooi B. L., (2003)**, "*A Dual-Mode Bandpass Filter with Enhanced Capacitive Perturbation*," IEEE Transactions on Microwave Theory and Techniques, vol. 51, no. 8, pp. 1906-1910.

97. **Zhu L. and Wu K., (1999)**, "*A Joint Field/Circuit Model of Line-to-Ring Coupling Structures and Its Application to the Design of Microstrip Dual-Mode Filters and Ring Resonator Circuits*", IEEE Transactions on Microwave Theory and Techniques, vol. 47, no. 10, pp. 1938-1948.

98. **Kundu A. C., Awai I. , Kajitani T., (1999)**, "*Attenuation Pole Frequency Control of a Dual-Mode Circular Microstrip Ring Resonator BPF*", IEEE Transactions on Microwave Theory and Techniques, vol.49, no. 6, pp. 1113-1117.

99. **Kundu A. C., Awai I., Kajitani T., (1997)**, "Theory on Rotated Excitation of a Circular Dual-Mode Resonator and Filter", IEEE MTT-S Digest, vol.2, pp.781-784.

100. **Kundu A. C., Awai I., (2001)**, "Control of Attenuation Pole Frequency of a Dual-Mode Microstrip Ring Resonator Bandpass Filter," IEEE Transactions on Microwave Theory and Techniques, vol. 49, no. 6, pp. 1113-1117.

101. **Kundu A. C., Awai I., (2000)**, "Effect of External Circuit Susceptance upon Dual-Mode Coupling of a Bandpass Filter," IEEE Microwave and Guided Wave Letters, vol. 10, no. 11, pp. 457-459.

102. **Karacaoglu U., Robertson I. D., Guglielmi M., (1993)**, "*A Dual-Mode Microstrip Ring Resonator Filter with Active Devices for Loss Compensation*", IEEE M'IT-S Digest, pp. 189-192.

103. **Misra D. K., (2001)**, "*Radio Frequency and Microwave Communication Circuit: Analysis and Design,*" John Wiley and Sons Inc.

104. **Lee Y. D., Lee M. H., Lee K. H., Hong W. P. , Hong U. S.,** "*Voltage-Controlled Hair-Pin Resonator Oscillator with New Tuning Mechanism*", Electronics Letters, vol. 36, no. 17, pp. 1470–1471.

105. **Hwang J. H., Cho J. S., J. H. Kim, Lee J. C., Kim B. K., Kim N. Y. , Hong U. S., (1999)** ,"*Effective Structure of a Push-Push Oscillator Using a*

Hair-Pin resonator for K Band Application," IEEE MTT-S, International Microwave Sympousim Digest, pp. 452–455.

106. **Yu C. C. and Chang K., (1997)**, *"Transmission-Line Analysis of a Capacitively Coupled Microstrip-Ring Resonator"*, IEEE Transactions on Microwave Theory and Techniques, vol. 45, no. 11, pp. 2018-2024.

107. **Oruc S., (2010)**, "Electronically Tunable Microwave Bandstop Filter Design and Implementation", MSc Thesis, Middle East Technical University.

108. **Advanced Wave Research Software Inc, (2009)**, *"Getting Started Guide, Release 9"*, 2009.

109. **Sonnet *em***, *"Sonnet Software"*, North Syracuse, NY. [Online]. Available: http://www.sonnetusa.com.

110. **Suarez A., (2009)**, *"Analysis and Design of Autonomous Microwave Circuits"*, John Wiley & Sons.

111. **Waterhouse R. B., (2003)**, *"Microstrip Patch Antennas: A Designer's Guide"*, Kluwer Academic Publishers.

112. **Swanson D. G., (2007)**, *"Narrow-band Microwave Filter Design"*, IEEE Microwave Mag., vol.8 , no. 5, pp. 105-114.

113. **Swanson D. G., Hoefer W.J.R., (2003)**, *"Microwave Circuit Modeling Using Electromagnetic Field Simulation"*, Dedham, MA: Artech House.

114. **Gianvittorio J. P., (2003)**, *"Fractals, MEMS, and FSS Electromagnetic Devices; Miniaturization and Multiple Resonances"*, PhD Thesis, University of California.

115. **Hsieh L. H., Chang K., (2003)**, *"Tunable microstrip bandpass filters with two transmission zeros,"* IEEE Transactions on Microwave Theory and Techniques, vol. 51, no. 2, pp. 520-525.

116. **Mezaal Y. S., Ali J. K., (2010)**, *"Design of Compact Hilbert Microstrip Bandpass Filter For Modern Wireless Communication Systems"*, journal of engineering and technology, vol.28, no.12, pp.2454-2468.

117. **Mahdi A. A., Aziz J. S., (2011)**, *"Miniaturized Koch Pre-Fractal Bandpass Filter"*, Journal of Mobile Communication, vol.5, pp.57-61.

118. **Husain N. N., (2008)**, *"Performance Enhancement of Bandpass Filters for Wireless Applications"*, *M.Sc Thesis*, University of Technology, Baghdad.

119. **Booppha P., et al, (2012)** , *"A Novel Structure of Microstrip Coupled Bandstop Filter Based on Shorted Step-Impedance Transmission Lines"*, 4th International Science, Social Science, Engineering and Energy Conference, pp. 1-9, Thailand .

120. **Mokhtaari M., Jens B., Amari S., (2006)**, *"New Reduced-Size Step-Impedance Dual-Band Filters with Enhanced Bandwidth and Stopband Performance"* , IEEE MTT-S Int. Microwave Symp. Dig., pp.1181-1184, San Francisco, USA.

121. **Illero R. Q., Barliarda C. P., (2008)**, " Multilevel and Space-Filling Ground Planes for Minature and multiband antenna",United States Patent, Patent No.:US7,362,283,B2, pp. 2-3.

122. **Barliarda C. P., et al, (2008)**, *"Fractal and Space-Filling Transmission Lines, Resonators, Filters and Passive Network Element"*, United States Patent, Pub. No.:US2008, 0011509A1, pp. 4-5.

123. **Noori A. A.-E. , (2010)**, *"A Novel Microstrip Dual-Mode Band-pass Filter for Second Harmonic Suppression"*, Engineering and Technology Journal, vol.28, no.11, pp. 2207-2212.

124. **Mezaal Y. S., Eyyuboglu H. T. , Ali J. K., (2013)** ,"*New Dual Band Dual-Mode Microstrip Patch Bandpass Filter Designs Based on Sierpinski Fractal Geometry*", 3rd International IEEE Conference on Advanced Computing and Communication Technologies, pp. 348-352, Rohtak , India .

APPENDICES

APPENDIX A

A.1 Determination of the Guided Wavelength in Ring Resonators

In this appendix, an uncomplicated transmission-line model is used to compute frequency modes of ring resonators of any common shape. Moreover, it gives an explanation for dual-mode behavior.

A.2 Frequency Modes for Ring Resonators

Figure (A.1) explains the arrangements of the one-port square and annular ring resonators. For a ring of any general shape, the overall length l can be divided into l_1 and l_2 sections.
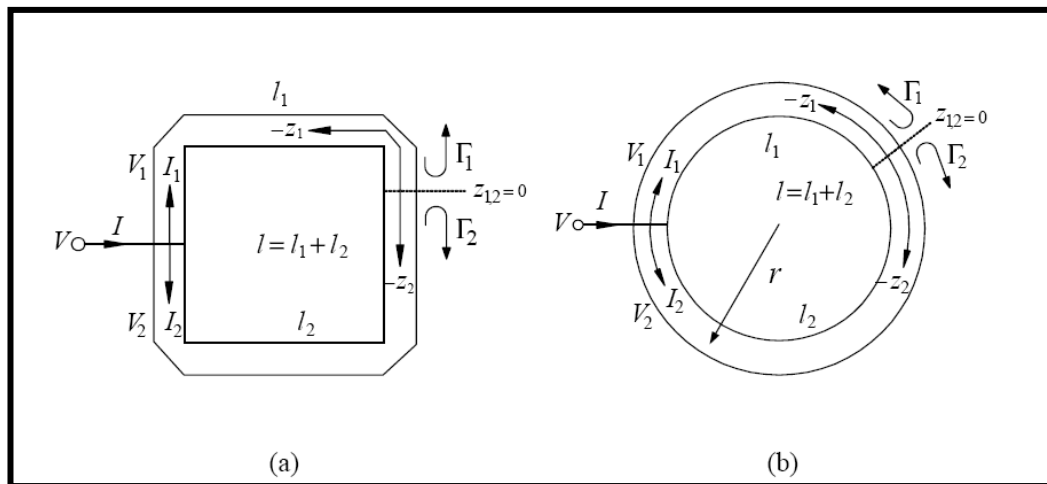

Figure (A.1) The configurations of one-port (a) square and (b) annular ring resonators

In the case of the square ring, each section represents a transmission line, z_1 and z_2 are the coordinates related to sections l_1 and l_2, respectively. The ring is fed by the

source voltage V at somewhere with $z_{1,2} < 0$. The positions of the zero point of $z_{1,2}$ and the voltage V are randomly selected on the ring. For a lossless transmission line, the voltages and currents for the two sections are given as follows:

$$V_{1,2}(Z_{1,2}) = V_o^+(e^{-j\beta Z_{1,2}} + \Gamma_{1,2}(0)\, e^{j\beta Z_{1,2}}) \tag{A.1a}$$

$$I_{1,2}(Z_{1,2}) = \frac{V_o^+}{Z_o}(e^{-j\beta Z_{1,2}} - \Gamma_{1,2}(0)\, e^{j\beta Z_{1,2}}) \tag{A.1b}$$

where $V_o^+ e^{-j\beta Z_{1,2}}$ is the incident wave propagating in the $+Z_{1,2}$ direction $V_o^+\Gamma_{1,2}(0)$ $e^{j\beta Z_{1,2}}$ is the reflected wave propagating in the $-Z_{1,2}$ direction, β is the propagation constant, $\Gamma_{1,2}(0)$ is the reflection coefficient at $z_{1,2} = 0$, and z_o is the impedance characteristic of the ring.

At resonance, standing waves set up on the ring. The least length of the ring resonator that maintains these standing waves can be gotten from the positions of the highest values of these standing waves. These positions can be determined from the derivatives of the voltages and currents in (A.1). The derivatives of the voltages are:

$$\frac{\partial V_{1,2}}{\partial Z_{1,2}} = -j\beta V_o^+(e^{-j\beta Z_{1,2}} - \Gamma_{1,2}(0)e^{j\beta Z_{1,2}}) \tag{A.2}$$

Letting

$$\left.\frac{\partial V_{1,2}(Z_{1,2})}{\partial Z_{1,2}}\right|_{Z_{1,2}=0} = 0 \tag{A.3}$$

The reflection coefficients can be found as:

$$\Gamma_{1,2}(0) = 1 \tag{A.4}$$

Substituting $\Gamma_{1,2}(0) = 1$ into (A.1), the voltages and currents can be rewritten as:

$$V_{1,2}(Z_{1,2}) = 2V_o^+ \cos(\beta Z_{1,2})$$

$$I_{1,2}(Z_{1,2}) = \frac{-j2V_o^+}{Z_O}\sin(\beta Z_{1,2}) \tag{A.5}$$

Therefore, the absolute values of the maximum voltages on the ring can be found as:

$$\left|V_{1,2}(Z_{1,2})\right|_{max} = 2V_o^+ \quad \text{for} \quad Z_{1,2} = m\frac{\lambda_g}{2} \quad , m\text{=0,-1,-2,-3} \tag{A.6}$$

In addition, the currents $I_{1,2}$ at the positions of $z_{1,2} = m\frac{\lambda_g}{2}$ are

$$\left.I_{1,2}(Z_{1,2})\right|_{Z_{1,2}=m\frac{\lambda_g}{2}} = 0 \tag{A.7}$$

A2

Also, the absolute values of the maximum currents can be found as:

$$\left|I_{1,2}(Z_{1,2})\right|_{max} = \frac{2V_O^+}{Z_O} \text{ for } z_{1,2} = \frac{(2m-1)}{4}\lambda_g, \quad m = 0, -1, -2, -3 \tag{A.8}$$

the voltages $V_{1,2}$ at the positions of $z_{1,2} = \frac{(2m-1)}{4}\lambda_g$ are:

$$V_{1,2}(Z_{1,2})\Big|_{Z_{1,2}=\frac{(2m-1)}{4}\lambda_g} = 0 \tag{A.9}$$

Figure (A.2) explains the absolute magnitudes of voltage and current standing waves on each section l_1 and l_2 of the square ring resonator. Inspecting Figure (A.2), the standing waves replicate for multiples of $\frac{\lambda_g}{2}$ on the each section of the ring. Thus, to sustain standing waves, the shortest length of each section on the ring has to be $\frac{\lambda_g}{2}$,which can be considered as the elementary mode of the ring. For higher order modes:

$$l_{1,2} = n\frac{\lambda_g}{2} \qquad \text{for } n = 1,2,3 \tag{A.10}$$

where n is the mode number. Therefore, the total length of the square ring resonator is:

$$l = l_1 + l_2 = n\lambda_g$$

l = total length of any ring loop resonator

Then:

$$f_o = \frac{nc}{l\sqrt{\varepsilon_{eff}}} \tag{A.11}$$

In terms of the annular ring resonator with a mean radius r as shown in Figure (A.1b),

$$l = n\lambda_g = 2\pi r \tag{A.12}$$

Equation (A.10) explains a general expression for frequency modes and can be used at any configuration of microstrip ring resonators including the dual-mode filter.
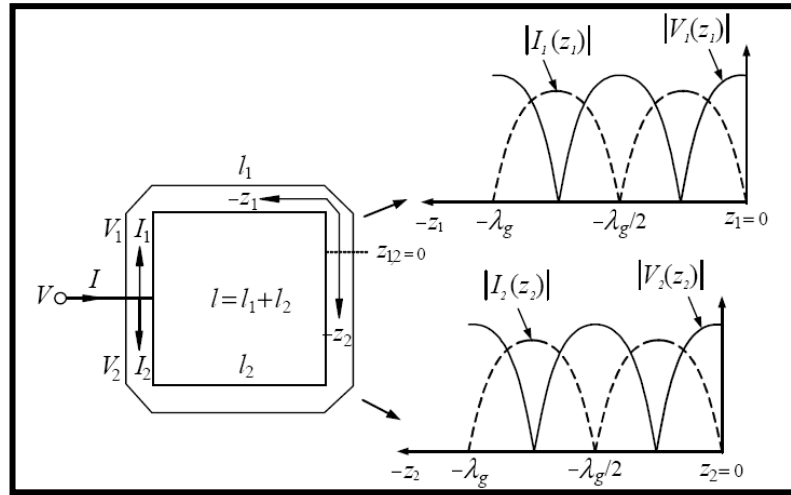
Figure (A.2) Standing waves on each section of the square ring resonator

PUBLICATIONS RELATED TO Ph.D THESIS

The following papers have been published during the course of Ph.D Reseach:

1. Yaqeen Sabah Mezaal, Jawad Kadhim Ali and Halil Tanyer Eyyuboglu, "Minaiturized Microstrip Bandpass Filters Based on Moore Fractal Geometry with higher Harmonics Suppression", International Journal of Electronics,2014, http://dx.doi.org/10.1080/00207217.2014.971351.

2. Yaqeen Sabah Mezaal, Halil Tanyer Eyyuboglu and Jawad Kadhim Ali, "A New Narrow Band Dual-Mode Microstrip Slotted Patch Bandpass Filter Design Based on Fractal Geometry" , Presented and published at 7th International IEEE Conference on Computing and Convergence Technology (ICCIT, ICEI and ICACT), 3-5, December, 2012, Seoul, South Korea.

3. Yaqeen Sabah Mezaal ,Halil Tanyer Eyyuboglu and Jawad Kadhim Ali, "New Microstrip Bandpass Filter Designs based on Stepped Impedance Hilbert Fractal Resonators" ,IETE Journal of Research,Vol.60,No.3 ,2014.

4. Yaqeen Sabah Mezaal ,Halil Tanyer Eyyuboglu and Jawad Kadhim Ali," A Novel Design of Two Loosely Coupled Bandpass Filter Based on Hilbert-zz Resonator with Higher Harmonic Suppression", Presented and published at the 3rd International IEEE Conference on Advanced Computing and Communication Technologies , 6-7 ,April , 2013, Rohtak, India.

5. Yaqeen Sabah Mezaal ,Halil Tanyer Eyyuboglu and Jawad Kadhim Ali, " A New Design of Dual Band Microstrip Bandpass Filter Based on Peano Fractal Geometry: Design and Simulation Results " , Presented and published at IEEE Mediterranean Microwave Symposium (MMS2013), 2-5 Septemper,2013, Saida, Lebanon.

6. Yaqeen Sabah Mezaal, Halil Tanyer Eyyuboglu and Jawad Kadhim Ali, "New Designs of Wide Bandpass and Narrow Bandstop Microstrip Filters Based on Hilbert Fractal Geometry: Design and Simulation Results", PLOS ONE Journal, 2014.

7. Yaqeen Sabah Mezaal ,Halil Tanyer Eyyuboglu and Jawad Kadhim Ali, "New Dual Band Dual-Mode Microstrip Patch Bandpass Filter Designs Based on Sierpinski Fractal Geometry", Presented and published at the 3rd International   IEEE Conference on Advanced Computing and Communication Technologies , 6-7, April 2013, Rohtak, India.

<h1 style="text-align: center">CURRICULUM VITAE</h1>

PERSONAL INFORMATION

Surname, Name: DAYYENI, Yaqeen Sabah Mezaal

Nationality: Iraqi (IQ)

Date and Place of Birth: 20 June 1985, Baghdad,Iraq

Marital Status: Single

Phone: +905310853503

Email: yakeen_sbah@yahoo.com

EDUCATION

Degree	Institution	Year of Graduation
PhD.	Çankaya University ,Electronic and Communication Department, Ankara,Turkey	2014
M.Sc.	University of Technology, Electrical Engineering Department , Baghdad, Iraq	2009
B.Sc.	University of Technology , Electrical Engineering Department , Baghdad, Iraq	2007
High School	Al-Saydia for Boys, Baghdad, Iraq	2003

EXPERIENCE:

Taught (digital techniques ,8086 microprocessors and communication systems) courses for undergraduate studies in yermuk and diyala universities in Iraq,

Had good experience in engineering software relating to the electronic and communication applications such as Matlab, Microsoft Math, Microwave Office,

from Advanced Wave Research Inc., IE3D, from Zeland Software Inc, Sonnet Software Inc., Registered evaluator for IE3D software since 2008, Member IEEE Iraq section.

FIELDS OF INTEREST: Microstrip Filter Designs, Fractal Resonators, Digital Signal Processing, Digital Communication and MIMO wireless systems.

PUBLICATIONS: More than 18 papers in international and local conferences and peer reviewed journals.

All my publications with details can be seen from the following website:

https://www.researchgate.net/profile/Dryaqeen_Mezaal

DESIGNATED REVIEWER OF SCI JOURNAL

1. International Journal of Electronics
2. International Journal of Electronics Letters
3. China Communication
4. IET Microwaves, Antennas and Propagation

HONOURS AND AWARDS

1. The first PhD student in ECE department in Cankaya University during PhD courses stage with GPA average (AA) in 2012.

2. Winner of TUBITAK scholarship for highly qualified PhD students in 2012.

3.Best paper award at the 3rd International IEEE Conference on Advanced Computing and Communication Technologies , 6-7 ,April , 2013, Rohtak ,India for the presented paper titled with " New Dual Band Dual-Mode Microstrip Patch Bandpass Filter Designs Based on Sierpinski Fractal Geometry" .

FOREIGN LANGUAGES

Arabic, English and Turkish .

HOBBIES

Reading of engineering books, Learning languages, Watching TV and Travelling.